Measurement and Characterization of Low Volatility Organic Compounds in the Atmosphere

by

Jonathan Pfeil Franklin

B.A., Chemistry, Connecticut College (2009)

Submitted to the Department of Civil and Environmental Engineering

In partial fulfillment of the requirements for the degree of

Doctor of Philosophy in Environmental Chemistry

at the

MASSACHUSETTS INSTITUTE OF TECHNOLOGY

~~May, 2018~~ [June 2018]

© Massachusetts Institute of Technology 2018, all rights reserved.

Signature redacted

Author.....

Department of Civil and Environmental Engineering

May 17, 2018

Signature redacted

Certified by.....

Jesse H. Kroll

Associate professor of Civil, Environmental, and Chemical Engineering

Thesis Supervisor

Signature redacted

Certified by.....

Jesse H. Kroll

Associate professor of Civil, Environmental, and Chemical Engineering

Chair, Graduate Program Committee

MASSACHUSETTS INSTITUTE OF TECHNOLOGY

JUL 26 2018

LIBRARIES

ARCHIVES

Measurement and Characterization of Low Volatility Organic Compounds in the Atmosphere

By

Jonathan Pfeil Franklin

Submitted to the Department of Civil and Environmental Engineering on May 17th, 2018, in partial fulfillment of the requirements for the degree of Doctor of Philosophy in Environmental Chemistry

Abstract

Organic aerosol is a central topic in environmental science due to its role in climate forcing and negative health effects. The transformation of organic species from primary gas phase emissions to secondary organic aerosol (SOA) is highly complex and poorly understood, proving difficult for even state-of-the-art computational models to predict. This thesis describes the in-depth characterization and re-design of a previously developed technique for the quantification of intermediate volatility organic compounds (IVOCs), which are compounds with saturation vapor pressures of 10^3-10^7 $\mu g/m^3$. This analytical technique, the thermal-desorption electron ionization mass spectrometer (TD-EIMS) provides a volatility separated, bulk measurement of IVOCs and will be used to investigate the primary emissions as well as production and evolution of IVOCs in a series of experiments described in this thesis. Primary emissions of IVOCs have been previously measured in vehicle exhaust and have been theorized as a significant precursor to secondary organic aerosol (SOA) in urban atmospheres. IVOCs are predominately emitted during cold start periods, but maintain a similar chemical composition across all engine states. As emissions controls have tightened, emissions of non-methane hydrocarbons and primary particulate matter have decreased, however emissions of IVOCs have only decreased significantly (as much as 80%) between the newest ULEV and SULEV emissions control tiers. Laboratory studies examining the atmospheric oxidation of common biogenic and anthropogenic SOA precursors in environmental "smog" chambers show different production and evolution profiles of IVOCs. The comparison of IVOCs measured by the TD-EIMS with other analytical techniques sampling in parallel show the TD-EIMS may detect a previously characterized fraction of carbon. Production of secondary low volatility organic compounds can also occur in low oxygen systems, such as in planetary atmospheres or in the process of soot formation. Ultraviolet light or heat can form radical hydrocarbon species, which, in low oxygen environments, will react with other hydrocarbon or radical species, undergoing oxidation by molecular growth. Particles made from ethane and ethylene are composed of very saturated compounds. The particles produced from the photolysis of acetylene are fundamentally different showing significantly larger molecule sizes and substantially higher degrees of unsaturation. The results from this thesis demonstrate measurements of the production and evolution of primary and secondary low volatility organic gases by new analytical techniques and provide a new insight to the complex chemical processes in the atmosphere leading to the production of secondary organic aerosol.

Thesis Supervisor: Dr. Jesse H. Kroll

Title: Associate Professor of Civil, Environmental, and Chemical Engineering

Acknowledgements:

This research was funded through the National Aeronautics and Space Association (Grant: NNX12AG58G) as well as by a training grant in environmental toxicology through the National Institute of Environmental Health sciences (Grant: P30---ES002109).

I would like to start off by thanking Jesse Kroll for being an amazing principle investigator as well as mentor throughout my six years at MIT. Jesse has an amazing skill for keeping in touch and guiding research while letting us students grow as scientists and learn how to solve issues and learn ourselves and I cannot put into words the amount I have learned throughout this process. I would also like to extend my extreme appreciation to my other thesis committee members, Dan and Colette. We might have only met annually to discuss research, but I always knew if I needed help I could reach out to them. I would also like to thank John Jayne and Scott Herndon at Aerodyne Research Inc. for all their help before and during graduate school.

Six years is a long chunk of anyone's life, and I truly appreciate all the friends I have made at MIT, in Parsons and especially in the Kroll Group. Thanks to Chris, David, Anthony and Kelly for being amazing friends and making routine lab work fun. I am especially grateful to all of the postdocs that have come through the lab. I will forever be indebted to Eben, who I have spent numerous months in the field with. I would never have gotten through 6 weeks in Brent, AL or El Monte, CA without him. A thankyou is also due to Ellie, who helped so much early on in my PhD as I learned what it took to run my own research projects especially during the late nights at the Berkeley National Lab.

I would lastly like to thank my family (Joe, Kate, Jane, Ray), who have been incredibly supportive throughout my PhD. The biggest thankyou goes to my wife, Mariana. Thank you for being the best partner I could ever have asked for. Thank you for all the support throughout traveling for work, late nights in the lab, and always pushing me to be the best version of myself.

Contents

List of Tables

List of Figures

Commonly Used Acronyms

IVOC – Intermediate volatility organic compound

TD-EIMS – Thermal Desorption – Electron Ionization Mass Spectrometry

VOC – Volatile organic compound

PM – Particulate Matter

OA – Organic Aerosol

POA – Primary Organic Aerosol

SOA – Secondary Organic Aerosol

$\overline{(OS_C)}$ – Average carbon oxidation state

n_c, n_H – number of carbon/ hydrogen

H:C, O:C – Hydrogen to carbon and oxygen to carbon elemental ratios

c* - saturation vapor pressure

DBE – double bond equivalents

LEV – Low Emissions Vehicle

LEV2 – Low Emissions Vehicle tier 2

ULEV – Ultra Low Emissions Vehicle

SULEV – Super Ultra Low Emissions Vehicle

CIMS – Chemical Ionization Mass Spectrometry

AMS/ SP-AMS – Aerodyne Aerosol Mass Spectrometer (Soot-Particle AMS)

ToF – Time of Flight mass spectrometer

PTR – Proton Transfer Mass Spectrometer

DMCH – cis-1,4 Dimethylcyclohexane

PTM – Process Test Mixture

Chapter 1

Introduction

Atmospheric fine particulate matter has important implications for visibility, climate forcing on a regional and global scale, as well as human health (*1-3*). Particulate matter (PM) contribute the largest uncertainty in radiative forcing and therefore have large implications in the understanding of climate change on a global scale (*4*). Aerosol particles in the atmosphere directly impact global climate positively by absorbing incoming solar radiation, leading to a warming of the upper atmosphere (*5*). These particles also contribute to a cooling effect on global temperatures by both reflecting and scattering incoming radiation as well as contributing to cloud formation, which increases the albedo of the planet, thus reflecting a larger fraction of incoming solar radiation leading to a cooling effect(*5*). Particulate matter has been shown to negatively affect health by increasing risk of cardiopulmonary disease as well as contributing to respiratory illnesses and a strong correlation has been shown between poor air quality effects with hospital admissions as well as mortality rates (*2*, *6*). Of total fine particulate matter, between 18 and 80% (*7*, *8*) is comprised of organic aerosol (OA) and can be directly emitted to the atmosphere as primary organic aerosol or be formed through condensation of low volatility organic gas phase compounds, forming secondary organic aerosol (SOA).

The transformation of primary gas-phase organic compounds to condensed-phase SOA is highly complex and poorly understood leading to a large degree in uncertainty surrounding aerosol formation and composition, proving too difficult even for state-of-the-art models to accurately predict. Models often under predict production of secondary organic aerosol by an order of magnitude or greater (*9*, *10*). One contribution to this uncertainty arises from the highly complex mixture of organic gases in the atmosphere which serve as precursors to organic aerosol. Gas phase organic compounds range from

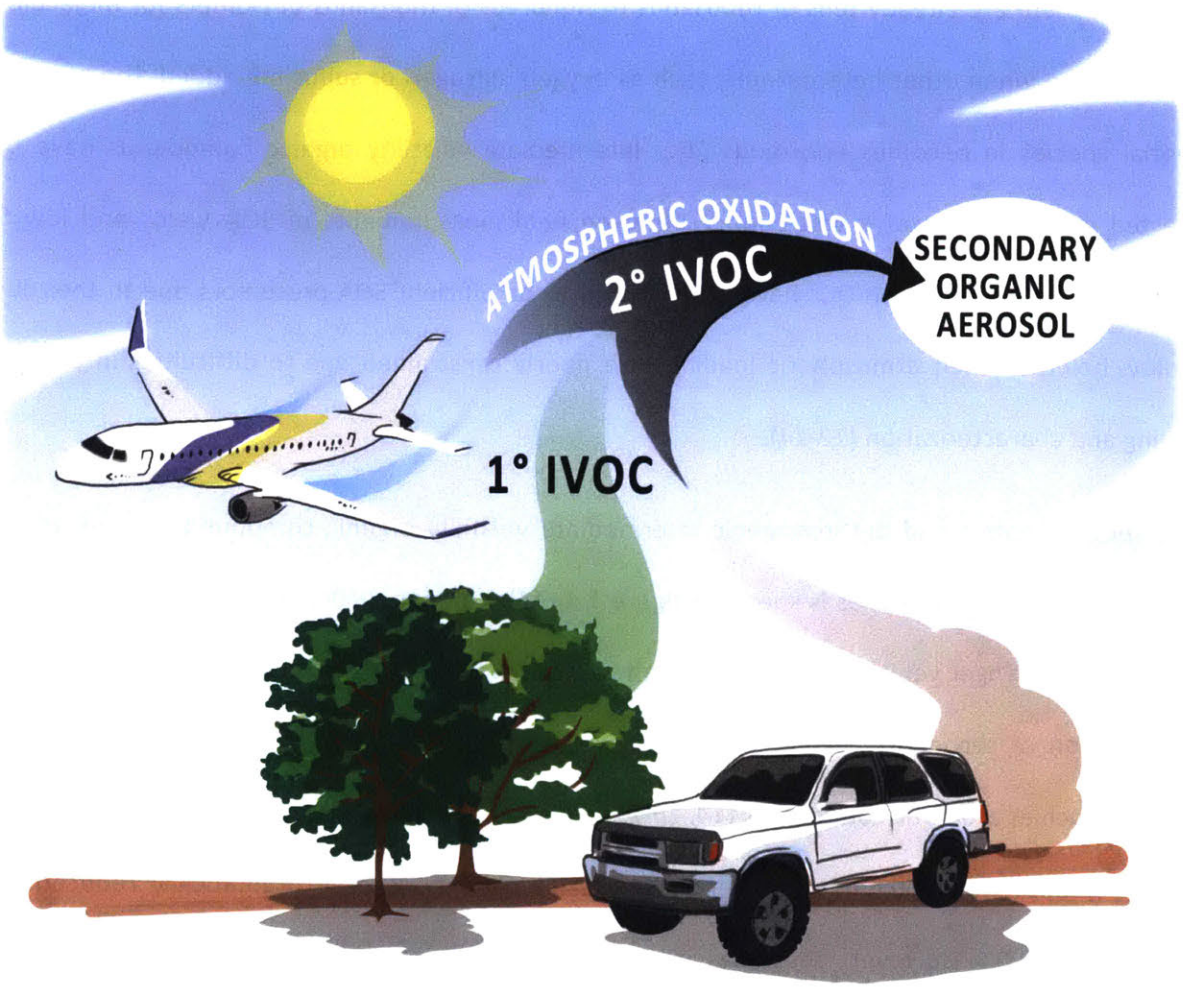

Figure 1.1. Production and evolution of intermediate volatility organic compounds. Primary IVOCs are emitted by both anthropogenic, such as passenger vehicles, and biogenic sources. Secondary IVOCs are produced by atmospheric photochemical oxidation of volatile organic compounds (VOCs) as well as other IVOCs. As IVOCs are oxidized they continue to reduce in vapor pressure and eventually partition into the particulate phase as secondary organic aerosol (SOA).

volatile organic compounds (VOCs), which exist completely in the gas phase, and have a saturation vapor pressure greater than 10^7 μg/m^3, to semivolatile organic compounds, which have a saturation vapor pressure (c*) between 1000 and 0.1 μg/m3 and exist in equilibrium between the gas phase and the particulate phase. Intermediate volatility organic compounds (IVOCs), which will be the focus of this thesis, are defined as organic species with effective saturation concentrations(c^*) falling between those of VOCs and SVOCs (between 10^3 and 10^6 μg/m^3.) These compounds have approximate n-alkane equivalent molecule sizes between decane ($C_{10}H_{22}$) and eicosane ($C_{20}H_{42}$). If just carbon and hydrogen are

considered, there are already tens of thousands to hundreds of thousands of isomers for molecules of these sizes and when other heteroatoms, such as oxygen, nitrogen or sulfur are added, the number of potential species in becomes enormous (*1*). Intermediate volatility organic compounds have been suggested as the source of a discrepancy between field measurements of SOA yields and low SOA production in models (*11*). IVOCs have been shown to be efficient SOA precursors due to their lower volatility, however their atmospheric loadings are poorly constrained due to difficulties in detection, sampling and characterization (*12-14*).

Both biogenic and anthropogenic Intermediate volatility organic compounds can be released directly into the atmosphere, as is shown in figure 1.1 (*15*). Primary IVOCs have been measured in the emissions of passenger vehicles as well as aircraft and can negatively affect air quality and human health via production of secondary organic aerosol as well as from the toxicity of primary components of emissions, such as aromatic compounds (*14, 16-21*). Primary emissions of VOCs and particulate matter is fairly straight forward to characterize and as a result regulations have dramatically reduced these emissions (*22, 23*). However, decreases in SOA yields from vehicle emissions have lagged behind reductions in primary emissions and it has been hypothesized that this difference arises from IVOCs, which are efficient SOA precursors and whose primary emissions are poorly understood.

Emissions controls targeting reduction in ozone production have led to reductions in both primary and secondary organic aerosols (*18, 23, 24*). While the newest tier of regulations, the super ultra-low emissions vehicle (SULEV), have reduced the primary emissions of organic aerosol, it is unclear how these more modern emissions controls have affected the emissions of IVOC and thus the production SOA. Standardized vehicle emissions testing typically group emissions into averaged multi-minute measurement periods and measurements of IVOCs are slow and are typically aligned with these longer averaging periods (*17, 23, 25*). Therefore, the emissions profile as a function of drive state is relatively unknown. Recent highly time resolved measurements of VOCs in vehicle emissions report that organic

compounds fluctuate much faster than typical averaging periods. The majority of these emissions occurring within the first 60-200 seconds of engine on depending on the level of emissions control (*26*).

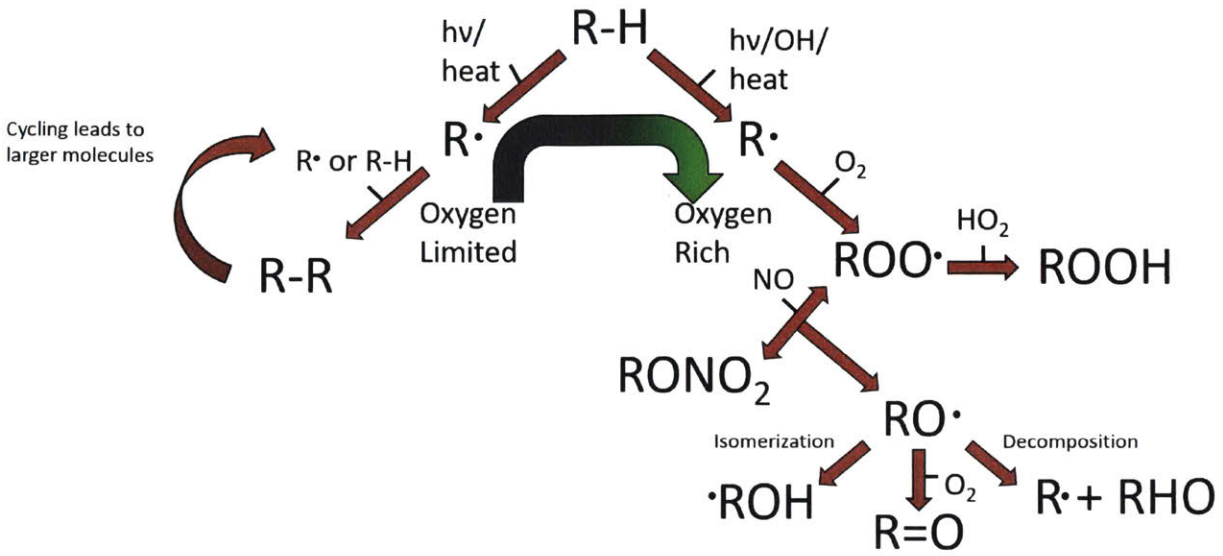

Figure 1.2. Simplified reaction pathways of oxidation occuring in oxygen limited systems (left branch) and oxygen rich environments (right). In oxygen limited systems, organics decrease in volatility via molecular growth. In oxygen rich systems, the addition of functional groups drives the decrease in volatility

In addition to being emitted directly as primary emissions, IVOCs can also be produced in the atmosphere via photo oxidation of VOCs and primary IVOCs producing secondary IVOCs. Through this process IVOCs can act as both precursors as well as intermediates to the production of secondary organic aerosol. Secondary production of IVOCs in the atmosphere occurs through oxidation of volatile organic compounds or primary IVOCs. The general process of atmospheric oxidation involves the emission of a higher volatility gas phase compound into the atmosphere where it is oxidized via gas phase reactions. Figure 1.2 shows a general schematic for reactions of gas phase organic species in the atmosphere. Typically, atmospheric oxidation occurs when some organic compound reacts with a reactive oxidant, such as the OH radical, removing a hydrogen resulting in an alkyl radical(*27*, *28*). This radical species is then quenched by atmospheric molecular oxygen producing an alkyl peroxy radical. This type of atmospheric radical species can be quenched by the HO_2 radical, forming an alkyl peroxide or isomerize producing a QOOH radical species. The alkylperoxy radical can react with nitric oxide (NO), which is common pollutant

gas in urban areas, producing alkyl nitrate compounds or alkoxy radicals (*29*). These alkoxy radicals undergo three major chemical reaction pathways: isomerization, functionalization, or decomposition. Isomerization leads to the relocation of the radical from the alkoxy oxygen to a carbon atom in the molecule, producing a radical alcohol species. In functionalization, the alkoxy radical reacts with atmospheric molecular oxygen producing a carbonyl functional group, such as a ketone or aldehyde. Lastly, the alkoxy radical can decompose, producing two smaller molecules. Every reaction in this process increases the average carbon oxidation state ($\overline{OS_C}$) in the molecule, and with the exception of the decomposition reaction where two smaller, and therefore more volatile, molecules are formed, every reaction leads to a product with a lower vapor pressure. (*30*).

The pathways leading to the production of secondary IVOCs as and eventually SOA in the atmosphere are not fully understood due in part to an inability to accurately measure the intermediates between primary gas phase emissions and produced SOA (*15*). Difficulties in detection and quantification will be examined below, but arise from a highly diverse mixture of organic gases in the atmosphere with extremely low atmospheric concentrations of individual compounds. Ambient IVOCs have been measured in urban areas as well as in forests, but little work has been done to investigate their chemical profile as they are photochemically aged in the atmosphere (*15*, *31*). Environmental "smog" chambers have been used extensively to investigate organic aerosol yields and production from a large range of precursor compounds and serve as a potent tool to understand the chemical processes in a controlled environment (*32-34*).

Secondary low volatility organic gases can also be produced in oxygen limited systems (left arm of figure 1.2). In this system, hydrocarbon species are radicalized via photolysis or heat, producing a radical product, which, in the absence of oxygen, can react with other hydrocarbons or radical species forming a product larger than either reactant. This process produces molecules with lower volatilities via

molecular growth rather than functionalization, which occurs in the presence of oxygen. This chemical process occurs in planetary atmospheres, such as Saturn's moon, Titan, where haze particles are formed in the upper atmosphere via VUV-photolysis of methane, which makes up a major fraction of the atmosphere(*35-37*). This also resembles the process of lean combustion, where in the absence of oxygen, soot is formed due to an inability to fully oxidize the hydrocarbon. While both pathways depicted in figure 1.2 seem somewhat straightforward, they have been very simplified and only represent the first generation of oxidation for organic compounds. As organic gases undergo further oxidation their chemical makeup becomes exponentially more complex(*1*).

There are very few measurements of both primary and secondary IVOCs due to difficulties in sampling and quantification (*16*). Due to the complexity of organics in the atmosphere individual intermediate volatility organic compounds exist in exceptionally low concentrations in the atmosphere, most of which are at or below levels of detection for most analytical techniques. IVOCs are also difficult to sample due to their low vapor pressures, which lead to increased interaction with instrument inlets, leading to losses prior to measurements are able to be performed. Traditional measurements of IVOCs have relied on inferences from SOA production, differences between non-methane organic gases (NMOG) and VOCs, or offline techniques. These methods, especially offline techniques, can provide useful information on IVOC loadings and composition, but typically lack high time resolution and have difficulties measuring highly oxidized compounds due to instrumental limitations. Recent research has leveraged high resolution mass spectrometry, which is the separation of ion by charge, with "soft" chemical ionization techniques to characterize SOA production. These methods are very effective at detecting oxygenated species, including atmospheric oxidation products, and provide chemical information, including the molecular formulas of analytes. CIMS instrumentation has been used extensively in atmospheric oxidation experiments as they are sensitive to lower volatility oxygenated hydrocarbons, especially organic acids (*38*, *39*). However, these methods also have difficulties in calibration, often possess

different responses for different compounds. These techniques also exhibit varying responses to different chemical species types. For example, in the case of H^+ CIMS, analytes must possess affinities for the H^+ ion to be detected leaving them blind to saturated compounds such as alkanes (*38*, *40*, *41*).

Recent work has utilized high resolution mass spectrometry with an online collection and thermal desorption collection attempts to produces time resolved volatility separated measurements of IVOCs. The thermal desorption – electron ionization mass spectrometer (TD-EIMS) is a novel technique designed to provide a time-resolved characterization of IVOCs and has been utilized previously to measure IVOCs in emissions from diesel vehicles and aircraft as well as in a forest (*14-16*). This technique utilizes physical adsorption of target IVOCs using cryogenic preconcentration followed by thermal desorption to provide volatility information of collected sample. Unlike "softer" chemical ionization, electron ionization, which is utilized in the TD-EIMS, does not provide molecular formulas, rather it fractures analyte species with a 70 eV electron beam, splitting apart molecules producing ion fragments, which are detected by the mass spectrometer. Electron ionization does not provide specific molecular composition, rather it provides a more comprehensive and easily quantifiable bulk measurement of chemical mass and composition.

1.1 Research Objectives

In this thesis low volatility organic compounds, in both the condensed and gas phase, are characterized by bulk electron ionization mass spectrometry. The development and use of these techniques has been performed to specifically address the following four research objectives:

1) ***Characterize and Improve upon a previously designed analytical technique for measuring intermediate volatility organic compounds.***
2) ***Quantify emissions of primary intermediate volatility organic compounds from gasoline vehicles.***

3) ***Measure production and evolution of secondary IVOCs in the context of atmospheric "smog" chamber experiments.***

4) ***Characterize differences in particle formation from hydrocarbons in oxygen-free environments.***

To address these questions high resolution mass spectrometry will be utilized in a series of experiments detailed in the following chapters:

Chapter 2: The thermal desorption – electron ionization mass spectrometer is an analytical technique developed to provide a bulk, volatility separated quantification of intermediate volatility gases in the atmosphere. This thesis work characterizes the instrument as it had previously been developed, including its state for deployment to measure primary emissions of IVOCs from in vehicle exhaust. Limitations of the original instrument design prompted the necessity to re-design the sampling, collection, and transfer components of the instrument. The development, and characterization of this new front end is described in detail in chapter two of this thesis.

Chapter 3: Intermediate volatility organic compounds are measured in vehicle exhaust and are hypothesized as a potential source for the discrepancy in measured ambient concentrations of secondary organic aerosol and predicted model SOA concentrations in urban areas. Emissions from a series of vehicles with emissions controls ranging from the older Low Emissions Vehicle (LEV) tier to the most modern super ultra low emissions vehicle (SULEV) were measured as the vehicles were driven through a standardized drive cycle on a chassis dynamometer. In this chapter emission indices as well as composition of intermediate volatility organic compounds were examined as a function drive cycle and emissions controls.

Chapter 4: Here, the modified version of the TD-EIMS is utilized to characterize IVOC production and evolution in the scope of atmospheric "smog" chamber oxidation experiments. α-pinene, the most common monoterpene biogenic emission, is oxidized via ozone as well as the OH radical. Cis-1,4-

dimethylcyclohexane is also oxidized via the OH radical as an example of an anthropogenic molecule emitted into the atmosphere. Both the evolution of the starting material as well as the production of secondary IVOCs are characterized by composition as well as volatility. How these measurements fit into the scope of the total evolution of carbon in chamber experiments are also discussed by comparing IVOC concentrations with other measurements of organic compounds also sampling during the chamber experiments.

Chapter 5: In the absence of oxygen, gas phase hydrocarbons can undergo molecular growth via radical oxidation. Hydrocarbon radicals, produced by photolysis or heat, will grow in size, and therefore reduce in volatility, by reacting with other hydrocarbons. This process can happen at extreme cold temperatures, such as planetary atmospheres, as well as in high temperature environments, such as combustion. A flow reactor was designed to photolyze two-carbon precursors with varying degrees of saturation. The photolysis initiates molecular growth decreasing volatility of molecules enough condense into the particulate phase, which can then nucleate particles to be detected and characterized using an Aerosol Mass Spectrometer, a bulk measurement of the composition of fine particulate matter. Produced particles have very different chemical composition, which gives insight on the chemical pathways undertaken to initiate molecular growth.

1.2 References:

1. A. H. Goldstein, I. E. Galbally, Known and unexplored organic constituents in the earth's atmosphere. *Environ. Sci. Technol.* **41**, 1514–1521 (2007).

2. C. A. Pope III, M. Ezzati, D. W. Dockery, Fine-particulate air pollution and life expectancy in the United States. *New England Journal of Medicine*. **360**, 376–386 (2009).

3. Q. Zhang *et al.*, Ubiquity and dominance of oxygenated species in organic aerosols in anthropogenically-influenced Northern Hemisphere midlatitudes. *Geophys. Res. Lett.* **34**, L13801 (2007).

4. *Working Group I Contribution to the Fifth Assessment Report of the Intergovernmental Panel on*

Climate Change, Summary for Policymakers, IPCC.

5. D. Lamb, J. Verlinde, *Physics and Chemistry of CLouds* (Cambridge University Press, New York, 2011).

6. D. W. Dockery, C. A. Pope, X. Xu, An association between air pollution and mortality in six US cities. *Mass Medical Soc* (1993).

7. A. G. Carlton, R. W. Pinder, P. V. Bhave, G. A. Pouliot, To What Extent Can Biogenic SOA be Controlled? *Environ. Sci. Technol.* **44**, 3376–3380 (2010).

8. Y.-H. Lin *et al.*, Epoxide as a precursor to secondary organic aerosol formation from isoprene photooxidation in the presence of nitrogen oxides. *Proceedings of the National Academy of Sciences*. **110**, 6718–6723 (2013).

9. R. Volkamer *et al.*, Secondary organic aerosol formation from anthropogenic air pollution: Rapid and higher than expected. *Geophys. Res. Lett.* **33**, 4407 (2006).

10. C. L. Heald *et al.*, *Geophys. Res. Lett.*, in press, doi:10.1029/2005GL023831.

11. A. L. Robinson *et al.*, Rethinking Organic Aerosols: Semivolatile Emissions and Photochemical Aging. *Science*. **315**, 1259–1262 (2007).

12. D. R. Gentner, G. Isaacman, D. R. Worton, (2012).

13. Y. Zhao *et al.*, Intermediate-Volatility Organic Compounds: A Large Source of Secondary Organic Aerosol. *Environ. Sci. Technol.* **48**, 13743–13750 (2014).

14. E. S. Cross *et al.*, Online measurements of the emissions of intermediate-volatility and semi-volatile organic compounds from aircraft. *Atmos. Chem. Phys.* **13**, 7845–7858 (2013).

15. J. F. Hunter *et al.*, Comprehensive characterization of atmospheric organic carbon at a forested site. *Nature Geosci.* **9**, 5155 (2017).

16. E. S. Cross, A. G. Sappok, V. W. Wong, J. H. Kroll, Load-Dependent Emission Factors and Chemical Characteristics of IVOCs from a Medium-Duty Diesel Engine. *Environ. Sci. Technol.* **49**, 13483–13491 (2015).

17. Y. Zhao *et al.*, Intermediate Volatility Organic Compound Emissions from On-Road Diesel Vehicles: Chemical Composition, Emission Factors, and Estimated Secondary Organic Aerosol Production. *Environ. Sci. Technol.* **49**, 11516–11526 (2015).

18. Y. Zhao *et al.*, Intermediate Volatility Organic Compound Emissions from On-Road Gasoline Vehicles and Small Off-Road Gasoline Engines. *Environ. Sci. Technol.* **50**, 4554–4563 (2016).

19. D. R. Gentner *et al.*, Chemical Composition of Gas-Phase Organic Carbon Emissions from Motor Vehicles and Implications for Ozone Production. *Environ. Sci. Technol.* **47**, 11837–11848 (2013).

20. W. Choi *et al.*, Neighborhood-scale air quality impacts of emissions from motor vehicles and

aircraft. *Atmospheric Environment*. **80**, 310–321 (2013).

21. L. Morawska, Z. Ristovski, E. R. Jayaratne, D. U. Keogh, X. Ling, Ambient nano and ultrafine particles from motor vehicle emissions: Characteristics, ambient processing and implications on human exposure. *Atmospheric Environment*. **42**, 8113–8138 (2008).

22. M. Hallquist *et al.*, The formation, properties and impact of secondary organic aerosol: current and emerging issues. *Atmospheric ...*, 5155–5236 (2009).

23. A. A. May *et al.*, Atmospheric Environment. *Atmospheric Environment*. **88**, 247–260 (2014).

24. G. Saliba *et al.*, Comparison of Gasoline Direct-Injection (GDI) and Port Fuel Injection (PFI) Vehicle Emissions: Emission Certification Standards, Cold-Start, Secondary Organic Aerosol Formation Potential, and Potential Climate Impacts. **51**, 6542–6552 (2017).

25. Y. Zhao *et al.*, Reducing secondary organic aerosol formation from gasoline vehicle exhaust. *Proceedings of the National Academy of Sciences*. **114**, 6984–6989 (2017).

26. G. T. Drozd, Y. Zhao, G. Saliba, B. Frodin, Time Resolved Measurements of Speciated Tailpipe Emissions from Motor Vehicles: Trends with Emission Control Technology, Cold Start Effects, and Speciation. *Environmental ...* (2016), doi:10.1021/acs.est.6b04513.

27. E. C. Browne *et al.*, Chemical changes to soot form heterogeneous oxidation by OH and ozone. *Journal of physical Chemistry*, 1–16 (2014).

28. P. D. Lightfoot *et al.*, ORGANIC PEROXY RADICALS: KINETICS, SPECTROSCOPY AND TROPOSPHERIC CHEMISTRY. *Atmospheric Environment*. **26A**, 1805–1961 (1992).

29. A. L. Robinson, A. P. Grieshop, N. M. Donahue, S. W. Hunt, Updating the Conceptual Model for Fine Particle Mass Emissions from Combustion Systems Allen L. Robinson. *Journal of the Air & Waste Management Association*. **60**, 1204–1222 (2010).

30. J. H. Seinfeld, S. N. Pandis, Atmospheric chemistry and physics: from air pollution to climate change (2012).

31. B. B. Palm *et al.*, In situ secondary organic aerosol formation from ambient pine forest air using an oxidation flow reactor. *Atmos. Chem. Phys.* **16**, 2943–2970 (2016).

32. J. H. Kroll *et al.*, Chamber studies of secondary organic aerosol growth by reactive uptake of simple carbonyl compounds. *J. Geophys. Res.* **110**, D23207 (2005).

33. J. F. Hunter, A. J. Carrasquillo, K. E. Daumit, J. H. Kroll, Secondary Organic Aerosol Formation from Acyclic, Monocyclic, and Polycyclic Alkanes. *Environ. Sci. Technol.* **48**, 10227–10234 (2014).

34. A. J. Carrasquillo, J. F. Hunter, K. E. Daumit, J. H. Kroll, Secondary Organic Aerosol Formation via the Isolation of Individual Reactive Intermediates: Role of Alkoxy Radical Structure. *J. Phys. Chem. A*. **118**, 8807–8816 (2014).

35. E. L. Barth, O. B. Toon, Methane, ethane, and mixed clouds in Titan's atmosphere: Properties

derived from microphysical modeling. *Icarus*. **182**, 230–250 (2006).

36. M. G. Trainer *et al.*, Haze aerosols in the atmosphere of early Earth: manna from heaven. *Astrobiology*. **4**, 409–419 (2004).

37. M. G. Trainer, J. L. Jimenez, Y. L. Yung, O. B. Toon, M. A. Tolbert, Nitrogen Incorporation in CH 4-N 2Photochemical Aerosol Produced by Far Ultraviolet Irradiation. *Astrobiology*. **12**, 315–326 (2012).

38. P. S. Chhabra *et al.*, Application of high-resolution time-of-flight chemical ionization mass spectrometry measurements to estimate volatility distributions of α-pinene and naphthalene oxidation products. *Atmos. Meas. Tech.* **8**, 1–18 (2015).

39. D. Aljawhary, R. Zhao, A. K. Y. Lee, C. Wang, J. P. D. Abbatt, Kinetics, Mechanism, and Secondary Organic Aerosol Yield of Aqueous Phase Photo-oxidation of α-Pinene Oxidation Products. *J. Phys. Chem. A*. **120**, 1395–1407 (2016).

40. R. K. Pathak, C. O. Stanier, N. M. Donahue, S. N. Pandis, Ozonolysis of α-pinene at atmospherically relevant concentrations: Temperature dependence of aerosol mass fractions (yields). *J. Geophys. Res.* **112**, 1052 (2007).

41. W. Lindinger, A. Jordan, Proton-transfer-reaction mass spectrometry (PTR–MS): on-line monitoring of volatile organic compounds at pptv levels. *Chem. Soc. Rev.* **27**, 347 (1998).

Chapter 2

The Thermal Desorption–Electron Ionization Mass Spectrometer

2.1 Introduction:

Intermediate volatility organic compounds (IVOCs) have been shown to be efficient precursors to secondary organic aerosol (SOA), however direct measurements of atmospheric concentrations are lacking due to difficulties in detection and sampling (*1-5*). IVOCs are defined as organic species with effective saturation concentrations(c^*) between 10^3 and 10^6 $\mu g/m^3$, which correlates to approximate n-alkane equivalent molecule size between decane ($C_{10}H_{22}$) and eicosane ($C_{20}H_{42}$). If just carbon and hydrogen are considered, there are already tens of thousands to hundreds of thousands of isomers for molecules of these sizes. When other heteroatoms, such as oxygen, nitrogen or sulfur are added, the number of potential species in existence is enormous (*6*). This large pool of potential compounds leads to an immense difficulty in detection. Individual compounds will exist in very low atmospheric concentrations, often below detection limits for current measurement techniques (*3*). There are a few exceptions for a handful of compounds that are major products of photochemical oxidation of primary gas phase emissions. However, these primary oxidation products can also undergo further oxidation, producing another level of complexity in the functionalization of IVOCs (*4*, *6*, *7*). This immense diversity in composition leads to difficulty in quantification of IVOC concentrations in the atmosphere as low concentrations of individual compounds prove difficult to detect. Measurements of IVOCs are also lacking due to difficulties in sampling. The low saturation vapor pressures of IVOCs lead to increased interaction with instrument inlet surfaces, leading to losses prior to collection and detection.

Traditionally, IVOCs have been preconcentrated on a sorbent then analyzed offline via gas chromatography (*1*, *8*, *9*). However, the majority of these measurements have been focused on primary emissions of IVOCs from combustion sources due to the inability of gas chromatography to quantify oxygenated compounds. The purpose of gas chromatography is to separate out individual compounds via interactions with a stationary phase along a long capillary while ramping the temperature. While the technique is very efficient at separating out certain types of compounds it has difficulties with oxygenates, as they interact with the stationary phase differently than non-oxidized hydrocarbons. Soft chemical ionization techniques, coupled with high resolution mass spectrometry have also been utilized to measure oxidation products. Chemical ionization mass spectrometry (CIMS) refers to the use of a chemical ion (H^+, I^-, NO_3^-, $C_2H_3O_2^+$) to ionize sample molecules, making samples detectable by mass spectrometry (*10-14*). These techniques are efficient at measuring oxygenated compounds, but struggle with quantification, as different molecules are capable of producing different instrument response rates. These analytical techniques also allow for specificity in detection of certain compounds but at the cost of comprehensively measuring all organics. For example, CIMS are highly efficient at measuring organic acids, but are effectively blind to fully saturated organic compounds, such as alkanes. Recently, work has been performed to quantify total IVOC concentrations by focusing on a bulk measurement top-down method, rather than focusing on individual compounds and a bottom up measurement of IVOC (*2-4*). While this technique will lose specific chemical composition, the use of high resolution mass spectrometry allows for the measurement of bulk chemical composition, including elemental ratios. The Thermal Desorption – Electron Impact Mass Spectrometer (TD-EIMS) is a novel technique designed to quantitatively provide this type of measurement of IVOCs (IVOCs).

This chapter focuses on two versions of the TD-EIMS. The first version of which was already built and utilized prior to this thesis work(*2-4*). Included in the scope of this thesis is substantial characterization of the original instrument construction at its use in characterizing primary IVOCs at the

California Air Resources Board (Chapter 3). Also included in this thesis is the application of the newly designed instrument (Chapter 4) the development of which will be described below. Both instrument designs, as deployed to the California Air Resources board to measure primary IVOC emissions as well as newest design are described as well as the development of the instrument to the updated version used during chamber oxidation experiments performed at the Massachusetts Institute of Technology will be described in this chapter.

2.2 6-Way Valve Instrument State:

2.2.1 Hardware:

The first iteration of this instrument (Figure 2.1) was previously described by Cross et al. The instrument was designed to cryogenically preconcentrate IVOC samples, then measure the bulk composition of IVOCs with volatility information as they are thermally desorbed off of the collection loop. In this version of the instrument, samples are pulled through a sample inlet constructed of heated ¼" stainless steel tubing passivated with a proprietary coating by AMCX inc. to reduce any effects of heated stainless steel on sampled IVOCs as well as maximize the transmission of organics (*15*). The entire inlet is heated to 250 °C to prevent condensation of sample to the walls of the inlet keeping organic compounds in the gas phase. The sample is then pulled through a similarly heated and passivated metal particulate filter, in order to remove inorganic particulate matter, before reaching the 6-way valve (VICI Valco Instruments Co. Inc.). The 6-way valve is operated in two different modes as depicted in figure 2.1. In Collection mode, sample is pulled through the sample loop by the pump while helium is fed directly into the ToF Mass spectrometer. The sample loop is made from passivated 1/16" stainless steel tubing wrapped around a copper block. The sample loop is cooled with liquid nitrogen to just above the dew point to condense out IVOC samples without condensing water. Collection temperatures are limited by water condensation in the sample loop as water will saturate the detector and quench the electron

ionization filament upon desorption. In the second mode, the desorption mode, the 6-way valve is rotated to direct helium flow through the sample loop into the mass spectrometer. At this point the collection

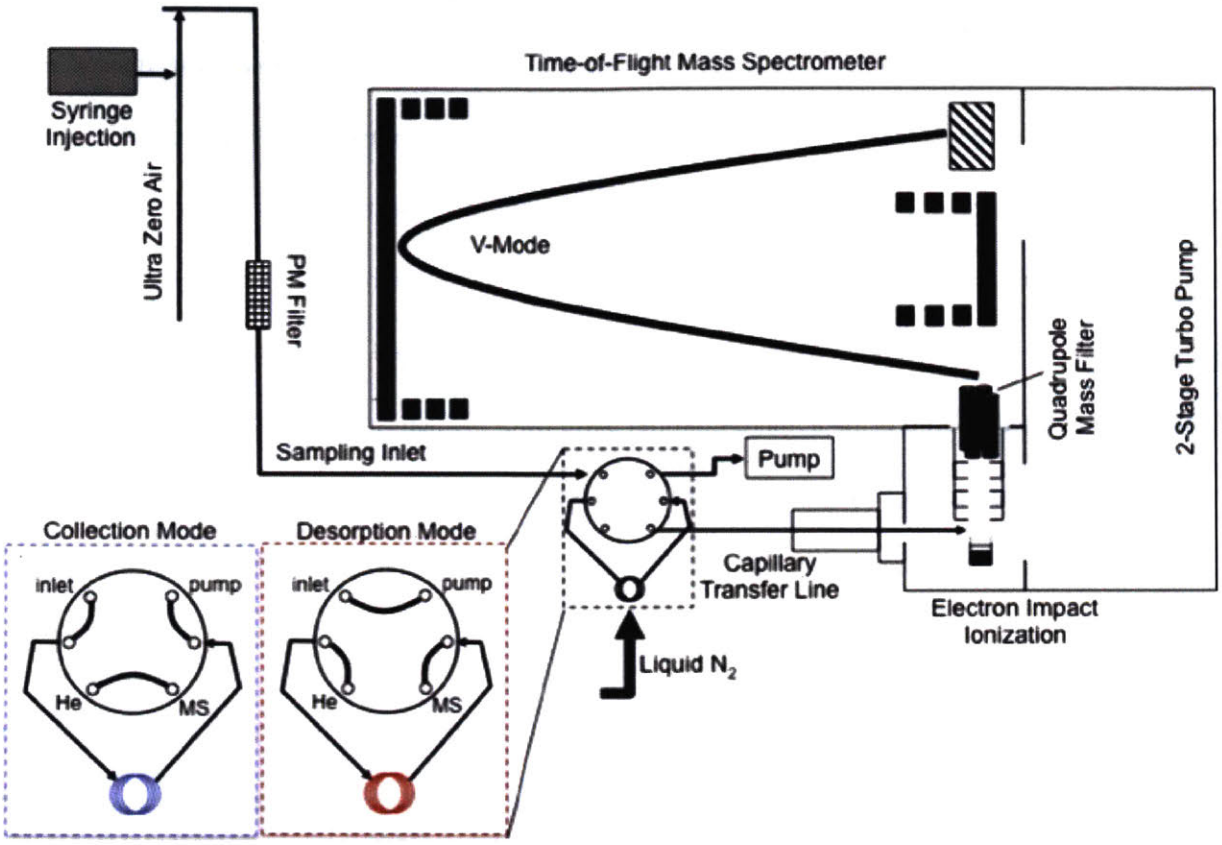

Figure 2.1 TD-EIMS instrument diagram depicting the heated 6-way valve in collection and desorption mode. The entire front end of the instrument is maintained at a high temperature to ensure samples stay in the gas phase. The collection loop is cooled by liquid nitrogen in collection mode and is then heated via temparature ramp in desorption mode to provide a thermogram of organics.

loop is heated via 100 W heater cartridge following a temperature ramp, desorbing the collected organic sample into the mass spectrometer. The desorption of collected organics will occur based on volatility, the higher volatility organics desorbing at lower temperatures, while lower volatilities desorb at higher temperatures, allowing for volatility determination of collected organics.

The high resolution time-of-flight mass spectrometer (ToF-Werk) used is a similar model to that used in the Aerodyne High Resolution Aerosol Mass Spectrometer (*16*). The model used for the TD-EIMS has a gas chromatograph coupling, which allows the passage of a capillary from the 6-way valve into the

ionization region of the mass spectrometer. The collected sample is vaporized on a 600 °C tungsten heater before being ionized with a standard electron impact filament Balzer ion cube operating at 70 electron volts. The produced ion fragments are then directed by a voltage stack through a quadrupole mass filter, which prevents helium ions from entering the ToF. The mass spectrometer can be operated in 'V' mode, where ions are directed in a 'V' trajectory, producing a peak resolution between 2000 and 2500. The mass spectrometer can also be operated in 'W' mode, where the ions are reflected 3 times instead of only once, producing a resolution between 4000 and 5000, however, the increased resolution comes at the expense of signal, as ions are lost during increased flight time. All data discussed in this thesis has been taken in "V" mode. Ions are detected using a micro-channel plate (MCP) which is an array of electron multipliers. Signals are transmitted to an acquisition computer with an Agilent AP-250 data acquisition card capable 2 GHz bandwidth, allowing for the detection of nanoscale differences in flight time for the ions in the mass spectrometer.

Heating and cooling of the TD-EIMS sample loop was controlled via custom visual basic software designed to program PID temperature controllers as well as trigger new collections as well as control the 6-way valve. Also controlled by the software is the signal to initiate data acquisition by the ToF-MS. Data acquisition is performed using the Aerodyne Research Inc. (Billerica, MA, USA) AMS-DAQ software. This data acquisition is designed for use with the high resolution aerosol mass spectrometer, which the TD-EIMS was originally based (*16*). Full mass spectra are acquired at a rate of 1 hz, allowing for accurate alignment of IVOC signal with temperature.

2.2.2 Calibration:

Instrument response was calibrated via syringe pump injection (Harvard Apparatus) of known concentrations of known hydrocarbon species via septum injection port. Figure 2.2 shows the linear correlation between injection concentration and integrated total organic signal. This calibration was

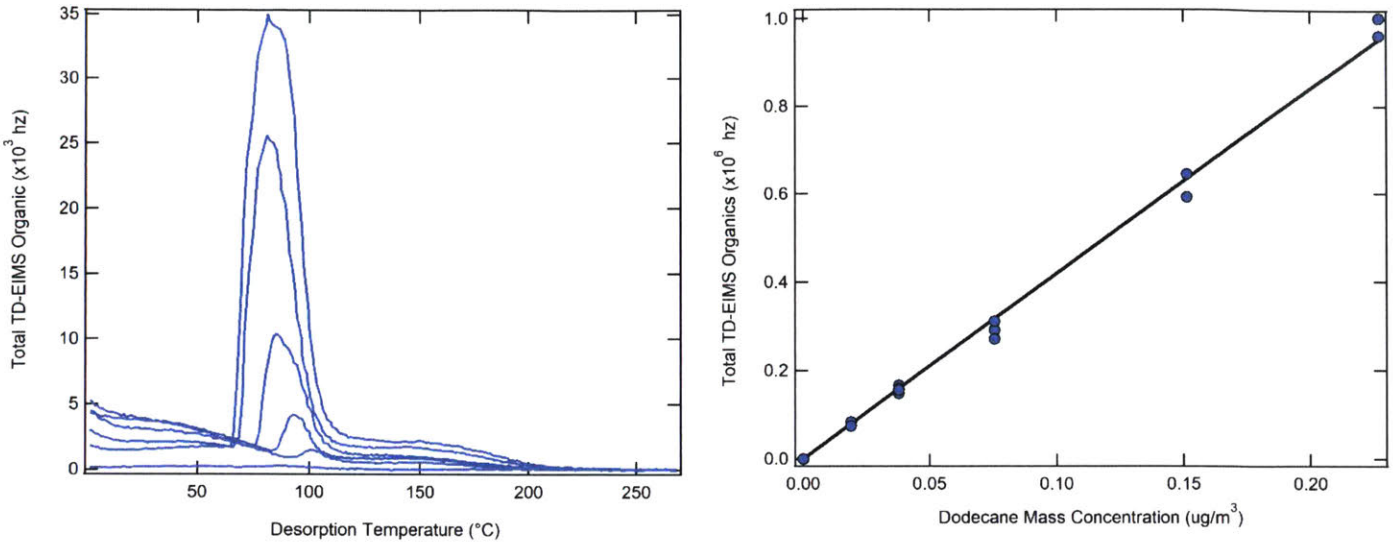

Figure 2.2 Calibration desorptions (left) and linear response curve from the calibration of dodecane. The calibration desorptions show the loading dependent desorption temperature issue, where higher loadings of organics desorb as much as 30 °C lower than lower concentrations.

performed using dodecane, as that was the n-alkane with the closest volatility to the IVOC sampled during the ARB vehicle emissions study. N-alkane standards are injected via septum injection into a stream of heated ultra-zero air to ensure complete volatilization with a known flow rate. Samples are also passed through a mixing tube to completely mix the sample into the air stream preventing any sample mixing artifacts when the instrument subsamples the calibration flow. More details on the analysis of calibrations will be discussed in the following data analysis section as the methodology for calibration analysis is identical to the new version of the instrument.

2.2.3 Limitations of the Original Design:

In an attempt to improve the functionality of the TD-EIMS, the collection and desorption front end of the instrument was identified as possessing a number of limitations in the initial design. The first, and arguably most important is a degraded sample loop. The sample loop was constructed out of 1/16" passivated stainless steel (*15*). In the initial publications of this instrument the collection loop provided very clear separation between different n-alkanes in a mixture. This separation was most likely due to an

unknown coating on the sample loop most likely formed during the initial testing and calibration of the instrument. While this coating likely increased the collection efficiency of certain organics onto the sample loop, it provided an inconsistent desorption surface for collected organics, especially as it aged. The desorption temperature changed with increased organic loading, where higher loadings of organics would desorb at lower temperatures. This effect can be seen in the dodecane calibration performed for the ARB vehicle study (figure 2.2(left)) where the highest loadings desorb as much as 30 degrees below the lowest concentrations. This is most likely due to an inconsistent interaction between the sample and whatever coating was on the sample loop. This coating also likely degraded over the years of applied use of the instrument culminating in a heater failure, which overheated the sample loop causing irreparable damage.

The second issue facing this instrument design was a rapidly degrading tungsten ionization filament. The filament rapidly degraded and required replacement annually, as opposed to every second or third year for other similar ToF systems. This degradation is due to a burst of air that filled the collection loop following the 6-way valve rotation from the collection to desorption position. This air burst quenches the filament emission current and degrades the filament emission enough during an experiment to require a correction for a change in ionization efficiency. In addition to damaging the filament this burst injects air into the ToF, contributing to a high background signal in the TD-EIMS. Both the software and hardware associated with the ARB version of the TD-EIMS only had the capability to control the heat and cooling temperature zones as well as the position of the 6-way valve. An increased control capability is a key factor leading to an instrument redesign. For example, a solenoid valve feeding helium upstream of the 6-way valve solves this issue by purging the air from the sample loop.

2.3 Valve-less Injection System & Characterization:

2.3.1 Hardware:

To improve instrument performance, the entire sample collection and transfer interface of the TD-EIMS was redesigned. The 6-way valve was replaced by a valve-less injection system which is designed to direct flow via pressure controlled zones (*17*). This system, depicted in figure 2.3, uses two flow paths

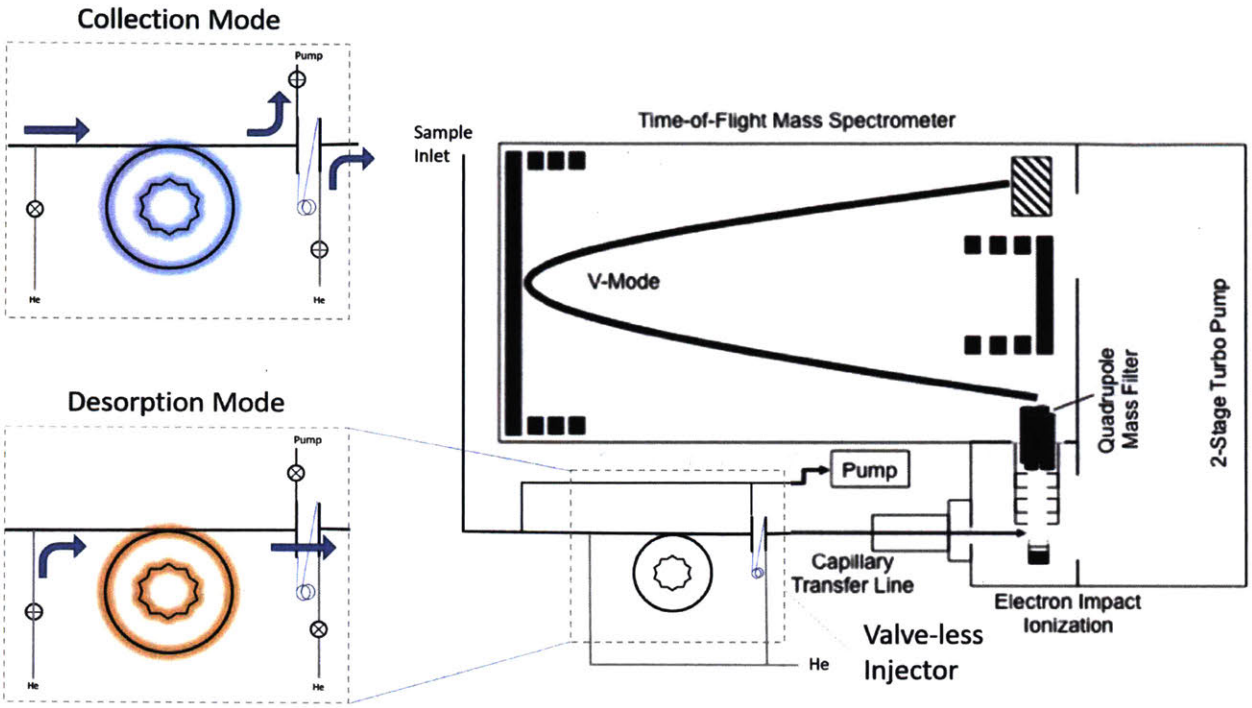

Figure 2.3 Instrument diagram of the new valve-less injection version of the TD-EIMS. The Mass spectrometer is identical to the 6-way valve version of the instrument. In collection mode valves to the sample pump as well as the ToF-MS He are open directing sample flow through the sample loop, which is being cooled by liquid nitrogen, while the ToF is protected by helium. In desorption mode both the sample and ToF He valves are closed, while a sample stream of He is opened in front of the collection loop. This He serves as a carrier gas to carry IVOC samples to the mass spectrometer as they are thermall desorbed off the sample loop.

connected by a restrictive capillary. In the collection mode a supply of helium protects the mass spectrometer while the sample pump pulls through the sample loop. The sample pump also pulls a constant flow past the inlet of the instrument in order to minimize sample inlet transfer time, which is kept below 10 seconds. A trickle flow of helium through the restrictive capillary prevents any sample flow from entering the mass spectrometer during the sampling mode also ensuring the ToF sees only helium and no ambient air, thus maintaining a low background signal. After a timed sample collection, the valve-less injection system is switched to desorption mode by closing the valves providing helium to the ToF as

well as the sample pump, and opening the valve to the upstream helium line. This allows the ToF to pull He through sample loop as it is heated via temperature ramp, desorbing organics based on their vapor pressure.

The sample loop is a 20 cm length of MXT-1 (RESTEK) non-polar metal gas chromatograph column. The dimethyl-polysiloxane stationary phase of the column provides increased affinity for organic samples allowing for higher collection efficiency when compared to the sample loop in the original iteration of the instrument. Transmission of oxygenated samples is more difficult due to differing interactions between the non-polar phase compared to reduced compounds. However, typical column lengths for gas chromatographs, techniques that these columns are designed for, are on the order of 10s of meters, not centimeters, which is the length of the collection loop in the TD-EIMS. The transmission and retention of oxygenates for the TD-EIMS front end collector will be detailed in the calibration section of this chapter. The collection loop is wrapped around a "Mini GC" which is simply an aluminum cylinder designed for even temperature distribution (*17*). The MiniGC is designed to be cooled with air blown through a central hole in the cylinder with fins for increased heat exchange. Instead of using room air to cool, the TD-EIMS uses high pressure liquid nitrogen (230 psi) delivered to a nozzle designed to spray the liquid nitrogen laterally at the MiniGC from the central hole. This allows for faster cooling, decreasing the duty cycle of the instrument by removing the longer air-cooling cycle. Liquid nitrogen cooling also allows for colder collection temperatures. With the new front end and collection loop, the system is still limited by dew point, but in systems with low or no water, liquid nitrogen allows collections to extremely cold temperatures (-50 - -70 C) allowing for the quantification of much higher volatility organic gases.

The new front end of the instrument is controlled via new control boxes developed by Aerodyne Research Inc. combined with new control and data logging software. The control boxes, which were developed for the TAG system (*18*) provide temperature control for the heat and cooling circuits. In addition to the temperature control for the sample loop, the new control setup allows for 8 PID type

temperature controls, which allows for a centralized control and logging of all the temperature zones associated with the TD-EIMS sampling setup. The main TAG control box not only controls the PID temperature controllers associated with the heating and cooling cycles, but it provides eight 24 VDC control lines, which allows for complete control of peripheral devices associated with the TD-EIMS valve-less injection system such as solenoid valves controlling a ToF He flow, a sample loop He source, as well as a valve to open and close the sample pump. In addition to 24 VDC control lines, the box has 4 digital I/O lines, one of which is used to trigger ToF acquisition through the AMS-DAQ software, similar to how it was controlled in the ARB variant of the instrument.

2.3.2 Calibration:

Calibrations were performed with the modified front end to the TD-EIMS similarly to those performed with the initial sampling configuration with minimal improvements. The septum injection port was replaced by a 1/16" capillary with a lure-lock syringe. This removes an inconsistency in calibration

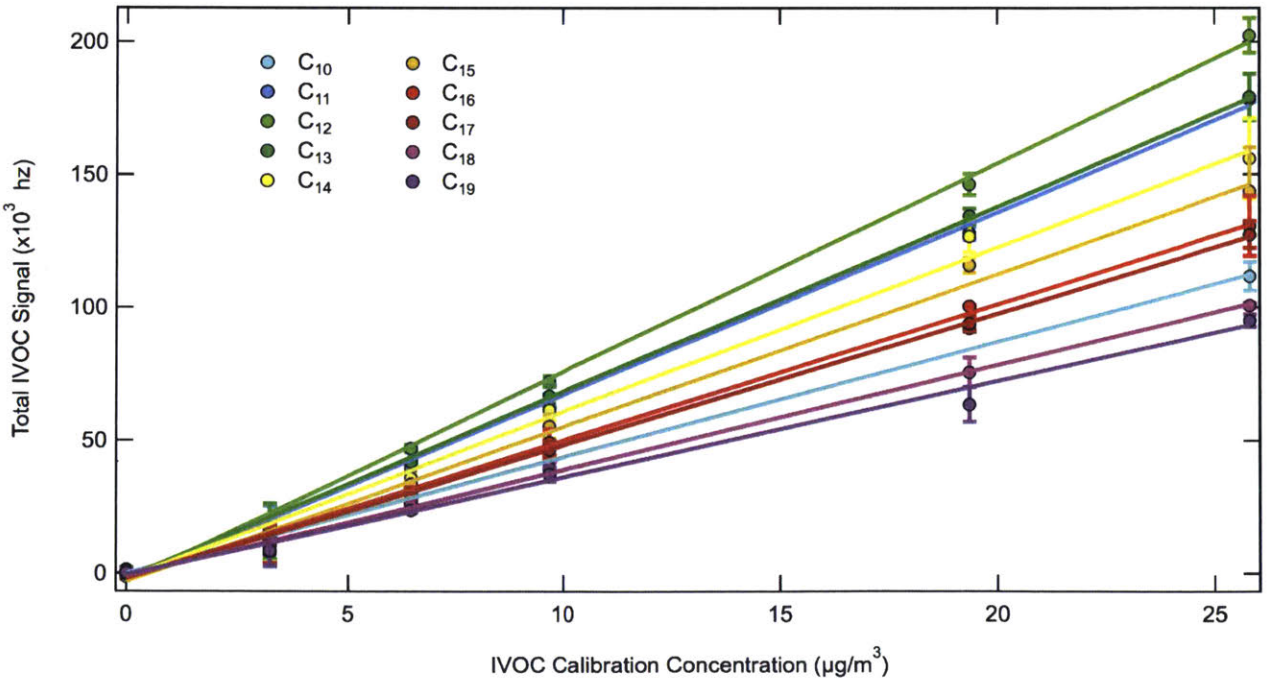

speciFigure 2.5 Calibration curve for n-decane through n-nonadecane. Calibrations are highly linear, but vary deso across volatilty bins, allowing for the targeted mass calibration for each volatlity bin sampled.

response factors based on the position of the needle in typical septum injections. Mass calibrations are performed using a C8-C20 n-alkane mixture at 30 mg/L in hexane solvent (Sigma Aldrich PN#: 04070-5ML) injected via syringe pump between 100 and 2000 nl/min. Injections are vaporized and diluted into dry hydrocarbon free house air (Aadco 737 A/C). Figure 2.4 shows a desorption profile for the n-alkane mixture. The large peak at low temperatures is the hexane solvent present in the injections. The n-alkane series provides clearly separated peaks for each alkane included in the mixture. This collection was taken at -25 °C which does not allow for the collection and thus quantification for n-octane and n-nonane, the two components of the mixture with the highest volatilities. The peak area is correlated to the mass of the given alkane collected. A calibration curve can be constructed using the different injection rates, which is depicted in figure 2.5. There are differing response factors for each n-alkane, which arises from different inlet interactions and collection efficiencies between compounds due to the spread in vapor pressures between n-octane (C_8) and n-eicosane (C_{20}). However, this difference is accounted for by calibrating multiple species across a large vapor pressure window, not just with a single compound, such as was done for the dataset acquired at the California Air Resources Board. This mass calibration is used in the analysis presented in the analysis of IVOC concentrations during environmental smog chamber oxidation experiments. By using an n-alkane mixture to create a mass response curve, the mass of each volatility bin will be in n-alkane equivalent masses. For example, any IVOC mass that elutes in the bin associated with tetradecane ($C_{14}H_{26}$) will be represented as a n-tetradecane equivalent mass.

The number of peaks visible in the desorption is dependent on collection temperature. Higher collection temperatures reduce the collection efficiency of higher volatility compounds. Each n-alkane, and corresponding volatility, will have a different collection efficiency at different collection temperatures. In order to calibrate for the collection efficiency, the same n-alkane mixture used for the mass calibration is injected at a constant rate into a constant dilution flow, creating a stable sample concentration. The collection temperature is then varied extremely cold temperatures (-65 C) to hot

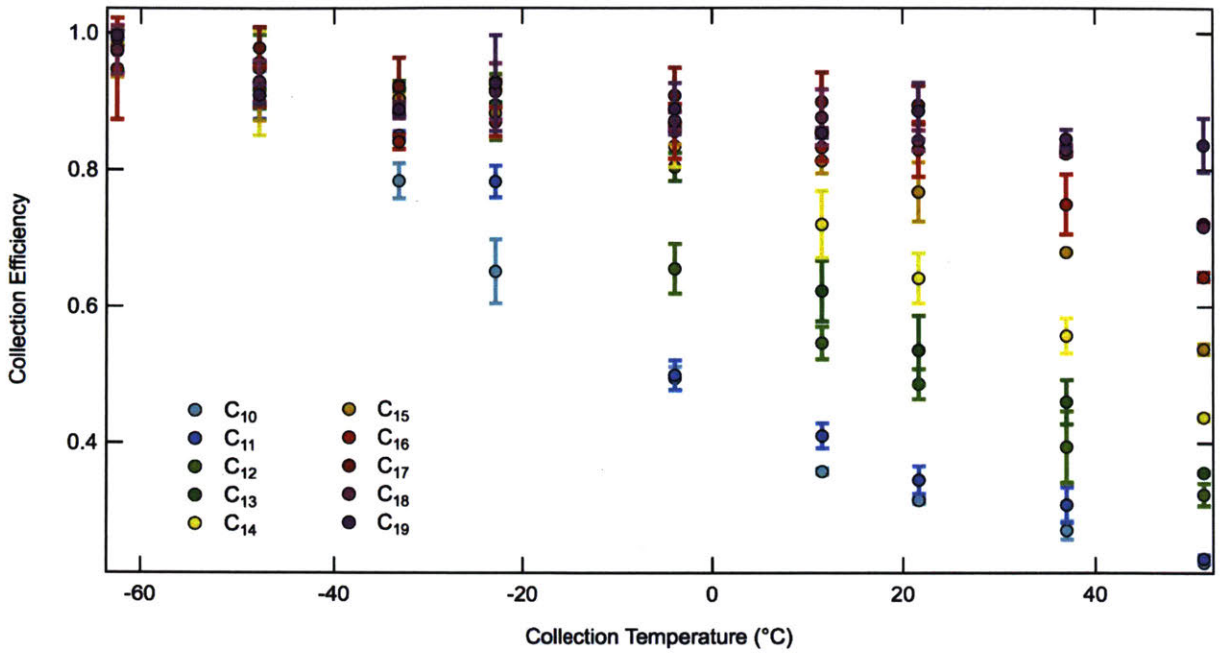

Figure 2.6 Collection efficiency calibration. The n-alkane calibration mixture was collected at varying temperatures. Lower volatility compounds show stable collection effieciecies, however, more volatile compounds (C_{10}-C_{14}) decrease rapidly in collection efficiency as the collection temperature is increased.

temperatures (50 C) (Figure 2.6). This gives a collection efficiency profile vs temperature for each volatility associated with the n-alkanes with the assumption that the TD-EIMS is quantitatively collecting all the masses at a collection temperature of -65 °C. Figure 2.6 shows the collection efficiency profiles for n-decane through n-nonadecane. The larger n-alkanes have much more stable collection efficiencies as they are less volatile and will condense onto the collection loop at higher temperatures. N-decane drops off at colder temperatures due to its significantly higher vapor pressure. Curves are fit to each calibration to adjust for collection temperatures which allows for a correction to be applied across the TD-EIMS desorption profile.

2.3.3 Vapor Pressure Calibration:

In order to provide I/SVOC mass as a function of vapor pressure, TD-EIMS desorptions are binned by the saturation vapor pressure of the n-alkane calibration. Figure 2.7 (left) shows the curve correlating saturation vapor pressure with desorption temperature. The volatility range on this instrument is

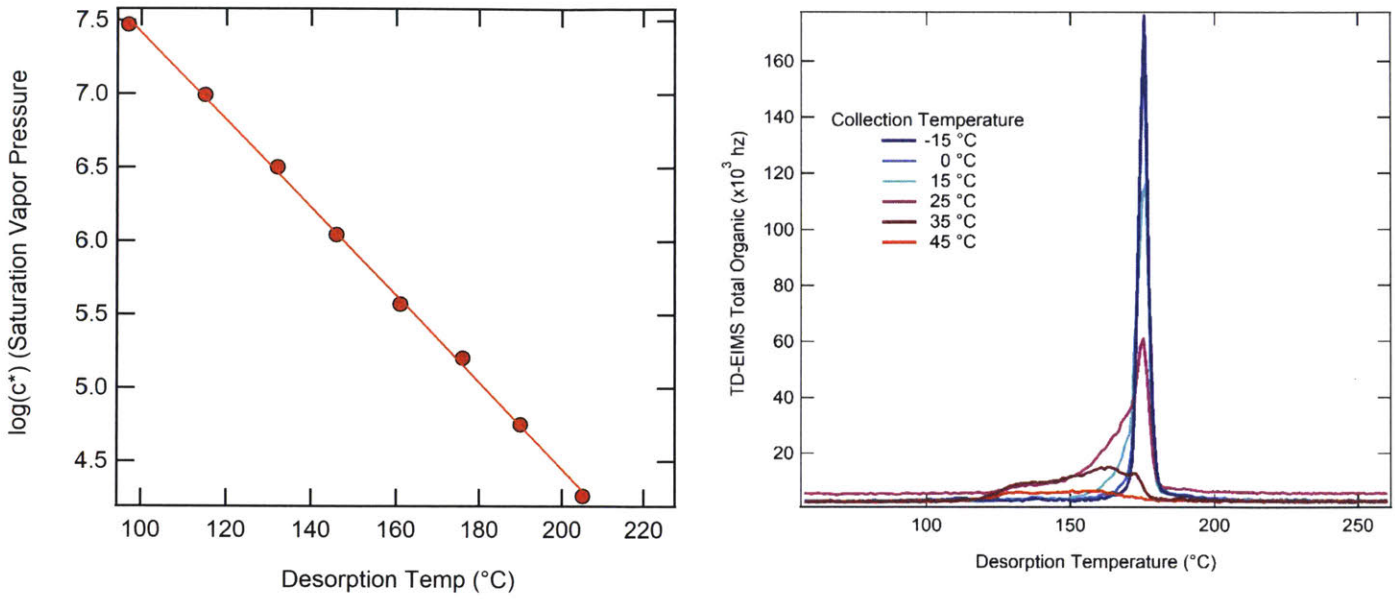

Figure 2.7 Left: volatility calibraion aligning the saturation vapor pressures (log(c*)) of the components of the n-alkane calibration mixture with desorption temperature. Right: IVOCs desorb at the same temperature independent of loading. As the collection temperature increases, IVOC samples will breakthrough the sample loop leading to peak broadening and eventually no collection.

centered on n-alkanes between decane and eicosane which correlates between a log(c*) between 7 and 2. Unlike the previous iteration of this instrument, compounds have been shown to consistently desorb at the same temperature in the valve-less system. This effect is shown in figure 2.7 (right), where a constant concentration of tetradecane ($C_{14}H_{26}$) is sampled at different collection temperatures. Figure 2.6 (right) shows at the coldest temperature (-15 °C) the collection efficiency is close to 1. However, as the temperature is raised, the peak begins to broaden, with some mass desorbing at lower temperatures, while the majority of the mass continues to desorb at the same temperature (~175 °C). This leading edge broadening shape is due to an inefficient collection of tetradecane at warmer temperatures where some of the mass at 15 °C and indeed all of the mass at 45 °C, has broken through the sample loop and is not collected. Because masses desorb at the same temperature peak, along with the linear relationship between vapor pressure and temperature, a correlation between vapor pressure and temperature is achieved (figure 2.7, left panel).

2.3.4 Calibration Validation:

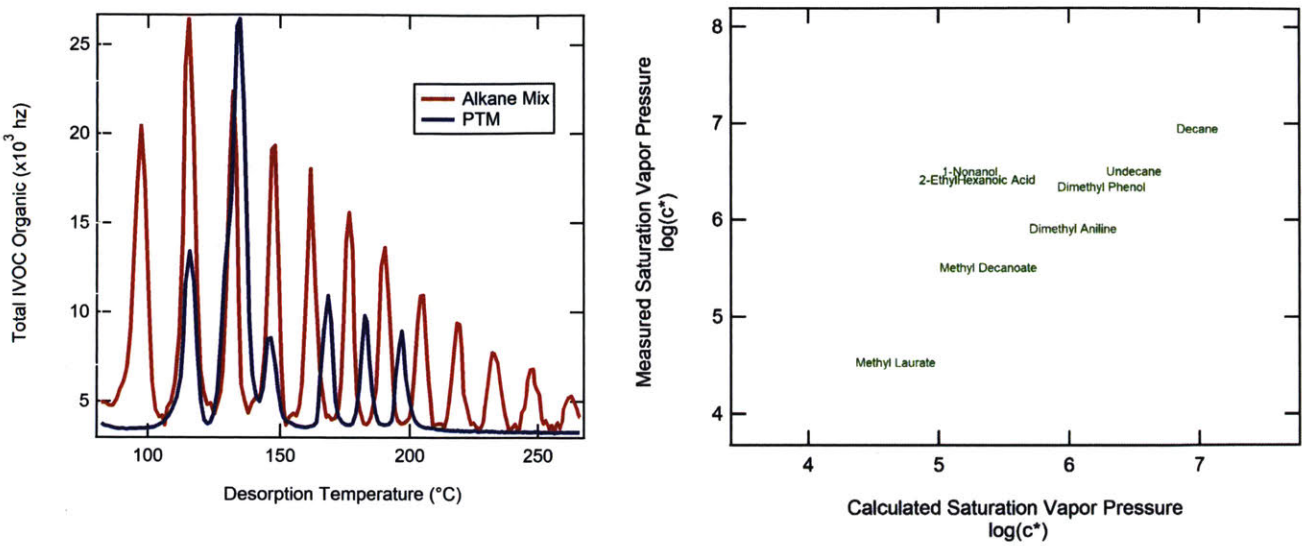

Figure 2.8 Left: Overlay of alkane calibration desorption with the PTM mixture. Alkane components of the PTM align with identical components of the PTM. Right: Calculated saturation vapor pressures of the components of the PTM plotted vs the measured saturation vapor pressure. Results are highly linear, with only two outliars. This could be due to the polar nature of these molecules, but also due to difficulty identifying where these componenets desorb.

The mass calibration and vapor pressure calibration were both performed using the same n-alkane series calibration standard. To ensure that the calibrations held true on non-alkane mixtures, a calibration was performed using a "programmed test mixture" (Sigma: 47304), which is a mixture of compounds with varying functionality such as alkanes, alcohols, aromatics, esters, and amines in dichloromethane. The calibration was performed in the same manner as the n-alkane series standard and the desorption of the PTM mixture plotted on top of the alkane mixture used to calibrate is shown in figure 2.8a. Both decane and undecane are components of the PTM mixture and desorb at the same temperature, 115 °C and 145 °C respectively, as the alkane mixture. The three low volatility peaks in the PTM correspond to C_{10}, C_{11}, and C_{12} methyl esters (methyl decanoate, methyl undecanoate, and methyl laurate). The remaining components of the mixture are either outside of the volatility range of the TD-EIMS or desorb in the large peak centered around 125 °C. Figure 2.8b shows the measured c* values of the identifiable components of the PTM mixture vs the values calculated from literature values of vapor

pressure. The values line up well, with only a few compounds falling off the 1:1 line. The compounds that fall off of the 1:1 line, n-nonanol and 2-ethylhexanoic acid, have terminal alcohol (-OH) groups which could interact with stationary phase of the sample loop, altering their perceived volatility and therefore saturation vapor pressure. However, while these alcohol groups could be negatively interacting with the sample loop, it is of note that component ions in from the NIST library of these compounds were not detected in the desorption and their desorption profile was inferred from other ion fragments

2.3.5 Data Analysis Methodology:

A brief overview of the analysis procedures used to manipulate the high resolution mass spectral data is shown as a flow chart in figure 2.9. The broad methodology can be broken down into four major steps from the acquisition of raw time-of-flight mass spectra and finish with fully processed TD-EIMS data. Data analysis of the TD-EIMS data takes place completely using user-written analysis procedures written in Igor Pro (Wavemetrics inc.). The first step of the analysis involves the processing of raw data using the squirrel AMS-analysis panel (*16*) allowing for initial analysis of unit resolved mass spectra. The time of flight- mass/charge calibration is then performed using strong ion signals from a perfluoromethyldecalin dopant in the He carrier gas to accurately align the elapsed nanoseconds with corresponding ion fragment size in atomic mass units (amus). This compound was chosen as it fragments over a large range of ion sizes (m/z 50 – 493) as well as possess negative mass defects in its fragments, making them much simpler separate from IVOC signals during resolution peak fitting. The mass spectra are then pre-processed before undergoing high resolution analysis, consisting of peak shape and width fitting. High resolution peak fitting is performed by assigning specific organic ion fragments (C_xH_y+ etc.) to ToF peaks. ToF peaks to specific organic ion fragments. These fits are applied to all mass spectra, which are then exported to be analyzed by the TD-EIMS analysis procedures.

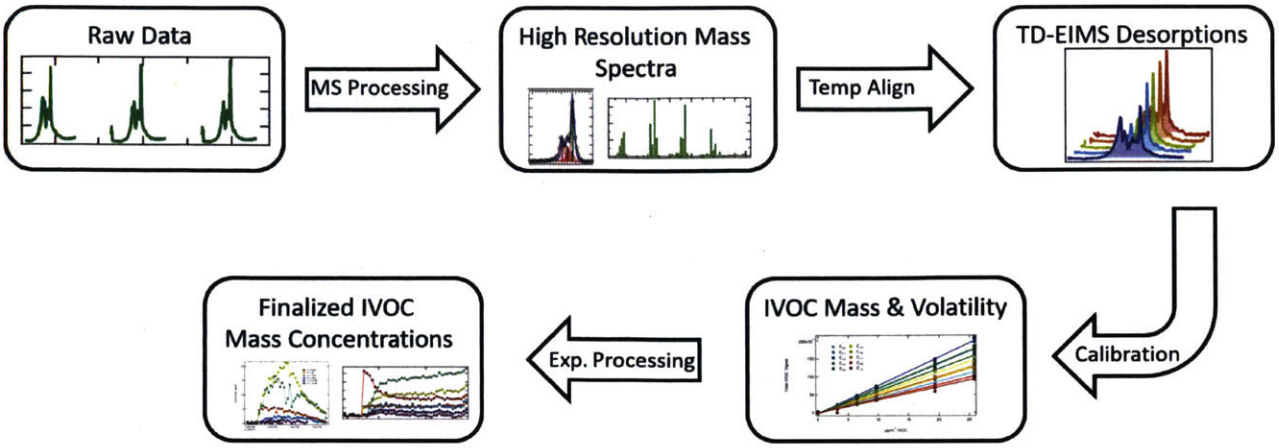

Figure 2.9. Methodology for data analysis for the TD-EIMS broken down by major steps. Raw data is processed producing high resolution mass spectra, which are then aligned with temperature data from the TD-EIMS, producing desorptions. Calibrations and further experiment specific processing is then applied to produce final IVOC mass concentrations.

The second step of data processing involves aligning the high resolution mass spectra with temperature and TD-EIMS desorptions. At this point, any raw data corrections, such as removal of contaminations and background corrections, are applied. The third major step in the data analysis the application of calibrations, starting with the volatility calibration. This process bins the high resolution mass spectra by temperature, based on the volatility calibration described above. Once the mass spectra are binned, the mass calibrations and collection efficiency calibrations are applied. Also performed at this stage of the data analysis is any elemental analysis of the mass spectra. Elemental analysis is calculated using the method described by Aiken et. al., with no correction for fragmentation arising from electron ionization(*19*) The elemental analysis requires the high resolution mass spectra prior to the application of mass calibrations, but can be performed in parallel as elemental ratios normalize out any other corrections.

2.4 Conclusions and Further Work:

The development of the TD-EIMS from the original instrument state has allowed for more reliable measurements of intermediate volatility organic compounds. Initial measurements of IVOCs at the provided measurements of IVOC mass concentration with an approximation of volatility, however due to

a degraded sample loop complete volatility information was lost. The valve-less injection system has allowed for a significantly more stable measurement technique, making analysis of larger datasets more efficient as instrument conditions do not change throughout the course of an experiment. In-depth characterization of the new collection system producing calibrations for collection efficiency, instrument signal response, and volatility have allowed for the accurate determination of ambient IVOC loadings binned by saturation vapor pressure.

While significant calibration and characterization of the instrument has been performed, this work only represents the first step in fully understanding the potential utility of the thermal desorption-electron ionization mass spectrometer (TD-EIMS). The use of a collection loop with a non-polar stationary phase, has significantly increased the collection efficiency of the sample loop. Traditionally non-polar columns affect the transmission of oxygenated compounds differently than non-polar compounds, though the majority of this effect is due to the use of significantly longer column lengths, tens of meters instead of the ten centimeters used in the TD-EIMS. Initial calibrations using oxygenated compounds proved positive, however much more work needs to be done to completely characterize desorption patterns of different types of molecules with different sizes, oxidation states, and functionality. A better understanding of the fraction of total carbon measured by the TD-EIMS will also prove invaluable. Sample is currently pulled through a heated inlet, where organic compounds in the particulate phase could revolatilize. Adding a denuder to strip the gas phase while allowing the particulate phase to pass through to the collection loop would allow for differentiation in signal between the gas and particulate phase. Similar apparatuses have been applied to other analytical instrumentation attempting to better understand gas/ particle partitioning and could be adapted for use on the TD-EIMS (*12*, *20*, *21*).

2.5 References:

1. Y. Zhao *et al.*, Intermediate-Volatility Organic Compounds: A Large Source of Secondary Organic

Aerosol. *Environ. Sci. Technol.* **48**, 13743–13750 (2014).

2. E. S. Cross, A. G. Sappok, V. W. Wong, J. H. Kroll, Load-Dependent Emission Factors and Chemical Characteristics of IVOCs from a Medium-Duty Diesel Engine. *Environ. Sci. Technol.* **49**, 13483–13491 (2015).

3. E. S. Cross *et al.*, Online measurements of the emissions of intermediate-volatility and semi-volatile organic compounds from aircraft. *Atmos. Chem. Phys.* **13**, 7845–7858 (2013).

4. J. F. Hunter *et al.*, Comprehensive characterization of atmospheric organic carbon at a forested site. *Nature Geosci.* **9**, 5155 (2017).

5. Y. Zhao *et al.*, Intermediate Volatility Organic Compound Emissions from On-Road Gasoline Vehicles and Small Off-Road Gasoline Engines. *Environ. Sci. Technol.* **50**, 4554–4563 (2016).

6. A. H. Goldstein, I. E. Galbally, Known and unexplored organic constituents in the earth's atmosphere. *Environ. Sci. Technol.* **41**, 1514–1521 (2007).

7. A. L. Robinson *et al.*, Rethinking Organic Aerosols: Semivolatile Emissions and Photochemical Aging. *Science*. **315**, 1259–1262 (2007).

8. Y. Zhao *et al.*, Intermediate Volatility Organic Compound Emissions from On-Road Diesel Vehicles: Chemical Composition, Emission Factors, and Estimated Secondary Organic Aerosol Production. *Environ. Sci. Technol.* **49**, 11516–11526 (2015).

9. Y. Zhao, A. T. Lambe, R. Saleh, G. Saliba, A. L. Robinson, Secondary Organic Aerosol Production from Gasoline Vehicle Exhaust: Effects of Engine Technology, Cold Start, and Emission Certification Standard. *Environ. Sci. Technol.* **52**, 1253–1261 (2018).

10. W. Lindinger, A. Jordan, Proton-transfer-reaction mass spectrometry (PTR–MS): on-line monitoring of volatile organic compounds at pptv levels. *Chem. Soc. Rev.* **27**, 347 (1998).

11. P. S. Chhabra *et al.*, Application of high-resolution time-of-flight chemical ionization mass spectrometry measurements to estimate volatility distributions of α-pinene and naphthalene oxidation products. *Atmos. Meas. Tech.* **8**, 1–18 (2015).

12. F. D. Lopez-Hilfiker *et al.*, A novel method for online analysis of gas and particle composition: description and evaluation of a Filter Inlet for Gases and AEROsols (FIGAERO). *Atmos. Meas. Tech.* **7**, 983–1001 (2014).

13. F. D. Lopez-Hilfiker *et al.*, Phase partitioning and volatility of secondary organic aerosol components formed from α-pinene ozonolysis and OH oxidation: the importance of accretion products and other low volatility compounds. *Atmos. Chem. Phys.* **15**, 7765–7776 (2015).

14. M. Ehn *et al.*, nature13032. *Nature*. **506**, 476–479 (2014).

15. N. C. Bouvier-Brown, A. H. Goldstein, J. B. Gilman, W. C. Kuster, J. A. de Gouw, In-situ ambient quantification of monoterpenes, sesquiterpenes, and related oxygenated compounds during BEARPEX 2007: implications for gas- and particle-phase chemistry. *Atmos. Chem. Phys.* **9**, 5505–

5518 (2009).

16. P. F. DeCarlo *et al.*, Field-Deployable, High-Resolution, Time-of-Flight Aerosol Mass Spectrometer. *Anal. Chem.* **78**, 8281–8289 (2006).

17. N. M. Kreisberg *et al.*, Development of an automated high temperature valveless injection system for on-line gas chromatography. *Atmos. Meas. Tech. Discuss.* **7**, 7531–7567 (2014).

18. B. J. Williams, A. H. Goldstein, N. M. Kreisberg, S. V. Hering, Atmospheric Chemistry Special Feature: In situ measurements of gas/particle-phase transitions for atmospheric semivolatile organic compounds. *Proceedings of the National Academy of Sciences.* **107**, 6676–6681 (2010).

19. A. C. Aiken, P. F. DeCarlo, J. L. Jimenez, Elemental Analysis of Organic Species with Electron Ionization High-Resolution Mass Spectrometry. *Anal. Chem.* **79**, 8350–8358 (2007).

20. Y. Zhao *et al.*, Development of an In Situ Thermal Desorption Gas Chromatography Instrument for Quantifying Atmospheric Semi-Volatile Organic Compounds. *Aerosol Science and Technology*. **47**, 258–266 (2013).

21. P. Eichler, M. Müller, B. D'Anna, A. Wisthaler, A novel inlet system for online chemical analysis of semi-volatile submicron particulate matter. *Atmos. Meas. Tech.* **8**, 1353–1360 (2015).

Chapter 3

Emissions of Primary Intermediate Volatility Organic Compounds from Modern Gasoline Vehicles

3.1 Introduction:

Vehicular emissions of organic compounds can negatively affect air quality and human health, both from the toxicity of primary species (gas-phase species such as benzene and toluene, and particulate species in the form of primary organic aerosol), and the formation of toxic secondary products (ozone and secondary organic aerosol)(*1-4*). Primary emissions of volatile organic compounds (VOCs) and particulate matter are relatively straightforward to characterize and quantify; however this is not the case for secondary species, namely secondary organic aerosol (SOA), due to the role of environmental conditions in controlling their formation, as well as the multiple precursors involved(*5*, *6*). As a result, while regulations have dramatically decreased the emissions of primary VOCs and PM from engines, the decreases in SOA production potential from emissions of lower volatility organic gases has lagged behind that of the primary NMOG and particulate emissions (*7*). It has been hypothesized that this difference arises from the important role of lower-volatility organic gases in SOA formation (*8*): intermediate volatility organic compounds (IVOCs), defined as organic species with effective saturation concentrations(c^*) between 10^3 and 10^6 $\mu g/m^3$, are not directly regulated, and so may not be decreasing as fast as VOCs. Since IVOCs readily form SOA upon oxidation(*9*, *10*), and may even dominate SOA

formation from vehicular sources (*11*), they may continue to contribute to SOA formation even as VOC emissions regulations become increasingly stringent.

Most previous work on primary IVOC emissions has relied on inferences from SOA formation, differences between non-methane organic gasses (NMOG) and VOCs(*7*, *12*), or offline techniques(*13*, *14*). Offline measurements and estimates of composition based on that of unburnt fuel show IVOC emissions are comprised of a large mixture of organic molecules including but not limited to alkanes, alkenes, cycloalkanes, single ring aromatic compounds, and polycyclic aromatic hydrocarbons(*11*). It is unclear what engineering advances have been made, but hydrocarbon emissions, including IVOC's, have dropped as vehicle emissions regulations have tightened(*15*). Low emission vehicles tier-2 (LEV2) vehicles have shown reductions in emissions when compared to the LEV-1 or pre-LEV vehicles (*12*, *15*). Emissions controls targeting reduction in ozone production have led to reductions in emissions of both primary and secondary organic aerosol (*12*, *15*, *16*). While the newest tier of regulations, the Super Ultra Low Emissions Vehicle (SULEV) have lower PM emissions than the slightly older Ultra Low emissions vehicles (ULEV), it is unclear how more modern emissions controls affect IVOC emissions because measurements for these cleaner vehicle classes are lacking. Therefore, it is unknown how emissions of IVOC, and thus production of SOA, is evolving as emissions regulations become more stringent.

How IVOC emissions profile with drive stage is also unclear as higher time resolved measurements have not been available. It has been shown that the majority of vehicle hydrocarbon emissions are produced before the engine and catalytic converter reach their operating temperature allowing partially combusted and unburned fuel to pass through vehicles' after treatment systems(*17*, *18*). While, emissions measurements are typically measured as averaged sample periods during the vehicle drive test, lasting between 5 and 20 minutes. Recent studies using faster time resolved measurements have reported volatile organic compound emission rates fluctuating much faster than the standard multi-minute averaging periods. The majority of these emissions occur within the first 60-200 seconds depending on

the emissions controls of the vehicle(*19*). However, preliminary work indicated a fundamentally different emissions profile, with cold and hot starts emitting comparable amounts (*20, 21*).

In this study we employ a recently-developed technique, the Thermal Desorption – Electron Ionization Mass Spectrometer (TD-EIMS)(*22-24*), to quantify and chemically characterize the IVOC emissions from a range of modern gasoline vehicles run under controlled driving conditions. The high time resolution of this technique (~1 min sample time) allows for the characterization of IVOCs to be made as a function of the specific part of the drive cycle. Here we examine how IVOC emissions in the first minute after the initial engine ignition ("cold start") compare with those during normal engine operation ("hot running") and after ignition of a warmed-up engine ("hot start"). A second major goal of this work is to understand how such IVOC emissions differ across tiers of emissions control technology. From these results, we are able to estimate that emissions rates during the cold start period have been reduced by as much as 80% while hot start and hot running stages have been reduced by as much as 100% as emissions controls have advanced from the LEV tier to the SULEV vehicles. As emissions controls become more efficient, emissions of IVOCs will be dominated by cold start events meaning they must be targeted for further reductions in IVOC emissions, and thus SOA production.

3.2 Methods:

3.2.1 Vehicle Tests:

Measurements of IVOC emissions from modern gasoline vehicles were made at the chassis dynamometer facility at California Air Resources Board's (CARB) Haagen-Smit Laboratory, enabling the characterization of emissions during typical driving conditions(*12*). This study examines emissions from 12 in-use vehicles, spanning a range of emission tiers (one each of Pre-LEV, tier 0, LEV, and LEV2 vehicles, as well as 4 ULEV vehicles and 4 SULEV vehicles). Table 1 shows the list of vehicles tested as well as which

Vehicle				TD-EIMS Collections		
Year	Make	Model	Emissions Tier	Cold Start	Hot Run	Hot Start
2012	Hyundai	Sonata	SULEV	✓		
2012	Buick	Lacrosse	SULEV	✓	✓	✓
2013	Chevrolet	Impala	SULEV	✓	✓	✓
2014	Kia	Optima	SULEV			
2013	Cadillac	CTS	ULEV	✓	✓	✓
2013	Hyundai	Accent	ULEV	✓	✓	✓
2013	Chevrolet	Tahoe	ULEV	✓	✓	
2013	Mazda	3	ULEV	✓	✓	✓
2008	Chevrolet	Uplander	LEV2	✓	✓	✓
1990	Buick	LeSabre	Tier0	✓		
2003	Ford	F-150	LEV	✓	✓	✓
1990	GM	Sierra	Pre-LEV	✓	✓	

Table 1. shows the vehicles sampled by the TD-EIMS during the study at the ARB Haagan-Smit facility in El Monte, California during the summer of 2014. Seven of the vehicles produced desorptions for all "bag" periods of the Unified Cycle. Either hot run (Bag 2) or hot start (bag 3) collections failed for, and therefor excluded, four vehicles due to condensation of water in the sample loop, which saturated the mass spectrometer upon desorption. The Optima was excluded due to abnormally high baseline signals producing biased emission index values.

collections were taken successfully for each vehicle. All vehicles were run through a cold-start unified cycle (UC), an approximately 40-minute-long drive cycle designed to mimic typical driving conditions in an urban setting. Prior to the cycle the vehicle is towed onto the dynamometer, ensuring that the engine is at ambient temperature at the time of engine ignition, thereby allowing for the examination of true cold-start emissions. The UC includes a number of different driving period ("bags"): the cold start and warm-up period ("bag 1", 300s in duration), which includes several accelerations and decelerations; a longer period ("bag 2", 1135s) that includes high-velocity portions (to mimic highway driving) and multiple rapid accelerations and decelerations; a 600s engine-off period ("hot soak") that mimics an extended stop; and a hot-start period ("bag 3", 300s) which is identical to the initial "bag 1" drive pattern but with the initial engine ignition occurring at a higher engine temperature.

3.2.2 IVOC Measurements:

IVOC measurements are made using the Thermal Desorption Electron Ionization Mass Spectrometer (TD-EIMS) with the six-way valve, as described in chapter 2.2. This instrument and analysis approach technique has been described previously for emissions measurements from aircraft and diesel engines(*22*, *23*) as well as ambient measurements(*24*); here we present a brief overview of the measurement technique, as well as details of the analysis specific to this work.

Sampled IVOC gases are cryogenically collected by pulling sample flow through a sample loop cooled with liquid nitrogen to -15°C (± 5°C). This is just above the dew point of the diluted sample, in order to avoid water condensing within the loop and saturating the mass spectrometer upon desorption. After one minute of collection, the collected sample is thermally desorbed via a controlled temperature ramp (60°C/min over 4.5 min, followed by a 1 min "soak" at 280°C) and sent into the ionization region of a time-of-flight mass spectrometer (described below) using helium as the carrier gas. The sample loop was then cooled back to the collection temperature for the next measurement, allowing for a measurement to be taken every ~9 min. A degraded sample loop prevented the accurate estimation of volatilities of the desorbed IVOCs, as in our previous work(*22*, *24*), but the desorption temperatures of the sampled emissions are in the same general range as those from C_{10}-C_{14} alkanes, corresponding to saturation vapor concentrations of approximately 10^7-10^5 μg/m3.

IVOCs desorbed from the sample loop are characterized and quantified using an electron ionization high-resolution time-of-flight mass spectrometer (Tofwerk AG), equipped with a quadrupole mass filter to prevent He carrier gas ions from reaching the detector. An average mass spectrum was saved every second. The mass spectrometer was run in "V mode", for a mass resolving power of ~1700, allowing for the identification of major ions in the mass spectrum, and clear separation of $C_xH_y^+$ and $C_xH_yO_z^+$ ions at masses below *m/z* 150. Mass spectra are analyzed via SQUIRREL and PIKA fast MS analysis

methodology in Igor Pro (Wavemetrics), developed for analysis of data from the Aerosol Mass Spectrometer, and adapted for analysis of TD-EIMS data. Elemental ratios are calculated using the method described in Aiken et al. with no correction for fragmentation arising from electron ionization(*25*). All carbon-containing ions were included in the analysis, with the exception of CO^+ and CO_2^+, which were present in very high levels in the blank (air) spectra, and thus are not reliable measures of IVOCs.

Mass calibrations (for converting mass spectrometric signal to IVOC concentration) were carried out via regular syringe injections of known concentrations of *n*-dodecane both at the tip of the inlet and just upstream of the six-way valve. Blanks during calibrations were performed using ultra zero air (Airgas). Inlet transfer calibrations performed by sampling a constant concentration of dodecane injected at the tailpipe as well as at the instrument showed a 75% transferal through the entirety of the sampling inlet. Mass calibrations were performed using *n*-dodecane, which exhibits a volatility (desorbing between 90-100 °C) similar to that of the measured vehicle emissions. All mass concentrations in this study are therefore given in "dodecane equivalents". While the calibrations are highly linear (precision of better than 5%), the absolute error is estimated at 30-50%, due to potential differences in detection efficiencies of different analyte species (*24*). Baseline measurements for vehicle tests were taken immediately prior to the vehicle test via the entire transfer line once it was attached to the vehicle's tail pipe by sampling ambient air pulled through the vehicle. Detection limits of IVOC measured in the ultra-zero air blank by the TD-EIMS were 3.28×10^{-3} µg total IVOC. This value is well below the range of baseline sample collections taken prior to each vehicle test which range from 1.16×10^{-3} to 1.61×10^{-3} µg. All vehicle collections were well above the detection limit and all collections, except for the hot start collections for the two SULEV vehicles, are significantly above their corresponding baseline collections.

3.2.3 Sampling Methods:

The TD-EIMS sampled from ~30 cm behind the tailpipe of the vehicles through a Fox-Venturi mini-eductor (Fox Venturi Products, Dover, NJ), allowing for subsampling and dilution of the high-pressure exhaust. Samples were collected at this location rather than from the constant volume sampler (CVS) traditionally used in these measurements due to concerns about losses of IVOCs to inlet walls. Sampling through the Venturi inlet was achieved using dry compressed air, which diluted the sample by a factor of ~5-15; this also lowered the dew point of the sample, allowing sampling at lower temperatures, thereby increasing the collection efficiency of IVOCs (as discussed below). The subsample was pulled at 10 LPM through a 9 m long, 3/8" O.D. PFA line heated to 50 °C, for a transfer time of ~10 seconds. While this sampling configuration served to minimize the interaction of IVOCs with the inlet/sampling surfaces, it bypasses the CVS, which complicates the determination of fuel consumption (as described below).

3.2.4 Emission Index Calculation:

IVOC emissions are quantified in terms of their emission indices, the mass of IVOC emitted per mass of fuel burned. Fuel consumption was not directly measured, but rather estimated from CO_2. Emission index is calculated from the following expression:

$$EI_{IVOC} = \frac{\Delta IVOC * F_{Cal} * N_A * EI_{CO_2} * F_{EF}}{\Delta CO_2 * F_{conv}} \qquad Eq\ 1.$$

where ΔIVOC is the measured IVOC signal above background (in counts per second, cps), F_{Cal} is the calibration factor($\frac{\mu g/m^3}{cps}$) determined from dodecane injections, and N_A is Avogadro's number. EI_{CO_2} is the emission index of CO_2 (g C/ kg fuel), ΔCO_2 is the increase in CO_2 above baseline (ppm), while F_{conv} represents the stoichiometry required to convert ΔCO_2 to grams of carbon (equal to 1.05 x 10^{21} $\frac{\frac{Molecules\ CO_2}{m^3}\ g\ CO_2}{ppm\ CO_2\ mol}$). Lastly, F_{EF} is an exhaust correction term, correcting for the variable exhaust flow throughout the experiment described blow.

3.2.5 Engine Exhaust Flow Correction:

The F_{EF} term is necessary because sampling was not done via the CVS; without this correction, estimated fuel consumption from CO_2 measurements will be biased towards periods of low engine power, since during these times exhaust flow is lowest while subsampling flows remain constant. Due to variations in exhaust flow, burned fuel mass could not be accurately measured using carbon dioxide concentrations in the TD-EIMS inlet alone. A correction factor, taking into account the variation in exhaust

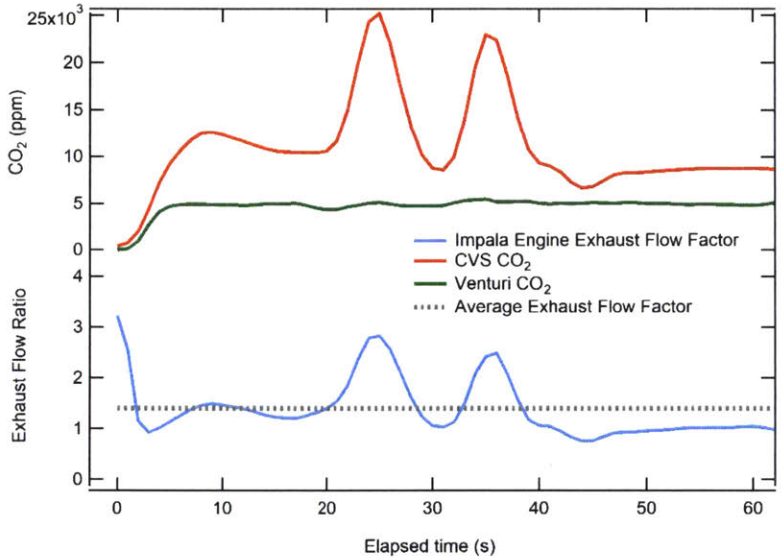

Figure 3.1. Ratio of CO2 for the Chevrolet Impala measured through the constant volume sampler (CVS) and TD-EIMS Venturi inlet used to calculate the exhaust flow correction factor due to biased sampling towards low engine flow periods.

flow, can be calculated from comparing CO_2 levels in the TD-EIMS inlet and those in the Constant Volume Sampler (CVS), which varies the dilution flow to maintain a constant flowrate through the sampler. By taking the ratio of CO_2 concentration in the CVS to the CO_2 concentration in the TD-EIMS inlet as well as the total flow through the CVS during a vehicle test, an estimate of the engine flow can be calculated.

An example of this correction for the cold start emissions from a Chevrolet Impala is shown in figure 3.1. The first 20 seconds of the UC has the vehicle sitting idle. While at idle, the CVS and TD-EIMS should see the same concentrations of CO2 due to a constant flow rate once corrected for the different

dilution rates between the CVS and venturi inlets. The red and green trace represent CO_2 measured through the venture inlet (green) and through the CVS (red) during different vehicle tests for the same vehicle (Chevrolet Impala). Observed differences in concentration are from differing amounts of dilution between the CVS and venture inlets. The CVS is variable due to the variable dilution required to maintain the constant flow rate in the CVS, while the venture sample line maintains a consistent dilution rate. By assuming this is the base flow rate the TD-EIMS will sample, anything higher would be the flow leading to low-biased measurements by the TD-EIMS. The difference between this constant value and the extra exhaust produced will be the fraction of exhaust flow missed by the TD-EIMS, which is proportional to the fraction of fuel that the TD-EIMS inlet will miss. The blue trace represents the ratio of exhaust flow above the flow rate during the initial 20 seconds of engine on where the engine is at idle and should be emitting a constant flow of exhaust. The average exhaust flow factor is ~1.4 (grey trace in figure 1), which means the TD-EIMS is only under-estimating the fuel burned by 40%, leading to an overestimation of emission indices by only ~28%. This value is an approximation made from one vehicle out of the 12 sampled as it was sampled through both the CVS and venutri inlets.

3.2.6 Additional Measurements:

Carbon dioxide measurements were made using a non-dispersive infrared absorption monitor (LI-COR Biosciences LI-840A). In order to accurately calculate consumed fuel in the exhaust, the CO_2 monitor sampled behind a Pt catalyst heated to 400°C, to fully convert any residual hydrocarbons in the exhaust to carbon dioxide (though emitted CO_2 dominates the signal).

In addition to online measurements by the TD-EIMS, IVOC and SVOC were also measured via collection and offline analysis, as in previous studies(*12*, *15*). One set of Tenax-TA sorbent tubes (Gerstel) collected gaseous emissions during the cold start phase while the combined emissions from the hot-

running and hot-start phases collected on a second set of sorbents. The sorbent tubes were housed in a heated enclosure (47 ± 5 °C) mimicking the CFR86 protocol. Sorbent tubes were analyzed using thermal desorption gas chromatography with mass spectrometry similar to Zhao et al.,(*15*).

The quantification of IVOC using electron impact ionization is similar to that of Zhao et al., except adapted for GCxGC methods(*13*, *15*). Slightly different methods were applied to quantify the material that fell into three categories: aliphatic, single ring aromatics (IVOC-SRA), and general IVOC (Gen-IVOC). These three categories are defined according to characteristic fragments in mass spectra and the polarity separation retention time. The aliphatics and IVOC-SRA have similar polarity retention times and are categorized by characteristic mass spectra. IVOC-Gen are compounds that are more polar and are defined by longer polarity separation retention times. All three classes of compounds were quantified by either direct calibration with known standards or relating the total ion chromatogram (TIC) signals to calibration standards of similar volatility and polarity. For example, n-alkanes were directly quantified, but compounds nearby in terms of polarity and volatility (i.e. branched alkanes) were quantified by relating their TIC signal to that of the nearest n-alkane. To this end, volatility bins were defined that are evenly spaced with their centers corresponding to each n-alkane. In GCxGC, the TIC signal corresponds to a "blob," or a region in volatility and polarity retention space, thus the TIC blobs were quantified using the calibration for the available standard of similar polarity in the same volatility bin. The GC-Image software package was used to create blobs from the generated GCxGC chromatograms. The complete analysis of this data is presented by Drozd et al (in prep).

3.3 Results & Discussion:

3.3.1 Measurement Overview:

For seven of the twelve vehicles studied, the TD-EIMS measured IVOCs in all three "bag" sampling periods (see Table 1); these are the focus of the present analysis and discussion. Figure 3.2 shows a time series of a typical UC drive cycle (for the Ford F-150, an LEV vehicle). The top panels show the vehicle

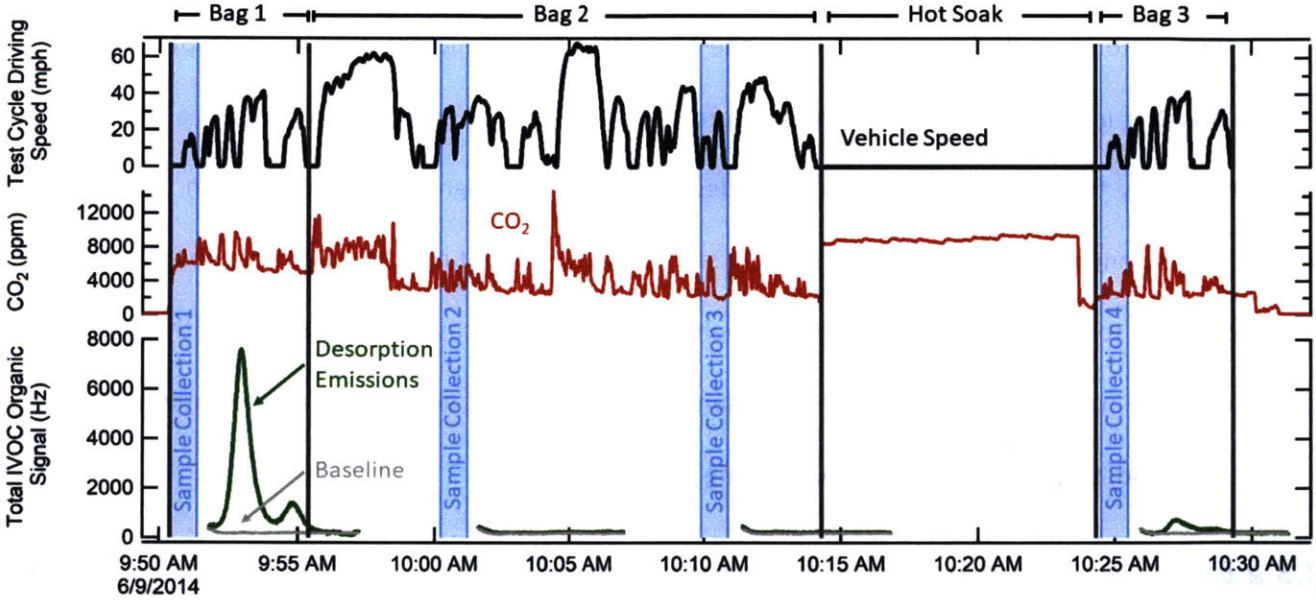

Figure 3.2. Sample data collected for a single UC drive cycle (from an LEV vehicle). Black trace: vehicle speed; red trace: measured CO_2 concentration at the TD-EIMS; green trace: total IVOC signal from the TD-EIMS; grey trace: IVOC signal during the blank experiment; blue boxes: periods during which the TD-EIMS was sampling.

speed profile of the UC test, and the measured CO_2. Blue boxes indicate the TD-EIMS sample collection periods. Sample 1 was timed to capture the cold start engine turnover by triggering collection at engine ignition, thus allowing for transfer line lags. The next two collections (Samples 2 and 3) were made during "hot run" (bag 2), taken to be representative of driving conditions after engine warm-up. However, the timing of these collection periods varied somewhat from vehicle to vehicle (due to differences in cooling times), leading to slightly varying duty cycles. Since engine speed varied rapidly during this period (top

panel), it is difficult to compare measurements from different hot run samples; nonetheless, these measurements provide a useful snapshot of the emissions during this sample period, once the vehicle has come to its operational temperature and runs at varying speeds. Additionally, while two collections were taken during the hot run period (Bag 2) for most vehicles, the second collection often failed due to the condensation of water in the collection loop of the TD-EIMS. Therefore, only the first hot-running collection period is examined for all vehicles. Finally, the 4th sample was taken at the engine turnover (beginning of bag 3) for each vehicle, in order to examine hot start emissions.

The bottom panel of Figure 3.2 shows the TD-EIMS total organic signal during desorption of the collected IVOCs into the mass spectrometer (green trace), as well as typical signal for a blank air desorption (grey trace). During the cold start, desorption signal is significantly higher than the blank, indicating substantial IVOC emissions during cold start. By contrast, hot run collections (samples 2 and 3) are much closer to the blank desorption for the vehicles and, in some cases are not significantly different from baseline. Finally, the hot start collection (sample 4) shows IVOC signal that is substantially higher than background, but also much lower than during the cold start.

3.3.2 Emissions as a function of Emissions Control Tiers:

IVOC emission indices for all vehicles studied, as a function of the drive stage (cold start, hot running, hot start), are given in Figure 3.3. The most striking feature is the very large contribution of cold start emissions to total emissions. This is seen for all vehicles studied, regardless of level of emissions control; however cold-start emission indices do generally decrease as the emissions tiers increase. LEV and LEV2 vehicles show an IVOC emission index of ~100 mg IVOC / kg fuel for the cold start, roughly 10-20 times higher than the emission indices of the hot run and hot start stages. The ULEV vehicles exhibit lower cold-start emission indices, closer to 80 mg IVOC/ kg fuel, with one exception (the Mazda 3). In this case the high emission index is driven not by a high IVOC mass collected, but rather an abnormally low

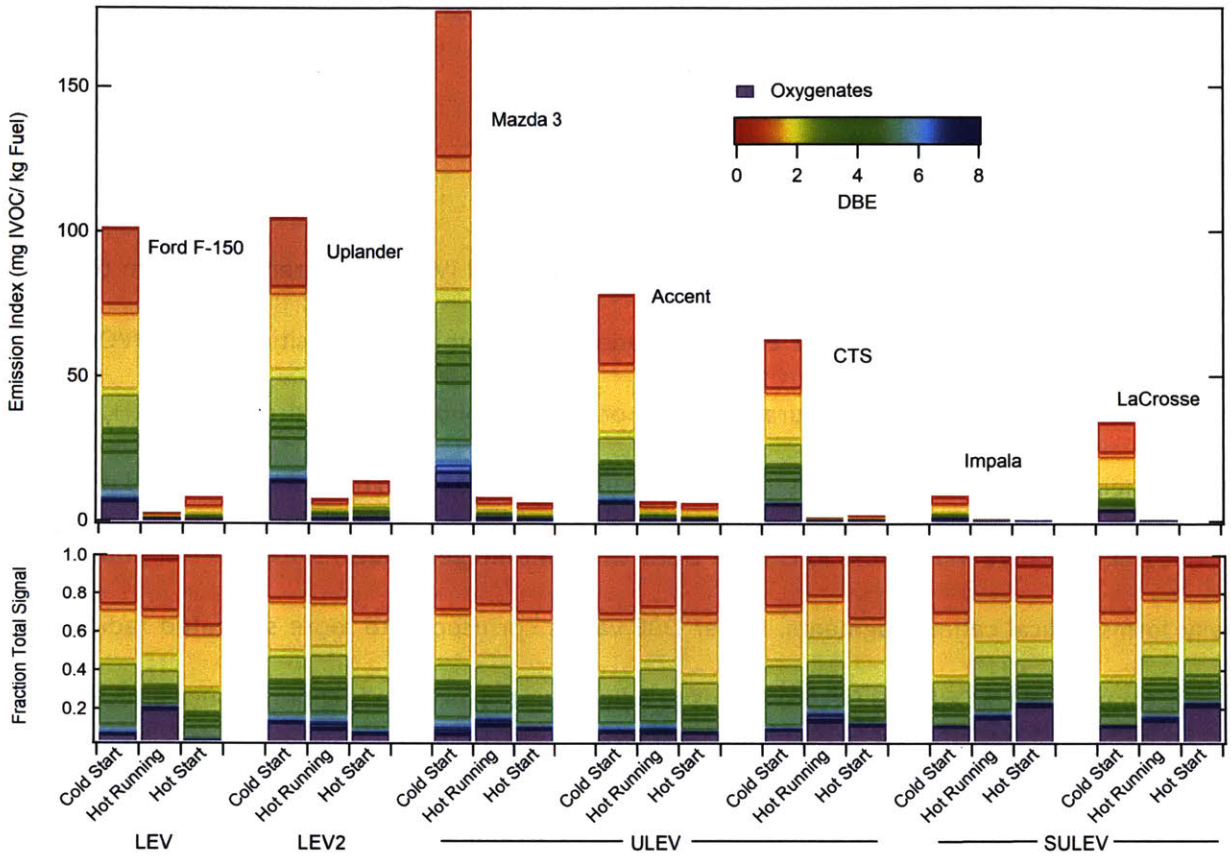

Figure 3.3. Amount and composition of IVOC emissions from various vehicles tested as a function of drive stage (cold start, hot run, and hot start). Upper panel: emission indices for each vehicle and drive stage. Colors provide information on IVOC composition, grouped by double bond equivalents of the ions in the average mass spectrum. Lower panel: fractional contribution of each ion type to total IVOC signal.

CO_2 value, corresponding to lower calculated fuel consumption. The cold-start emission indices from the SULEV vehicles are lower still (8-33 mg IVOC/kg fuel). The emissions during the hot run and hot start stages are low for all vehicles, and also generally decrease as emissions tier increases; For SULEV vehicles the hot run and hot start emissions were exceedingly low, just barely above (or in one case, below) baseline levels, with IVOC emission indices of 0.5 mg /kg fuel or lower. While in some cases (the two LEV and LEV2 vehicles studied) the hot start emissions are higher than that of the hot run stage, this is not true for all vehicles. This dominance of cold-start IVOC emissions is in contrast to the result of a previous study (*15*), which found cold-start and hot-start IVOC emissions to be roughly the same. The reason for this difference is

not clear, though it may be a function of the different set of vehicles sampled; as we show below, the present results are consistent with VOC emissions(*19*).

3.3.3 IVOC chemical composition:

Figure 3.3 also shows the chemical makeup of the emitted IVOCs, as determined from the TD-EIMS high-resolution mass spectrum for each desorption. The chemical composition of the IVOCs are described in terms of degrees of unsaturation (rings or double bonds), with hydrocarbon (C_xH_y+) ions grouped by their double bond equivalents, or DBEs (calculated using by from the number of C and H atoms in the ion: $DBE=n_c - n_H/2 + 1$). Most ions have DBEs with half-integer values, since electron ionization generally forms radical cation fragments. Lower DBE values correspond to more saturated radical ion fragments; for example, a DBE of 0.5 corresponds to fully saturated alkyl ion fragments, such as $C_3H_7^+$ and $C_4H_9^+$. Single-ring aromatic compounds have DBE values of 3.5 or higher, depending on the degree of unsaturation of the substituents on the aromatic ring. Any organic ions containing oxygen (other than CO_2^+ and CO^+), which are excluded from this analysis) are included in a separate "oxygenate" category.

The composition of the IVOC emissions remains fairly consistent across vehicle types as well as driving conditions (cold start, hot run, hot start). Mass spectra are dominated by ions with DBE values between 0.5 and 2.5, indicating aliphatic ion fragments; these make up 60-80% of the total IVOC mass. This is consistent with the composition of gasoline fuel, as well as previous studies showing that engine exhaust is dominated by alkanes and cycloalkanes (DBEs below 2)(*11*). Ions with higher DBE values (3.5-8) make up much of the remainder of the IVOCs (10-26% of the ions); these are likely compounds that include a single aromatic ring, a result that again is consistent with Gentner et al. Finally, oxygenates make up 3-20% of total IVOC mass (11). The vast majority of ions in this class only have 1 oxygen atom (CH_3O^+, $C_2H_3O^+$, $C_2H_5O^+$), and overall the IVOC O:C ratios are quite low (~0.1), a value consistent across all vehicles. These measurements are broadly consistent with earlier TD-EIMS measurements of IVOC emissions from

diesel engine exhaust, which found that alkanes and cycloalkanes make up the largest fraction of the emissions, with aromatic and oxygenated compounds accounting for a smaller fraction (10-20%) (*23*).

At the same time, the lack of observed variability in IVOC composition with drive stage contrasts with results from the previous diesel emissions study, which found dramatic changes in composition with engine load (specifically an increase in aromatic organic signal at higher loads)(*23*). Such differences may arise from the different systems being sampled: that earlier study involved a medium-duty diesel engine with no emissions control, and so emissions are likely to be quite different. Additionally, that study examined IVOC emissions at steady state, enabling the systematic examination of different engine loads. By contrast, the present study cannot resolve different engine load states, since over the 60-second sampling period, the UC involves several changes to vehicle speed (and hence engine load). Thus any changes to IVOC emissions arising from load changes will likely be averaged out in the present study, and so it is possible that the IVOCs emitted may be dependent on load, despite the relative uniformity shown in Figure 3.3.

3.3.4 Timing of IVOC emissions:

As shown in Figures 3.2 and 3.3 the vast majority of IVOCs measured by the TD-EIMS are emitted during the cold start. Here we compare TD-EIMS measurements with those from the offline measurements (in which IVOCs were collected in sorbent tubes and analyzed by GCxGC); this can provide confidence in measurements made by individual techniques, and also insight into the time dependence of IVOC emissions.

Figure 3.4 shows emissions indices from the TD-EIMS measurements plotted against those from the offline samples. The left panel uses the TD-EIMS emission indices determined from Eq. 1 (using the fuel consumption during the 60 s collection time only). The measurements are generally well-correlated, both showing the general trend of decreasing IVOC emissions with increasing emissions controls tier,

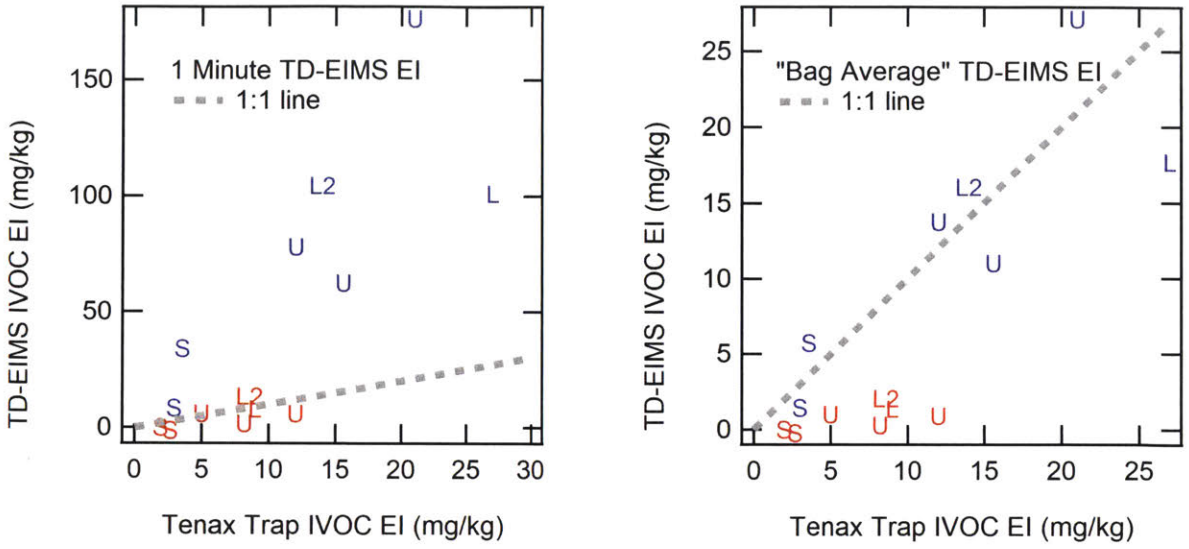

Figure 3.4 IVOC emission indices measured by the TD-EIMS vs those measured by offline GC-MS. Emission indices are labeled by emissions tier (L=LEV, L2 = LEV2, U=ULEV, S = SULEV). Red symbols represent hot start measured by the TD-EIMS vs hot start emissions measured by offline analysis and blue markers represent cold start emissions comparisons. Left panel: emission indices for 60-second TD-EIMS collections, assuming IVOC emissions continuously occur over the entire collection period. Right panel: the same emission indices except only TD-EIMS EI's are scaled by fuel burned during the whole 5-minute cold start collection period.

giving confidence in these general results. The overall emission factors for the hot-start/hot-run periods agree quite well; however, the TD-EIMS emission factors are about five times higher than those measured by the Tenax-GC measurements. This difference likely arises from two major differences between the two measurement techniques. Due to differences in sampling inlets as well as collection conditions, the "volatility window" defining which IVOCs are collected likely differ between the two techniques, so the set of IVOCs measured by each may not be exactly the same. The IVOC volatility window measured by the offline techniques is larger than the collection window of the TD-EIMS. The offline GC-MS measurements measure volatilities between n-alkane volatility bins of C_8-C_{34}, while the TD-EIMS measures between C_{10} – C_{14} (10^7 -10^5 µg/m^3). While the majority of the signal appears to be captured by both techniques, the differences in sampling volatility windows could lead to differing detected IVOC levels. More importantly, the length of the collection period of each technique also differs: the TD-EIMS collected sample for only

60 seconds, whereas the Tenax sampling occurred over the entire cold start period (300s) or the entire combined hot-run/hot-start period (1435s). Such a difference would not matter if the IVOC emissions stayed constant over the entire Tenax sampling period. However, previous work has shown that cold-start emissions of VOCs are quite transient, occurring mostly in the period immediately following ignition; this initial period is especially short for vehicles with the highest level of emissions control (*19*). It is likely that IVOCs behave similarly, in which case the measurements from TD-EIMS (which samples for the first 60s only) would suggest a higher cold-start emission factor than that of the longer-collection Tenax measurements'; this may explain the factor of 5 difference between the two techniques.

This difference in sampling times is taken into account in the right panel of figure 3.4, which shows the same comparison as in Figure 3.4(a), except it assumes that all IVOCs from the cold start are emitted within the first 60s (the TD-EIMS collection time) after ignition. The emission indices from the TD-EIMS (Eq. 1) are thus scaled by the fuel consumed over the entire 300s period (rather than the sampling period only). This decreases the TD-EIMS cold-start emission indices by a factor of ~5, so that they now align much more closely with the values from the Tenax measurements. This suggests that most IVOC emissions from these vehicles occur within the first minute after engine ignition, which is consistent with VOC emissions from similar vehicles (*19*). On the other hand, for the hot-run and hot-start cycles, the unscaled emissions (Fig. 3a) agree better than the scaled ones (Fig 3b). This suggests that, unlike cold-start emissions, such emissions (while very low) are more or less continuous, and not dominated by large transients. However, this is difficult to assess fully from the present dataset, since (1) emissions from the hot-run and hot-start cycles were collected together during sampling for offline analysis, so a comparison of these individual stages is not possible; and (2) during the hot run, only a small fraction of the highly variable drive cycle was sampled by the TD-EIMS, complicating comparisons with the longer-timescale collected samples.

3.4 Implications and Future Work:

In this work, we find that the IVOCs emitted from gasoline vehicles are relatively uniform in their overall chemical composition, primarily composed of alkanes and single-ring aromatics, regardless of the emissions control tier or stage of the drive cycle. However, the amount (emission indices) of IVOCs emitted is exceedingly dependent on both factors. IVOC emissions from all vehicles tested are far higher during the cold start than for any subsequent stage of the drive cycle. Such emissions are concentrated in the period immediately following engine turnover (first ~60 seconds after ignition), corresponding to distances of less than 0.1 miles of travel in the present tests. In fact, since the time resolution of the present measurements are limited by the collection period of the TD-EIMS, cold start emissions may occur over periods that are even shorter than the first minute after ignition. Thus, while these measurements represent some of the most highly-time resolved measurements of IVOC emissions from vehicles made to date, gaining a full description of the IVOC emissions profile upon engine ignition would require the use of still faster, more continuous measurements. This would enable an understanding of the exact factors contributing to IVOC emissions – for example, whether they are emitted only at the moment of ignition, or also during the initial driving period. Such an understanding would not only enable improved modeling of IVOCs (and hence air quality) within urban areas, but also provide insight into what changes to engines and emissions control technologies could decrease IVOC emissions still further.

Vehicles with more modern emissions controls generally emit the lowest levels of IVOCs, indicating that control technologies, originally designed to reduce VOC emissions (as well as emissions of NOx and POA), are also effective at controlling IVOC emissions. In fact, as is shown in figure 3.5, IVOC emissions from cold start events have shown a reduction of almost 80% with the new SULEV emissions tier. This however, comes after cold start emissions have remained constant from LEV through LEV2 and

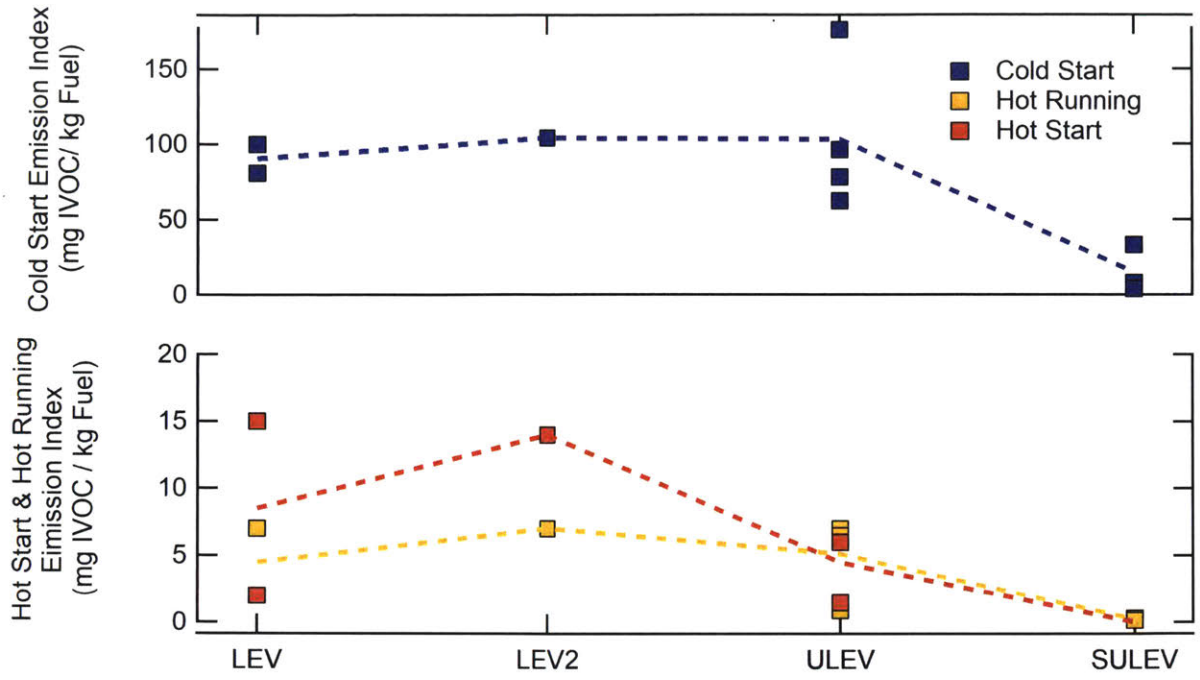

Figure 3.5. Cold start and Hot Running/ Hot Start IVOC Emission indices grouped by emissions tier. Cold start emissions stay constant from LEV to ULEV vehicles before having emissions reduced by a factor of ~80%. Hot running and hot start emissions are reduced by 100%, with emissions at or below the detection limit of the TD-EIMS.

to the ULEV emission tiers. Hot start and hot running emissions show higher variability, but also decrease significantly for the SULEV emissions tier. This profile in emissions reductions does not follow those of non-methane hydrocarbons, which show as much as an 80% reduction between the LEV and LEV 2(*12*). An order of magnitude decrease in total hydrocarbon as well as primary organic aerosol emissions has been measured between LEV and SULEV tiers (*16, 19*). This supports the notion by Robinson et al. and Gordon et al. that a disproportionate reduction in IVOC emissions has led to a smaller reduction in SOA production in urban atmospheres as both of these emissions classes have been consistently reduced as emission controls have modernized (*7, 8*). It should also be stated that while the vehicles used during this test were "in-use" vehicles from the California fleet in that they were borrowed from citizens for the purpose of these tests. This means they are likely to be representative of the California fleet than typical

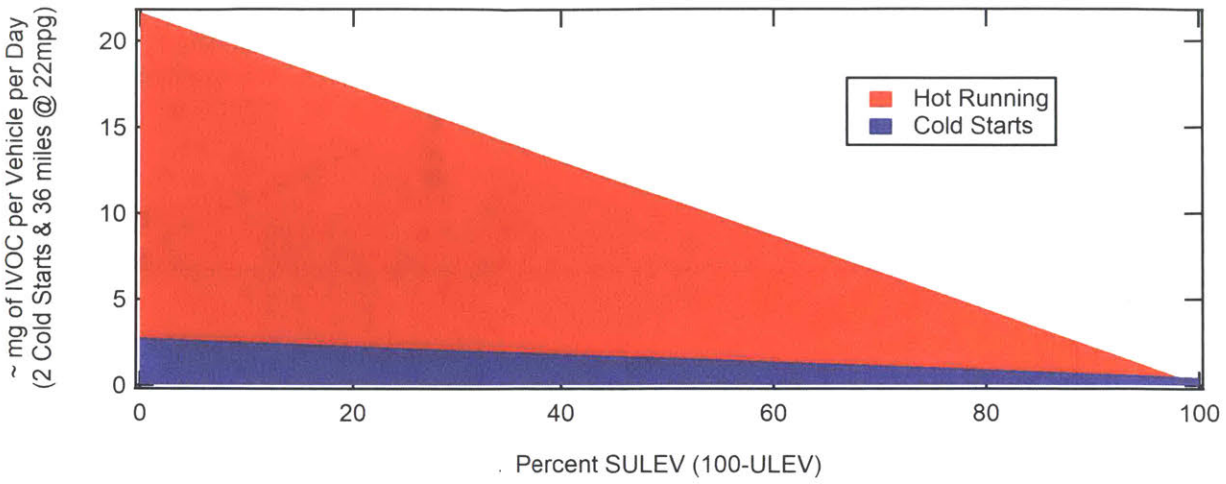

Figure 3.6 Total emitted IVOC (mg) per day based on the assumption of 2 cold start events and 36 miles driven per day @ 22 miles/gallon which is based on similar calculations presented in Drozd et. al. (*19*). The majority of the IVOC emissions by ULEV vehicles are emitted during the hot running stage, due to the large difference in fuel burned. However, as vehicle fleets become more modern, the majority of emissions will come from cold start events.

test vehicles used by auto manufacturers, but the sample size of seven vehicles is very small, and could easily be biased low or high based on which vehicles were measured.

Back-of-the-envelope calcultions for total IVOC mass emitted over the course of the day (figure 3.6) indicate that even for recent emissions control tiers, the majority of the mass is emittied during the hot running stages of engine use due to the vast difference in fuel burned between the hot running and the cold start period. However, as fleets become more modern and emissions controls effectively remove IVOC emissions during the hot running and hot start stages of engine operation, the cold start will be the dominant source of IVOCs emitted from gasoilne vehicles into the atmosphere. Combined with similar results for VOC emisisons (*19*), this work therefore suggests that modern gasoline vehicles will largely contribute to SOA during the cold start; decreasing emissions during this initial period is thus an important target for future emissions control improvements. Cold start emissions from this study also represent an "idealized" definition of a cold start as all test were performed during the summer in southern California. Emissions have been shown to be higher in cold temperatures by either increasing emissions rates or by

increasing time required for engines to come to operational temperatures , and it is not unreasonable to assume emissions of IVOCs will follow suit (*26*, *27*).

3.5 References:

1. C. A. Pope III, M. Ezzati, D. W. Dockery, Fine-particulate air pollution and life expectancy in the United States. *New England Journal of Medicine*. **360**, 376–386 (2009).

2. W. Choi *et al.*, Neighborhood-scale air quality impacts of emissions from motor vehicles and aircraft. *Atmospheric Environment*. **80**, 310–321 (2013).

3. L. Morawska, Z. Ristovski, E. R. Jayaratne, D. U. Keogh, X. Ling, Ambient nano and ultrafine particles from motor vehicle emissions: Characteristics, ambient processing and implications on human exposure. *Atmospheric Environment*. **42**, 8113–8138 (2008).

4. B. Brunekreef, S. T. Holgate, Air pollution and health. *The Lancet*. **360**, 1233–1242 (2002).

5. M. Hallquist *et al.*, The formation, properties and impact of secondary organic aerosol: current and emerging issues. *Atmospheric ...*, 5155–5236 (2009).

6. J. H. Kroll, J. H. Seinfeld, Chemistry of secondary organic aerosol: Formation and evolution of low-volatility organics in the atmosphere. *Atmospheric Environment*. **42**, 3593–3624 (2008).

7. T. D. Gordon *et al.*, Primary Gas- and Particle-Phase Emissions and Secondary Organic Aerosol Production from Gasoline and Diesel Off-Road Engines. *Environ. Sci. Technol.* **47**, 14137–14146 (2013).

8. A. L. Robinson *et al.*, Rethinking Organic Aerosols: Semivolatile Emissions and Photochemical Aging. *Science*. **315**, 1259–1262 (2007).

9. Y. Zhao *et al.*, Intermediate-Volatility Organic Compounds: A Large Source of Secondary Organic Aerosol. *Environ. Sci. Technol.* **48**, 13743–13750 (2014).

10. T. D. Gordon *et al.*, Secondary organic aerosol formation exceeds primary particulate matter emissions for light-duty gasoline vehicles. *Atmos. Chem. Phys.* **14**, 4661–4678 (2014).

11. D. R. Gentner *et al.*, Elucidating secondary organic aerosol from diesel and gasoline vehicles through detailed characterization of organic carbon emissions. *Proceedings of the National Academy of Sciences* **109**, 18318 (2012).

12. A. A. May *et al.*, Atmospheric Environment. *Atmospheric Environment*. **88**, 247–260 (2014).

13. Y. Zhao *et al.*, Intermediate Volatility Organic Compound Emissions from On-Road Diesel Vehicles: Chemical Composition, Emission Factors, and Estimated Secondary Organic Aerosol

Production. *Environ. Sci. Technol.* **49**, 11516–11526 (2015).

14. J. J. Schauer, M. J. Kleeman, G. R. Cass, B. R. T. Simoneit, Measurement of Emissions from Air Pollution Sources. 2. C 1through C 30Organic Compounds from Medium Duty Diesel Trucks. *Environ. Sci. Technol.* **33**, 1578–1587 (1999).

15. Y. Zhao *et al.*, Intermediate Volatility Organic Compound Emissions from On-Road Gasoline Vehicles and Small Off-Road Gasoline Engines. *Environ. Sci. Technol.* **50**, 4554–4563 (2016).

16. G. Saliba *et al.*, Comparison of Gasoline Direct-Injection (GDI) and Port Fuel Injection (PFI) Vehicle Emissions: Emission Certification Standards, Cold-Start, Secondary Organic Aerosol Formation Potential, and Potential Climate Impacts. **51**, 6542–6552 (2017).

17. I. Schifter, L. Díaz, R. Rodríguez, Cold-start and chemical characterization of emissions from mobile sources in Mexico. *Environmental Technology*. **31**, 1241–1253 (2010).

18. M. Weilenmann, J.-Y. Favez, R. Alvarez, Cold-start emissions of modern passenger cars at different low ambient temperatures and their evolution over vehicle legislation categories. *Atmospheric Environment*. **43**, 2419–2429 (2009).

19. G. T. Drozd, Y. Zhao, G. Saliba, B. Frodin, Time Resolved Measurements of Speciated Tailpipe Emissions from Motor Vehicles: Trends with Emission Control Technology, Cold Start Effects, and Speciation. *Environmental ...* (2016), doi:10.1021/acs.est.6b04513.

20. Y. Zhao, A. T. Lambe, R. Saleh, G. Saliba, A. L. Robinson, Secondary Organic Aerosol Production from Gasoline Vehicle Exhaust: Effects of Engine Technology, Cold Start, and Emission Certification Standard. *Environ. Sci. Technol.* **52**, 1253–1261 (2018).

21. Y. Zhao *et al.*, Reducing secondary organic aerosol formation from gasoline vehicle exhaust. *Proceedings of the National Academy of Sciences*. **114**, 6984–6989 (2017).

22. E. S. Cross *et al.*, Online measurements of the emissions of intermediate-volatility and semi-volatile organic compounds from aircraft. *Atmos. Chem. Phys.* **13**, 7845–7858 (2013).

23. E. S. Cross, A. G. Sappok, V. W. Wong, J. H. Kroll, Load-Dependent Emission Factors and Chemical Characteristics of IVOCs from a Medium-Duty Diesel Engine. *Environ. Sci. Technol.* **49**, 13483–13491 (2015).

24. J. F. Hunter *et al.*, Comprehensive characterization of atmospheric organic carbon at a forested site. *Nature Geosci.* **9**, 5155 (2017).

25. A. C. Aiken, P. F. DeCarlo, J. L. Jimenez, Elemental Analysis of Organic Species with Electron Ionization High-Resolution Mass Spectrometry. *Anal. Chem.* **79**, 8350–8358 (2007).

26. M. S. Reiter, K. M. Kockelman, The problem of cold starts: A closer look at mobile source emissions levels. *Transportation Research Part D: Transport and Environment*. **43**, 123–132 (2016).

27. A. L. Robinson, A. P. Grieshop, N. M. Donahue, S. W. Hunt, Updating the Conceptual Model for Fine Particle Mass Emissions from Combustion Systems Allen L. Robinson. *Journal of the Air & Waste Management Association*. **60**, 1204–1222 (2010).

Chapter 4

Formation and Evolution of Secondary Intermediate Volatility Organic Compounds

4.1 Introduction:

Particulate matter in the atmosphere is a central topic in environmental science due to its role in climate forcing and negative health effects (*1-3*). Organic aerosol (OA), which is a major fraction of PM globally, can be directly emitted into the atmosphere from combustion sources (primary organic aerosol) or can be photochemically produced through the oxidation of gas phase organic compounds leading to partitioning into the particulate phase (secondary organic aerosol) (*4-6*). There is a large and diverse collection of organics emitted into the atmosphere which undergo differing oxidation processes leading to countless products(*7, 8*). The chemical pathways leading to SOA production are complex and not fully understood due in part to an inability to accurately measure the intermediates between primary gas phase emissions and produced SOA (*9, 10*). Model calculations often under predict secondary organic aerosol formation in the atmosphere (*11, 12*). A better understanding of the production and evolution of SOA precursors, such as intermediate volatility organic compounds, may reduce the discrepancy between model prediction as and measured atmospheric production of SOA.

Intermediate volatility organic compounds (IVOCs) are defined as organic species with effective saturation concentrations(c^*) between 10^3 and 10^6 $\mu g/m^3$ and has been proposed as a substantial, yet unquantified source of potential secondary organic aerosol in the atmosphere(*8*). This class of compounds pose many challenges in quantification due to highly diverse chemical composition in terms of structure, properties and reactivity, all of which become more complex while undergoing atmospheric

oxidation (*10*). Primary IVOCs have been measured in anthropogenic emissions and have been shown to be a large potential source of SOA in urban areas (*13-17*). Ambient IVOCs have also been measured in urban areas as well as in forests, but little work has been done to investigate their chemical profile as they are photochemically aged in the atmosphere(*9, 10, 14*).

Environmental "smog" chambers have been used extensively to investigate organic aerosol yields and production from a large range of precursor compounds and serve as a powerful tool to understand chemical processes in the atmosphere in a controlled environment (*18-20*). Atmospheric chambers can allow for faster oxidation than in the actual atmosphere, allowing for a few days of equivalent oxidation over the course of a day. IVOCs often go unmeasured during chamber oxidation experiments. It has been suggested that they may be lost to chamber walls during the course of an experiment due to their lower volatiles (*21*).

In this study, we attempt to quantify intermediate volatility organic compounds as they evolve in the course of smog chamber oxidation experiments. The oxidation of α-pinene has been studied extensively as it is one of the most important SOA precursors emitted into the atmosphere ((*7, 22-26*)). IVOC have traditionally been measured by differences in non-methane hydrocarbons and volatile organic compounds (VOCs), online gas chromatography, or by collection on sorbent tubes followed by offline analysis(*27, 28*). However, these techniques have primarily been used to measure emissions of primary IVOCs due to difficulties measuring oxygenated species. Recent studies of secondary organic aerosol formation environmental chambers have employed a suite of new analytical techniques that leverage the information provided through high resolution mass spectrometry coupled with "soft" chemical ionization (*22, 29, 30*). These techniques exhibit sensitivity to oxygenated organic compounds and can provide molecular formulas as they do not fracture analyte molecules in the process of ionization but rather use a reagent ion which binds with analyte molecules preserving the molecule (*31*). Reagent ions provide selected sensitivity to a range of molecule, both inorganic and organic. These ions include H_3O^+, I^-, acetate,

and nitrate, which provide measurements of oxygenated organics, such as acids which are major oxidation products in the atmosphere. One drawback of CIMS is while the selectivity allows for detection of certain chemical classes, others are missed or have a different sensitivity, making bulk measurements via CIMS more difficult. H_3O^+ ionization, for example, is highly efficient at detecting oxygen containing compounds, but is effectively blind to reduced hydrocarbons, such as alkanes. While soft ionization provides a wealth of information, electron ionization is utilized in the thermal desorption – electron ionization mass spectrometer as it provides a more comprehensive detection of sampled organics. In this study we employ a novel mass-spectroscopic technique to provide a bulk, volatility separated measurement of IVOC mass and chemical composition. This technique has been applied to primary anthropogenic IVOC emissions as well as measurements of secondary IVOC in a forest, but this represents the first attempt to comprehensively monitor IVOC chemical evolution in the scope of a photochemical environmental smog chamber experiment(*10, 16, 32*).

4.2 Methods:

4.2.1 Chamber Experiments

All experiments presented in this chapter were performed in a 7.5 m^3 environmental chamber constructed out of 0.005" thick PFA Teflon (Ingeniven), which is housed in an environmental room capable of maintaining a constant temperature between 15 and 40 °C (figure 4.1). Experiments presented in this chapter were all performed at 20 C and between 0 and 5% RH, which is measured via Vaisala HMP50 RHT probe. While a lower relative humidity would facilitate colder collections by the TD-EIMS, other instruments sampling the same chamber for some of the experiments required a minimum of 2% RH. The interior walls of the environmental room are lined with two sets of 24 40-watt black lights. The lamps have a standard spectrum centered around 340 nm. The chamber is operated in "semi-batch" mode wherein the chamber maintains a consistent volume, and thus surface area to volume ratio, by balancing

a dilution flow into the chamber with the sample flow of the measurement suite sampling from the chamber. The total sample flow on the chamber during the experiments was 14 liters/ min allowing for a total chamber experiment duration of over 400 minutes.

Dilution in the chamber was monitored by injecting a non-reactive tracer, in this case hexafluorobenzene, which was measured with a proton transfer mass spectrometer. At the onset of each

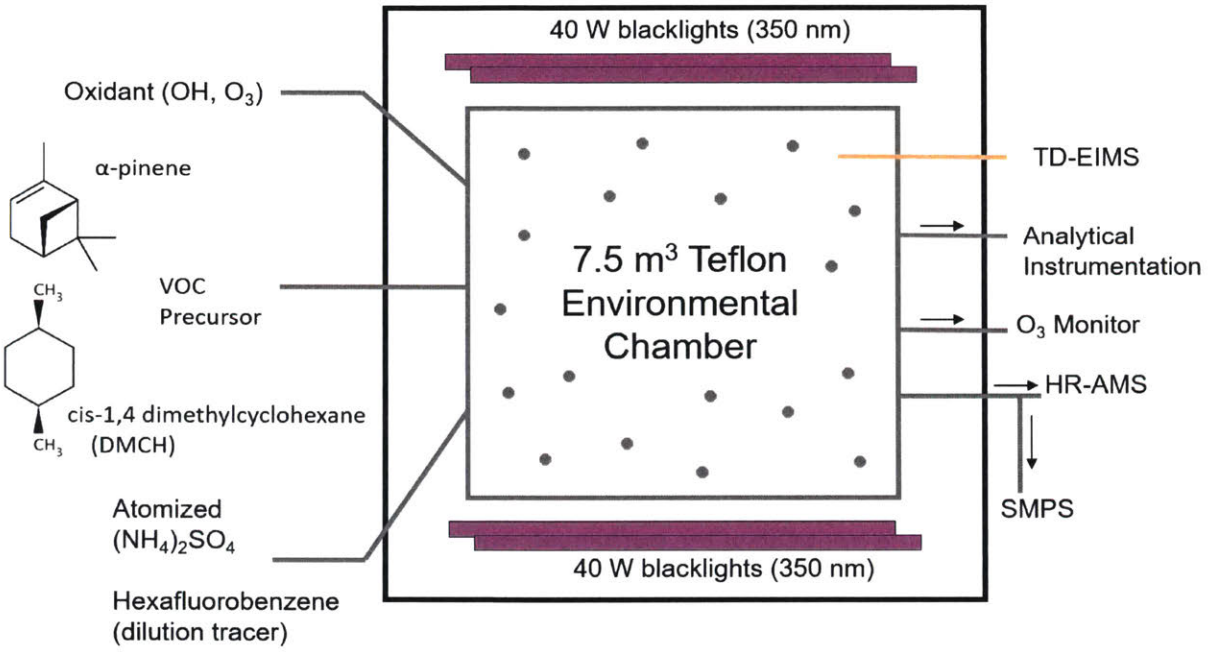

Figure 4.1 Schematic of 7.5 m^3 environmental smog chamber. Left side of figure represents compounds injected into the chamber. Right side depicts the analytical instrumentation used to characterize oxidation reactions. Oxidation is performed using ozone or by injecting HONO, which is then photolyzed using the 350 nm black lights, forming OH radicals.

experiment ammonium sulfate (reagent grade: Aldrich) seed particles were added to the chamber via TSI atomizer. These particles provide a surface for oxidation products to condense rather than the chamber walls. Oxidation in the chamber is performed with the OH radical which is introduced via photolysis of HONO by the black lights lining the chamber walls. Total OH concentrations provide a total equivalent atmospheric oxidation of approximately 14 hours. Also presented in this chapter are data from a chamber experiment taken during a previous intensive experiment period with new calibration and data processing techniques applied to the older data set. Hydrocarbon precursors utilized include α-pinene and 1,4-cis

dimethylcyclohexane (DMCH). These compounds were chosen because they demonstrate different chemical characteristics and represent differing sources including biogenic (α-pinene) and anthropogenic (DMCH). Precursor hydrocarbons are added to the chamber via syringe injection into a flow of clean air heated to 50 C to ensure all the precursor is transferred into the chamber.

4.2.2 IVOC Measurements

IVOCs are measured using the valve less-injection version of the TD-EIMS as described previously (Section 2.3). Due to the low relative humidity of the chamber, collections were taken at -25 C allowing for quantification organic compounds with c* values between 10^7 and 10^4 $\mu g/m^3$, which correlate with alkane equivalents of n-decane through n-eicosane. The TD-EIMS pre-concentrated the IVOC sample for 2 minutes to ensure sufficient mass was collected. The TD-EIMS sampled through a 1/8" OD PFA Teflon line which extruded approximately 5 cm into the chamber from the wall to minimize the effect of the chamber wall on the sampled IVOC concentration. The transfer line was heated to ~100 °C to ensure complete transfer of IVOC to the front end of the instrument, which was maintained at 200 °C.

Elemental composition of IVOCs is calculated using the method descried by Aiken et al. with no correction for fragmentation arising from electron ionization(*33*). Signal associated with the precursor hydrocarbons are removed by scaling the desorption profile of a collection of pure precursor, prior to the commencement of oxidation. Measurements by a PTR-MS also measuring these experiments was used to accurately remove the signal associated from precursors from the TD-EIMS desorptions. A contamination was also visible in the TD-EIMS desorptions, either originating from the inlet or chamber. This contamination had a chemical signature associated with siloxanes (with a series of mass spectral peaks starting at m/z = 280) and desorbed around 100 °C (figure 4.2). Removing these peaks was essential to account for the background instrument signal and could not be simply subtracted due to decay in contamination signal over the course of the experiment. To remove these peaks, a mass spectral

signature was created matching the desorption profile of the contamination peak. This profile was scaled by the contamination's decay profile then subtracted from each desorption throughout the experiment, allowing for the final IVOC loadings to be calculated accurately.

4.3 Results & Discussion

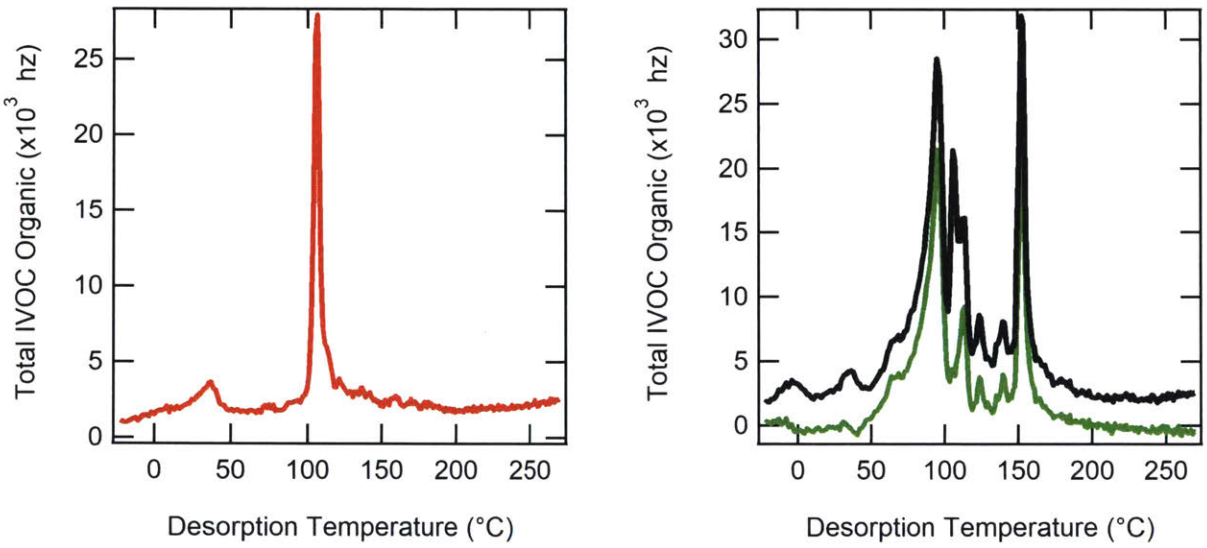

Figure 4.2. Left: Background desorption prior to chamber experiment showing contamination peak desorbing at approximately 100 C. Right: Desorption of IVOC during α-pinene chamber oxidation experiment showing raw data including background and contamination (black) as well as corrected desorption profile (green)

4.3.1 IVOC Chamber Profile

Total IVOC concentrations were measured during the oxidation of α-pinene with OH and O_3 as well as the oxidation of cis-1,4 dimethylcyclehexane by OH. The α-pinene plus ozone experiment was performed previously using different chamber conditions, specifically lower relative humidity and higher oxidation rates combined with higher precursor concentrations in the chamber. No contamination was detected during these experiments and therefore did not need to be corrected. Figure 4.3(a) shows the

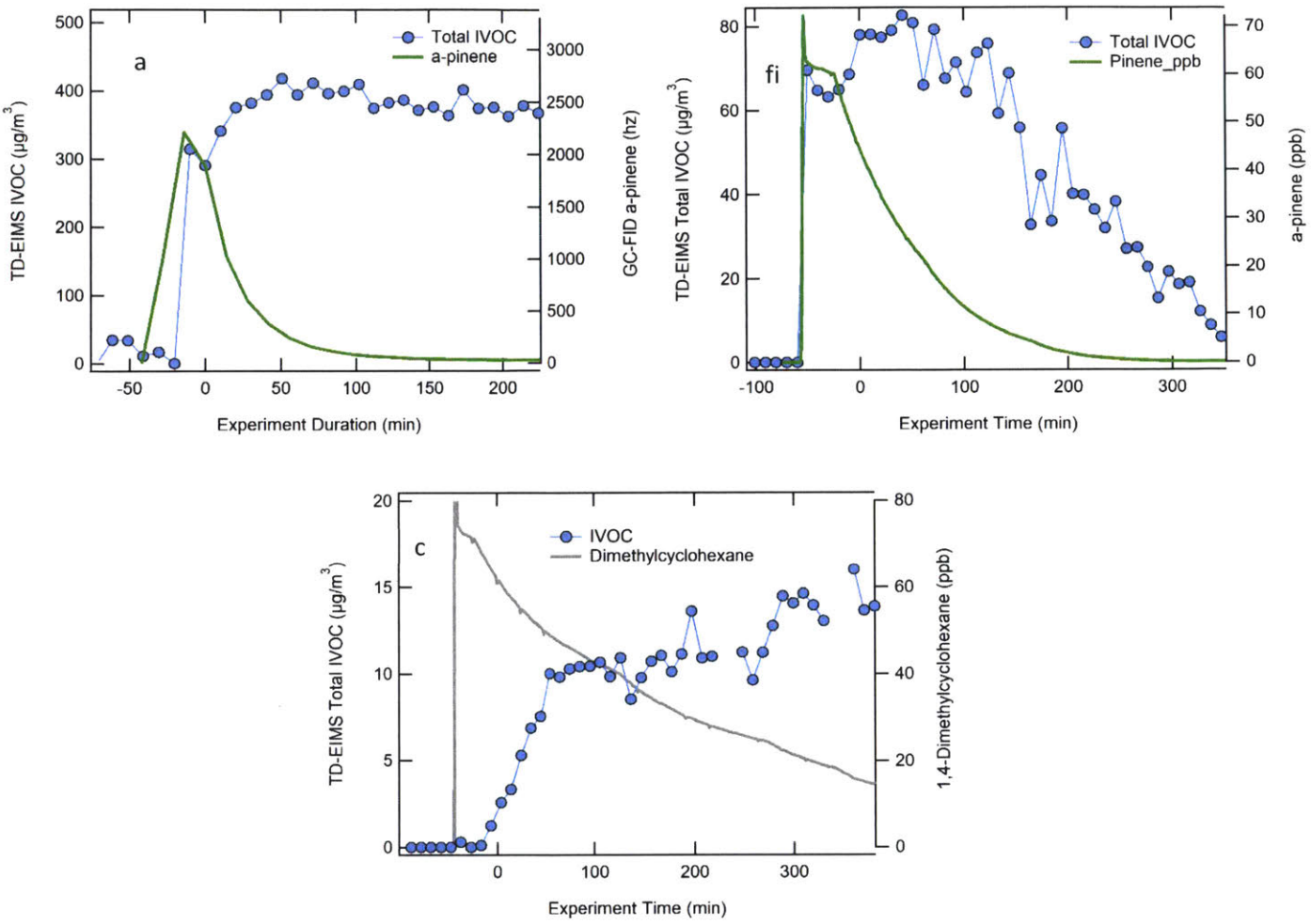

Figure 4.3 Time series of total IVOC mass measured by the TD-EIMS and time series of precursor compound. Precursors were measured by PTR which provides ppb concentrations in the chamber (α-pinene and DMCH + OH) or by GC-FID (α-pinene + O3) which was not quantifiable. Top Left: reaction of α-pinene with OH. Top Right: Reaction of α-pinene with o-zone. Bottom: reaction of cis-1,4-dimthylcyclohexane with OH

profile of total IVOC signal as well as signal associated with the precursor hydrocarbon as measured by other instrumentation sampling from the chamber. The blue trace, which contains both precursor hydrocarbons as well as oxidation products peaks just before addition of oxidant, which reacts away the precursor after approximately 90 minutes. Oxidation products grow in rapidly with the addition of oxidant and, once the data has been adjusted for dilution in the chamber, the products come to steady state. This suggests that there is no major wall loss of IVOC on the timescale detectable by the TD-EIMS as has been

reported by other measurement techniques measuring similar chamber systems (*21*). This profile is expected for the oxidation of α-pinene by ozone in this context as there is one major oxidation pathway in which ozone reacts with the double bond in α-pinene. Once one of the reactants, in this case α-pinene, reacts away, the chemistry in the chamber for the most part stops, which supports the IVOC profile seen where the IVOCs grow in and maintain a constant concentration.

Figure 4.3(b) shows the total IVOC as well as oxidation precursors for the α-pinene plus OH reaction. Unlike the reaction of α-pinene with O_3, IVOC concentrations decay away instead of coming to a stable concentration in the chamber. There are a few possible reaction pathways leading to the decay of the IVOC in this case. The first is that oxidation of IVOCs in the gas phase continue to reduce in vapor pressure driving then into the condensed particulate phase, which the TD-EIMS may not see. Also, instead of simply functionalizing and partitioning into the particulate phase, secondary IVOCs could fragment, producing products with much higher volatilities, which the TD-EIMS will be blind to due to higher volatility gases passing through the sample loop rather than being collected(*4*, *26*). It is also possible that oxidation products may get so oxidized that they are incapable of making it through the heated inlet of the instrument, either condensing to surface walls or thermally dissociating.

The chamber oxidation of DMCH by OH has an IVOC profile similar to that of α-pinene oxidation via ozone. Figure 4.3(c) shows IVOC concentrations that grow in once lights are turned on. This is due to DMCH having too high a saturation vapor pressure to effectively be trapped by the TD-EIMS at -25 °C. DMCH produces much less IVOC compared to α-pinene, totaling only 8-12 $\mu g/m^3$ and shows a different concentration profile. The IVOC concentration continues to grow, from a concentration of 8 $\mu g/m^3$ to as much as 12 $\mu g/m^3$ once lights are turned on. This growth in IVOC could be due to a re-volatilization of organics reacting on the surfaces of particles and undergoing fragmentation leading to higher volatility gas phase products. The grown in IVOC mass could also be from higher volatility organic species, such as VOCs, lowering in vapor pressure and producing secondary IVOCs as 2nd or later generation oxidation

products. The growth could also be due to slow reaction kinetics as the decay of DMCH (figure 4.2(c)) is much slower than either α-pinene reaction.

4.3.2 Volatility Resolved IVOC

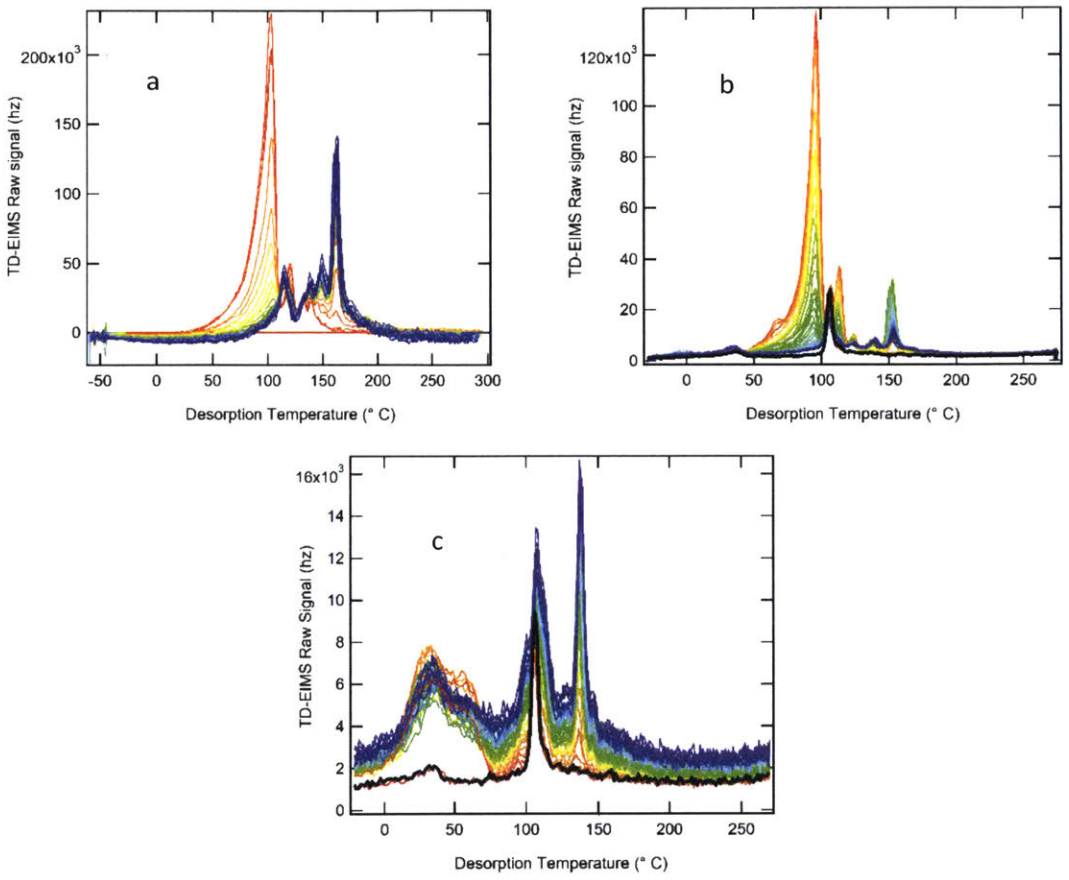

Figure 4.4. Desorption profiles of chamber experiments of α-pinene with OH (top left), α-pinene with OH (top right) and DMCH with OH (bottom). The color scale represents the progression during the experiment where red traces represent the beginning of the experiment and progress to purple traces which represent the end of the experiment. Black traces (top left and bottom right) are background desorptions showing the contaminant which had to be removed from data.

Because of the high time resolution of the ToF mass spectrometer, the TD-EIMS is capable of separating signal in desorptions by desorption temperature, providing for time-resolved information about the evolving volatility of the reaction mixture. Figure 4.4 shows the desorption profile for the three chamber experiments plotted versus desorption temperature (°C). The color bar shows the progression

of the experiment in time, progressing from the beginning of the experiment in red to the end in blue. Black traces in panels (b) and (c) show the contamination, which required removal. This trace is not visible in the reaction of α-pinene with O_3 because there was no contamination at the time of that experiment (figure 4.4a). A clear shift in volatility is visible in the collected IVOC for all precursors. As the experiments proceed, oxidation products grow in at higher temperatures, indicating lower effective saturation vapor pressures. Figure 4.4(a) shows desorptions from the oxidation of α-pinene with O_3. Two peaks desorbing right at 100 °C show the decay of α-pinene. There are two peaks for α-pinene due to a polymer product that arises from heating α-pinene and is likely formed in the inlet of the instrument (*34*). Oxidation products show a range of volatilities, desorbing from 100 °C to 150 °C, suggesting multiple products with varying sizes. The desorption profiles for the α-pinene reaction with OH (figure 4.4(b) has a clear peak associated with the precursor that starts with a high concentration and decays down to the baseline. Oxidation products are much less substantial in this figure when compared to the reaction of ozone with α-pinene. This could be due to the experiment conditions, such as precursor loadings or total oxidant concentrations but most likely is due to actual differences in the reaction pathways in the α-pinene + OH reaction as the ratios of product to α-pinene are different between the two oxidants. This suggests that the oxidation products formed from the oxidation of α-pinene with OH are either in the particle phase or highly volatile and thus outside of the volatility window of the TD-EIMS.

Figure 4.4(c) shows the desorption profiles for the reaction of DMCH with OH. As opposed to either of the reactions of α-pinene, the oxidation products make up the majority of the signal in the desorptions resulting from the oxidation of DMCH with OH. Unlike the reaction between α-pinene and OH, the contamination peak appears to be squarely in the middle of a grouping of oxidation products seeing as the profile of the contamination is to decay to about half its initial value throughout the course of an experiment. There are two main volatilities of oxidation products visible in the desorptions, the first centered around 105 C while the second has a lower volatility, desorbing around 140 C.

A convenient way to discuss the evolving volatility distribution of mixtures is to bin them by saturation vapor pressure (c*). Figure 4.5 shows the total mass of oxidation products binned by saturation

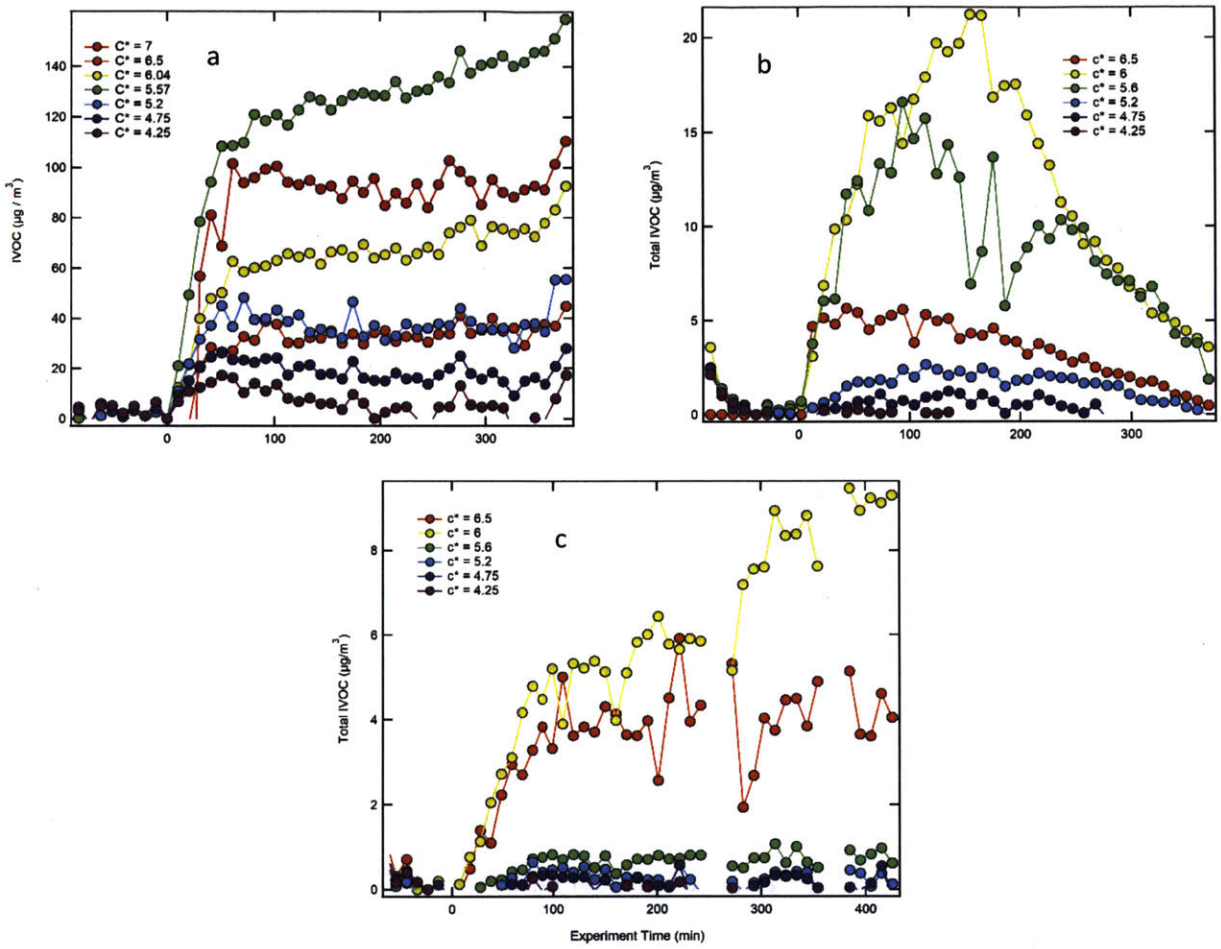

Figure 4.5 Evolution of secondary IVOCs during "smog" chamber oxidation experiments separated by volatility. Panel (a) shows the production of IVOCs from the oxidation of α-pinene with ozone. IVOC concentrations grow in and stabilize over the course of the experiment. Panel (b) shows the reaction of α-pinene with OH which exhibits a growth followed by a decay of all volatility bins. Panel (c) shows the oxidation DMCH by OH where IVOCs show a sharp growth right at the beginning of the experiment followed by a slow growth in total IVOC concentrations.

vapor pressure for the three chamber experiments. The overall pattern of the IVOC oxidation products follows the total mass of oxidation precursors depicted in figure 4.3. Figure 4.5(a) shows the growth of IVOCs during the reaction of α-pinene with O_3. In this experiment IVOCs with a log(c*) of 5.5 make up the majority of the mass followed by the most volatile bin (log(c*) = 7). The different volatility bins appear to have different concentration profiles. The bins with saturation vapor pressures of log(c*) = 5.5 and 6

appear to grow in slowly throughout the experiment, while the lower volatility bins (log(c*) <5) appear to slowly decay away. At the same time the highest volatility oxidation products (log(c*) = 7) maintains a constant concentration. The loss of low volatility IVOCs throughout the experiment is likely due to partitioning of gas phase organics into the condensed phase. However, the growth of the middle volatility bins must come from the production of IVOCs during the experiment. The precursor decay (shown in figure 5.2(a)) shows that all α-pinene has reacted away after two hours, meaning that production of IVOCs either comes from the evaporation of particulate phase organics, or the oxidation of VOCs to lower volatiles.

The oxidation of α-pinene with OH shows a very different pathway. The majority of the mass comes in the volatility bins associated with log(c*) values of 6.5 and 6. IVOCs rapidly grow in once the lights are turned on, and then decay. This shape is a clear contrast with the reaction of α-pinene with O_3 where the IVOC concentrations stabilize. The highest volatility bin (log(c*) = 6.5) shows a different profile, that grows in and slowly decays away throughout the course of the experiment. Lower volatility IVOCs, log(c*) = 5.2, show a slow growth followed by a slow decay. This could be a sign that the higher volatility IVOCs are passing through this bin as they partition to the particulate phase. IVOCs could also fragment while undergoing oxidation, leading to higher volatility products that are too volatile for the TD-EIMS to measure. These could also be other oxidation products that do not react away as slowly. It is clear in this experiment that chemistry continues throughout the experiment as the IVOCs of all volatility bins effectively react away.

Figure 4.5(c) shows the growth of IVOCs from the reaction of cis-1,4 dimethylcyclohexane by OH, which exhibits a very different profile from either reaction of α-pinene. Both the log(c*) bins of 6.5 and 6 grown in rapidly and then the log(c*) = 6 bin continues to grow while the log(c*) = 6.5 bin maintains a stable concentration. In this case, all IVOCs are produced by higher volatility organics decreasing in volatility as they oxidize because the all the starting materials were too volatile to be quantified by the

TD-EIMS. The oxidation of DMCH is much slower than α-pinene as evidenced by its significantly slower decay shown in figure 4.5(c). The slow growth of IVOCs over the experiment could simply be due to the oxidation of precursor hydrocarbon but could also be due to the production of secondary oxidation products.

4.3.3 Comparison with Other Measurement Techniques:

The final dimension of information that the TD-EIMS provides (in addition to IVOC mass and volatility) is information on chemical composition. Each data point collected contains a high resolution EI mass spectrum, which provides chemical information. While the TD-EIMS does not resolve individual compounds, it does provide elemental composition of the collected IVOC, which can be used to calculate the average carbon oxidation state ($\overline{OS_C}$). This is calculated using $\overline{OS_C}$ = 2* O:C – H:C, where O:C and H:C are the atomic elemental ratios of oxygen to carbon and hydrogen to carbon, respectively. $\overline{OS_C}$ is one of the properties of the two dimensional volatility basis set, which a useful way of visualizing organic compounds, especially as the evolve in the atmosphere. The 2D-VBS consists of oxidation state of compounds plotted versus their saturation vapor pressure (log(c*)) (*10*, *35*). Volatility separated IVOCs can be plotted in this space as there is an average volatility and $\overline{OS_C}$ for each bin (*10*). Similar experiments to comprehensively measure the chemical evolution of carbon from precursor to oxidation in the environmental chamber at MIT have been attempted previously (*36*). Shown in figure 4.6 are 2D-VBS figures representing the organic carbon measured in the chamber by a range of different techniques including both particulate and gas phase compounds after 1 hour of equivalent atmospheric oxidation (top) and 4 hours of equivalent atmospheric oxidation (bottom) (*36*). This figure includes measurements from and Aerosol Mass Spectrometer (particulate phase measurements), PTR-MS and I^- CIMS (gas phase organic measurements), as well as a TILDAS carbon monoxide measurement. The TD-EIMS data from the α-pinene + OH experiment has been overlaid onto these plots, since the TD-EIMS experiments were

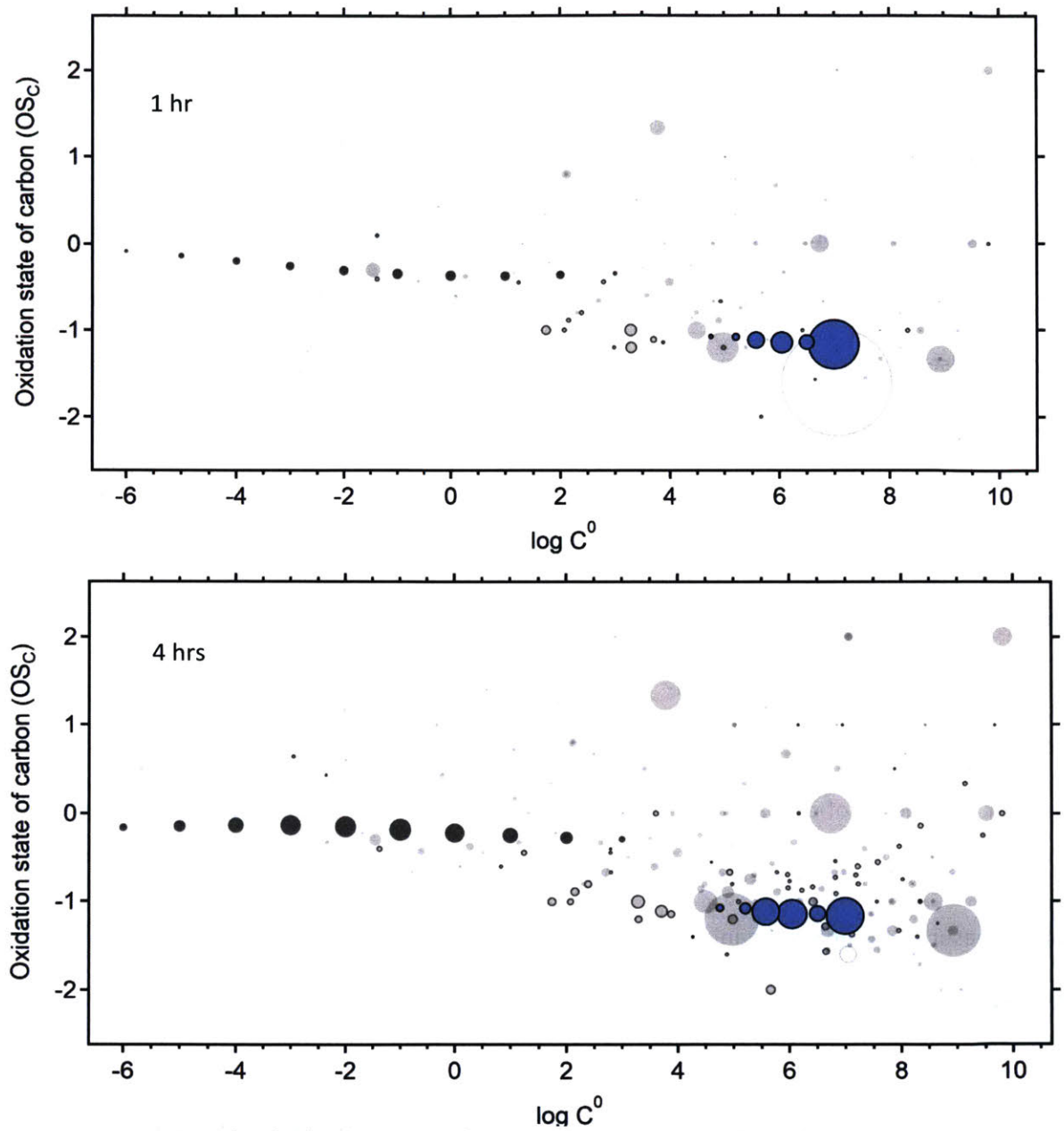

Figure 4.6. 2-Dimensional volatility basis sets showing all measured carbon during α-pinene + OH oxidation experiment from Isaacman-Vanwertz et al. (36) after 1 hour of oxidation (top) and 4 hours of oxidation (bottom)1. Markers are sized by relative concentration. Light grey markers are speciated gas phase compounds measured, while dark grey markers are particulate phase organics binned by volatility. Blue circles represent TD-EIMS data at these phases of oxidation.

carried out under similar conditions (in terms of NOx, oxidation timescale, and initial concentration of α-pinene). The largest concentration measured by the TD-EIMS after 1 hour of oxidation is associated with α-pinene, which was the precursor molecule and has not yet been fully reacted away. The signal associated with the precursor has decayed after 4 hours of oxidation leading to the growth of lower

volatility bins. The OSC for each of these bins shows a slight increase as it moves from higher volatility to lower volatility (right to left on the 2D-VBS), which is expected as the lower volatility oxidation products are expected to functionalize as they are oxidized in the chamber (*18*, *35*).

Total IVOC concentrations measured in the OH oxidation of α-pinene peak at ~35 μg/m^3. This represents a rather large fraction of the total mass. At the same point of the experiment, organic aerosol only comprises 25 μg/m^3. Figure 4.7 shows the composition of all measured carbon during an α-pinene experiment discussed in Issacman-VanWertz et al. The oxidation experiment presented in this figure was performed in the same environmental chamber, under similar conditions. The primary difference is total oxidation. The experiments presented in Isaacman-VanWertz et al encompass 24 hours of equivalent atmospheric oxidation, whereas the measurements discussed in this thesis only measure ~14 hours of equivalent atmospheric oxidation(*36*). The peak of IVOC measured by the TD-EIMS in recent experiments occurs at about 100 minutes of reaction time in this experiment. At this point, the majority of mass in the chamber is made up of oxidized VOCs, such as acetone and acetic acid, and is measured by the PTR-MS and iodide CIMS. The profile of secondary IVOCs during this experiment (figure 4.4(b)) does not track any of the measured gas phase organics. With the exception of pinonaldehyde, the majority of the gas phase compounds measured appear to grow in and stabilize in concentration. The IVOCs measured by the TD-EIMS have mostly reacted away by the end of the experiment, which corresponds to approximately 350 minutes of reaction time in figure 4.6. Figure 4.6(b) shows the mass profile of IVOCs measured by the TD-EIMS as well as compounds measured by the PTR-MS and Iodide CIMS which fall into the same volatility bins.

Figure 4.6 shows time series of carbon measured during the α-pinene oxidation experiment discussed in Isaacman-Vanwertz et al. While there is likely overlap in the measurements which is consistent with the 2D VBS figures in figure 4.6, by the end of the experiment all the carbon from the α-pinene precursor has been accounted for. However, there is missing carbon during the first 5 hours of

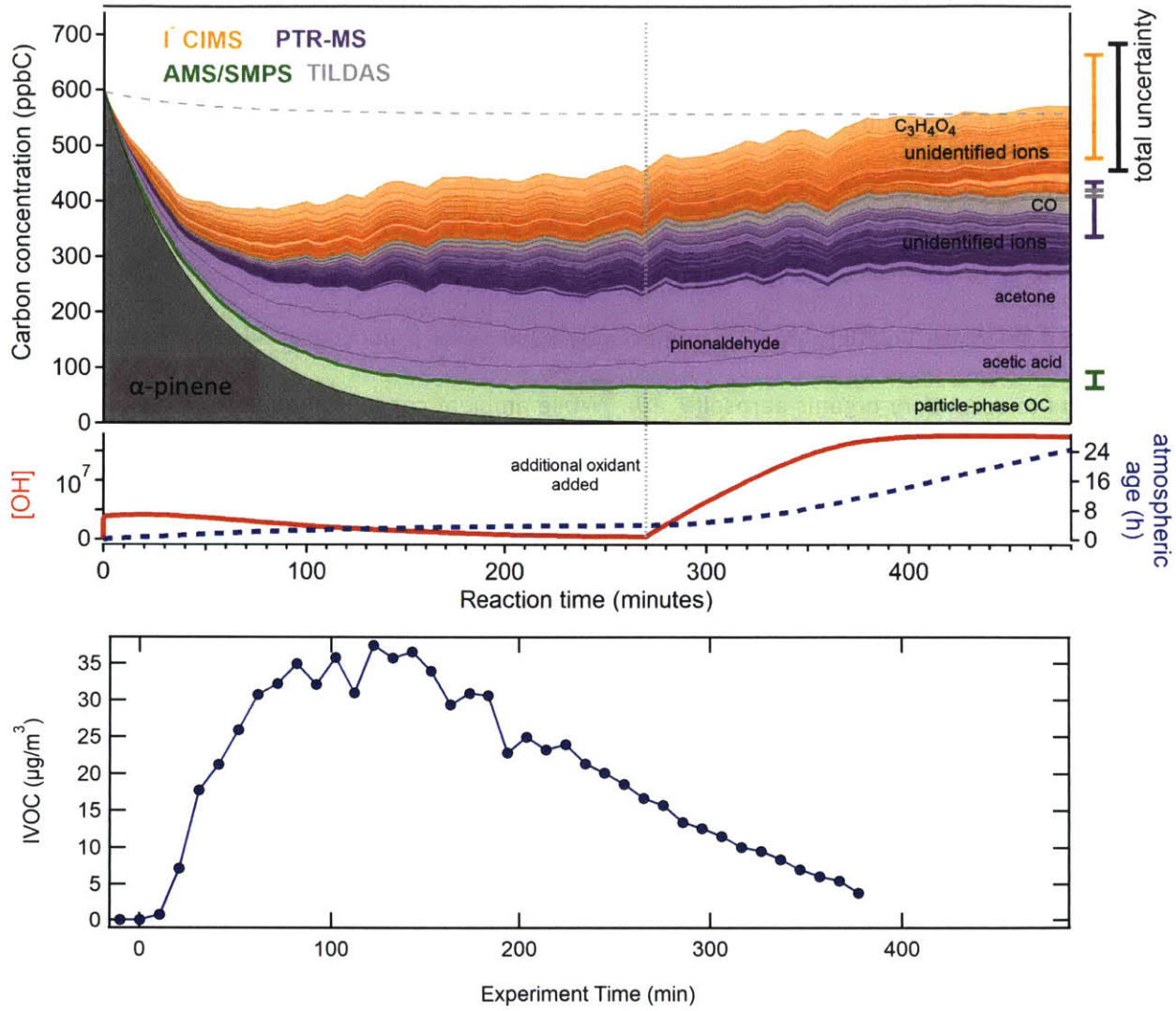

Figure 4.7 Top: Chemical evolution of measured carbon during an α-pinene oxidation by OH presented in Isaacman-VanWertz et al (*36*). Both gas and particle phase are characterized in this figure and all carbon has been accounted for by the end of the experiment. Bottom: IVOC concentrations measured by the TD-EIMS of α-pinene oxidation by OH. The profile of this measurement mimics the profile of the "missing" carbon during the Isaacman-VanWertz experiment.

the experiment (~14 hours of atmospheric oxidation). This "missing carbon" is likely early oxidation products and may not be easily measured by the techniques used during this experiment due to instrument sensitivity or could also be lost to the walls of the chamber quickly (*36*). While it is likely that the TD-EIMS does not measure exactly the missing fraction of carbon, the concentration profile of the oxidation products matches the gap in carbon closely and of any of the other quantified species, it is the

only measurement that grows in, and then slowly reacts away to zero. While the numbers do not align, the profile of the TD-EIMS measurements suggest that it is capable of quantifying some fraction of the carbon in the missing early oxidation products.

4.4 Conclusions:

Intermediate volatility organic compounds have been proposed as likely intermediates and precursors to secondary organic aerosol(*9*, *10*). While ambient concentrations or primary emissions of IVOCs have been studied, few studies have focused on measuring IVOC concentrations as they evolve in the atmosphere from emissions through intermediates to secondary organic aerosol. In this study the profile of IVOCs was examined in the context of environmental chamber experiments of α-pinene and 1,4-dimethylcyclohexane undergoing atmospheric oxidation. IVOCs were measured by a novel technique, the Thermal Desorption- Electron Ionization Mass Spectrometer (TD-EIMS), which provides a highly time resolved bulk measurement of volatility separated IVOC mass concentration and chemical composition. Three different IVOC evolution profiles were seen for α-pinene reacting with OH and O3 as well as DMCH reacting with OH. IVOC concentrations all grew in upon the commencement of oxidation in each experiment, but proceeded to decay back to zero for the reaction of α-pinene with OH, stay at constant concentration in the reaction of α-pinene with O3, and continue to grow in concentration in the case of DMCH reacting with OH. The TD-EIMS also provides chemical and volatility information for IVOCs and showed an increase in oxidation state $\overline{(OS_C)}$ in the oxidation products which also showed a lower volatility than the precursor molecule. The IVOC concentrations measured by the TD-EIMS may detect the gap of "missing carbon" inferred previously (*35*), suggesting that the "missing" carbon is likely in the form of IVOCs. Additional work still needs to be performed to understand how much overlap in compounds measured exists between the TD-EIMS and the other measurement techniques used during that study. This study represents the first time the TD-EIMS measured secondary IVOC in the context of atmospheric

chamber oxidation experiments. Analysis suggests that the TD-EIMS measures a large, potentially previously unmeasured fraction of carbon in these experiments.

4.5 References:

1. *Working Group I Contribution to the Fifth Assessment Report of the Intergovernmental Panel on Climate Change, Summary for Policymakers, IPCC.*

2. C. A. Pope III, M. Ezzati, D. W. Dockery, Fine-particulate air pollution and life expectancy in the United States. *New England Journal of Medicine*. **360**, 376–386 (2009).

3. D. W. Dockery, C. A. Pope, X. Xu, An association between air pollution and mortality in six US cities. *Mass Medical Soc* (1993).

4. N. M. Donahue *et al.*, Aging of biogenic secondary organic aerosol via gas-phase OH radical reactions. *Proceedings of the National Academy of Sciences*. **109**, 13503–13508 (2012).

5. N. M. Donahue, A. L. Robinson, E. R. Trump, I. Riipinen, J. H. Kroll, in *Atmospheric and Aerosol Chemistry* (Springer Berlin Heidelberg, Berlin, Heidelberg, 2012), vol. 339 of *Topics in Current Chemistry*, pp. 97–143.

6. C. R. Hoyle, G. Myhre, T. K. Berntsen, I. S. A. Isaksen, Anthropogenic influence on SOA and the resulting radiative forcing. *Atmos. Chem. Phys. Discuss.* **8**, 18911–18936 (2008).

7. A. H. Goldstein, I. E. Galbally, Known and unexplored organic constituents in the earth's atmosphere. *Environ. Sci. Technol.* **41**, 1514–1521 (2007).

8. A. L. Robinson *et al.*, Rethinking Organic Aerosols: Semivolatile Emissions and Photochemical Aging. *Science*. **315**, 1259–1262 (2007).

9. B. B. Palm *et al.*, In situ secondary organic aerosol formation from ambient pine forest air using an oxidation flow reactor. *Atmos. Chem. Phys.* **16**, 2943–2970 (2016).

10. J. F. Hunter *et al.*, Comprehensive characterization of atmospheric organic carbon at a forested site. *Nature Geosci.* **9**, 5155 (2017).

11. C. L. Heald *et al.*, *Geophys. Res. Lett.*, in press, doi:10.1029/2005GL023831.

12. R. Volkamer *et al.*, Secondary organic aerosol formation from anthropogenic air pollution: Rapid and higher than expected. *Geophys. Res. Lett.* **33**, 4407 (2006).

13. Y. Zhao *et al.*, Intermediate Volatility Organic Compound Emissions from On-Road Gasoline Vehicles and Small Off-Road Gasoline Engines. *Environ. Sci. Technol.* **50**, 4554–4563 (2016).

14. Y. Zhao *et al.*, Intermediate-Volatility Organic Compounds: A Large Source of Secondary Organic Aerosol. *Environ. Sci. Technol.* **48**, 13743–13750 (2014).

15. Y. Zhao, A. T. Lambe, R. Saleh, G. Saliba, A. L. Robinson, Secondary Organic Aerosol Production from Gasoline Vehicle Exhaust: Effects of Engine Technology, Cold Start, and Emission Certification Standard. *Environ. Sci. Technol.* **52**, 1253–1261 (2018).

16. E. S. Cross, A. G. Sappok, V. W. Wong, J. H. Kroll, Load-Dependent Emission Factors and Chemical Characteristics of IVOCs from a Medium-Duty Diesel Engine. *Environ. Sci. Technol.* **49**, 13483–13491 (2015).

17. E. S. Cross *et al.*, Soot Particle Studies—Instrument Inter-Comparison—Project Overview. *Aerosol Science and Technology*. **44**, 592–611 (2010).

18. J. H. Kroll *et al.*, Chamber studies of secondary organic aerosol growth by reactive uptake of simple carbonyl compounds. *J. Geophys. Res.* **110**, D23207 (2005).

19. A. J. Carrasquillo, J. F. Hunter, K. E. Daumit, J. H. Kroll, Secondary Organic Aerosol Formation via the Isolation of Individual Reactive Intermediates: Role of Alkoxy Radical Structure. *J. Phys. Chem. A*. **118**, 8807–8816 (2014).

20. J. F. Hunter, A. J. Carrasquillo, K. E. Daumit, J. H. Kroll, Secondary Organic Aerosol Formation from Acyclic, Monocyclic, and Polycyclic Alkanes. *Environ. Sci. Technol.* **48**, 10227–10234 (2014).

21. J. E. Krechmer, D. Pagonis, P. J. Ziemann, J. L. Jimenez, Quantification of Gas-Wall Partitioning in Teflon Environmental Chambers Using Rapid Bursts of Low-Volatility Oxidized Species Generated in Situ. *Environ. Sci. Technol.* **50**, 5757–5765 (2016).

22. P. S. Chhabra *et al.*, Application of high-resolution time-of-flight chemical ionization mass spectrometry measurements to estimate volatility distributions of α-pinene and naphthalene oxidation products. *Atmos. Meas. Tech.* **8**, 1–18 (2015).

23. J. E. Shilling *et al.*, Loading-dependent elemental composition of α-pinene SOA particles. *Atmos. Chem. Phys.* **9**, 771–782 (2009).

24. R. K. Pathak, C. O. Stanier, N. M. Donahue, S. N. Pandis, Ozonolysis of α-pinene at atmospherically relevant concentrations: Temperature dependence of aerosol mass fractions (yields). *J. Geophys. Res.* **112**, 1052 (2007).

25. F. D. Lopez-Hilfiker *et al.*, Phase partitioning and volatility of secondary organic aerosol components formed from α-pinene ozonolysis and OH oxidation: the importance of accretion products and other low volatility compounds. *Atmos. Chem. Phys.* **15**, 7765–7776 (2015).

26. K. M. Henry, T. Lohaus, N. M. Donahue, Organic Aerosol Yields from α-Pinene Oxidation: Bridging the Gap between First-Generation Yields and Aging Chemistry. *Environ. Sci. Technol.*, 121031135342008 (2012).

27. Y. Zhao *et al.*, Development of an In Situ Thermal Desorption Gas Chromatography Instrument for Quantifying Atmospheric Semi-Volatile Organic Compounds. *Aerosol Science and Technology*. **47**, 258–266 (2013).

28. D. R. Gentner *et al.*, Chemical Composition of Gas-Phase Organic Carbon Emissions from Motor

Vehicles and Implications for Ozone Production. *Environ. Sci. Technol.* **47**, 11837–11848 (2013).

29. F. D. Lopez-Hilfiker *et al.*, A novel method for online analysis of gas and particle composition: description and evaluation of a Filter Inlet for Gases and AEROsols (FIGAERO). *Atmos. Meas. Tech.* **7**, 983–1001 (2014).

30. D. Aljawhary, R. Zhao, A. K. Y. Lee, C. Wang, J. P. D. Abbatt, Kinetics, Mechanism, and Secondary Organic Aerosol Yield of Aqueous Phase Photo-oxidation of α-Pinene Oxidation Products. *J. Phys. Chem. A.* **120**, 1395–1407 (2016).

31. W. Lindinger, A. Jordan, Proton-transfer-reaction mass spectrometry (PTR–MS): on-line monitoring of volatile organic compounds at pptv levels. *Chem. Soc. Rev.* **27**, 347 (1998).

32. E. S. Cross *et al.*, Online measurements of the emissions of intermediate-volatility and semi-volatile organic compounds from aircraft. *Atmos. Chem. Phys.* **13**, 7845–7858 (2013).

33. A. C. Aiken, P. F. DeCarlo, J. L. Jimenez, Elemental Analysis of Organic Species with Electron Ionization High-Resolution Mass Spectrometry. *Anal. Chem.* **79**, 8350–8358 (2007).

34. J. J. Gajewski, I. Kuchuk, C. Hawkins, R. Stine, The kinetics, stereochemistry, and deuterium isotope effects in the α-pinene pyrolysis. Evidence for incursion of multiple conformations of a diradical. *Tetrahedron*. **58**, 6943–6950 (2002).

35. N. M. Donahue, S. A. Epstein, S. N. Pandis, A. L. Robinson, A two-dimensional volatility basis set: 1. organic-aerosol mixing thermodynamics. *Atmos. Chem. Phys.* **11**, 3303–3318 (2011).

36. G. Isaacman-VanWertz *et al.*, Chemical evolution of atmospheric organic carbon over multiple generations of oxidation. *Nature Chem*. **10**, 462–468 (2018).

Chapter 5

Organic Particle Formation in Oxygen-Free Environments

5.1 Introduction:

In systems characterized by a lack of oxygen, radical hydrocarbon species can be produced via photolysis or heat, producing a radical product, which, in the absence of oxygen, can react with other hydrocarbons or radical species forming a product. In this process, molecules will decrease in volatility via molecular growth rather than functionalization, which occurs in the presence of oxygen. As these molecules grow, they decrease in vapor pressure, eventually partitioning into the particulate phase. There has been much interest in these particles as they mimic particles that are thought to have formed in the atmosphere of the early Earth (*1*). In addition to planetary atmospheres, such as Saturn's moon, Titan, this chemistry also mimics "low temperature" combustion where the photolysis replaces high temperatures in the formation of reactive intermediate species and the production of molecular growth, such as soot, from simple hydrocarbon precursors.

Some planetary atmospheres are characterized by highly complex and dynamic organic chemistry in which methane and other small hydrocarbons react to form larger hydrocarbons (*2*, *3*). The radical intermediates in this growth mechanism, which are formed via short wave UV photolysis as well as absorption of cosmic rays (*4*, *5*). In the absence of oxygen these reactive intermediates, react with hydrocarbons and intermediates forming larger and more complex molecules(*6-8*). As this process continues, molecules will grow continually decreasing in vapor pressure until partitioning into the condensed phase, thus forming particles. These particles form a distinct haze layer in the atmosphere of

titan and are referred to as "tholin" particles (*9*). The presence of these tholin particles were confirmed by the Voyager spacecraft and could serve as cloud condensation nuclei (CCN) for the ethane clouds in the haze layer of Titan's atmosphere (*4*, *10*, *11*). There have been numerous laboratory simulations of haze particles similar to those of Titan. The majority of these experiments expose varying concentrations of methane to some sort of radiation, UV, spark, and cold plasma discharge (*1*, *2*, *5*, *12*) and detect the resulting particles via absorption and mass spectroscopy(*1*, *5*, *12*). While these laboratory analogs are not completely representative due to a differences in temperature and pressure compared to the atmosphere of titan they can be useful to provide information on the chemical pathways of molecular growth.

This study is designed to characterize particles produced using vacuum ultraviolet light initiated photolysis of two-carbon hydrocarbon precursors an oxygen free environment. While many studies mimic the atmosphere of Titan by focusing on methane photolysis (*5*, *12*, *13*), this study aims to examine the difference in particulate growth using starting materials with differing levels of saturation. Ethane, ethylene, and acetylene, the two-carbon precursors used in this experiment, range in H:C ratio from 3 in ethane, to 2 l ethylene, and 1 in acetylene. This difference in elemental composition as well as reactivity of the single, double, and triple bond between the carbons provide a simple test case for determining the difference in particle formation pathways from photolysis in oxygen free systems.

5.2 Methods:

Haze particles were formed in an airtight reaction vessel (Figure 5.1) in which C_2 hydrocarbon precursors were exposed to vacuum ultra-violet light from a Hamamatsu L1835 lamp, which has an emission spectrum between 115 and 170 nm with major peaks at 121.6, 125.4, and 160.8 nm. The flow reactor is constructed from aluminum KF-flanged vacuum fittings with a custom VUV lamp attachment flange to ensure it is vacuum tight. The volume of the reaction cell is ~150 cubic centimeters and with a

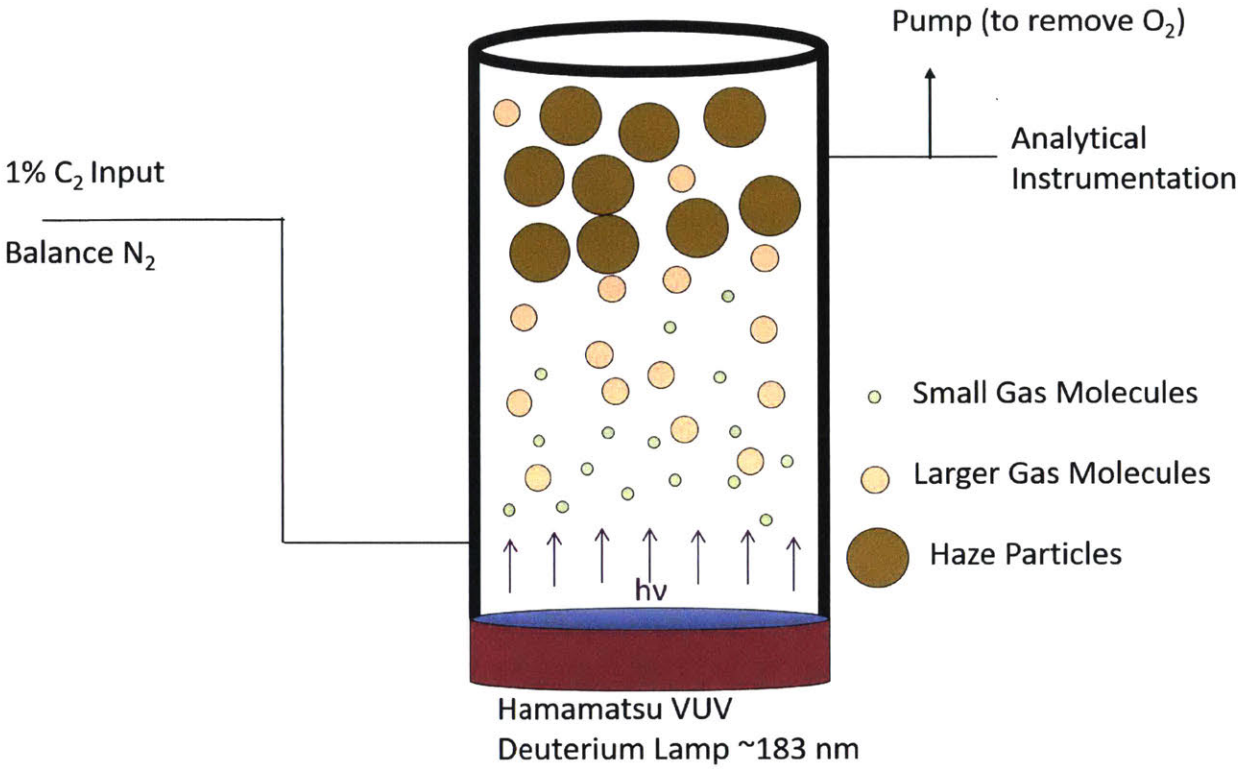

Figure 5.1 Diagram of photolysis reaction flow reactor. Hydrocarbon precursors are photolyzed via VUV photolysis lamp emitting a spectrum centered at 180 nm. The flow reactor is approximately 40 cm in length and has a diameter of 2.5 cm.

flow of 100 sccm, provides a residence time of approximately 1.5 minutes. All experiments were conducted at 25 C. Prior to experiments, the reaction cell was pumped down to 10^-4 torr to remove as much ambient air, specifically oxygen, as possible. It was then filled with a 1% mixture of ethane (C_2H_6), ethylene (C_2H_4), or acetylene (C_2H_2) (Airgas Inc.) in nitrogen and was held at ~ 350 torr for 10 minutes in the reaction cell before being directed to the measurement instrumentation to best mimic other laboratory simulations of these particles.

Particle composition and size were measured using an Aerodyne High Resolution Aerosol Mass Spectrometer, or AMS (Aerodyne Research Inc, Billerica, MA). This technique has been discussed previously (*14*) and has also been used in studies of tholin laboratory analogs(*5*, *13*). In short, particles are separated from the gas phase via aerodynamic lens and vaporized at ~600 C. Vaporized particles are then

ionized via electron ionization and passed into a TofWerk high resolution time-of-flight mass spectrometer. The AMS utilized in this study was a Soot Particle-AMS (SP-AMS), which uses an infrared (1064 nm Nd-YAG) laser to vaporize particles that absorb strongly in the IR, such as soot particles (*15*). Haze particles were examined under both SP and non-SP mode to determine the amount of IR absorbing mass, if any, produced and incorporated into particles. The HR-AMS was run in V-mode, which provides a mass resolving power of ~2200. This allows for clear separation of different $C_xH_y^+$ ions in the mass spectra. These are fitted using the software package (*14*), enabling the determination of individual ion formulas and the calculation of elemental ratios in the particles using the method developed by Aiken et. al. (*16*).

5.3 Results & Discussion:

5.3.1 Particle Composition

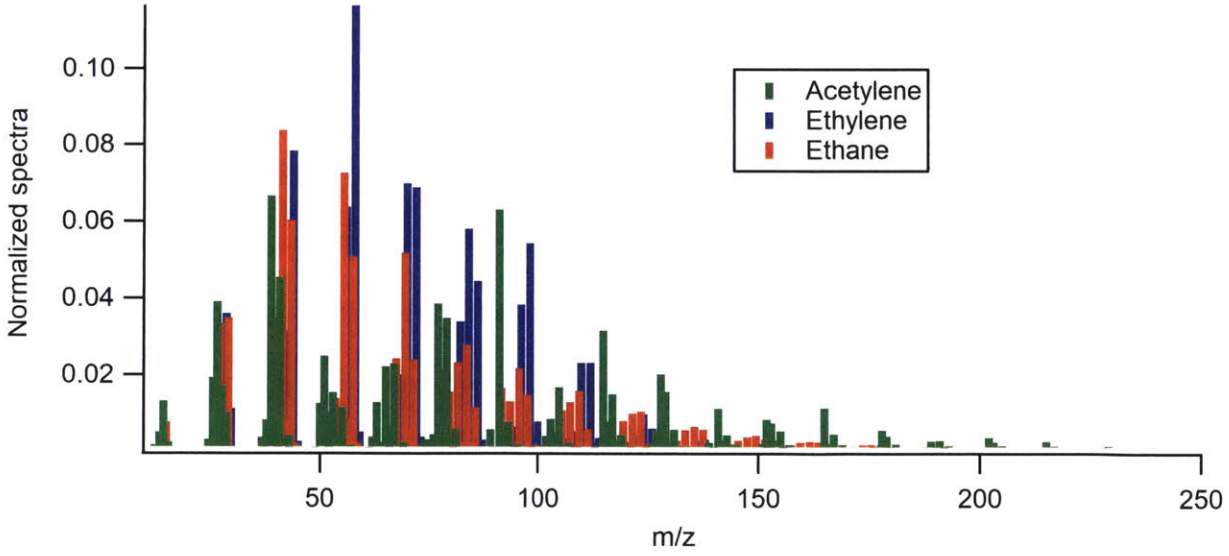

Figure 5.2 Mass spectra from the soot-particle aerosol mass spectrometer (SP-AMS) of particles formed via VUV photolysis of ethane (red), ethylene (blue), and acetylene(red). Particles formed from ethane and ethylene show a typical saturated hydrocarbon decay pattern, while particles formed from acetylene show aromatic characteristics.

Particles were produced using all three C_2 hydrocarbons: ethane, ethylene, and acetylene. Acetylene was capable of creating a stable stream of particles while ethane and ethylene could not sustain continuous particle formation with the conditions used in these experiments and only produced a pulse of particles that quickly decayed away. All data shown are from thermal vaporization mode in the AMS only, as the use of SP (IR vaporization) showed no additional signal. Figure 5.2 shows the mass spectra for the three different starting materials, which are highly complex, suggesting a wide variety of products. The mass spectra of particles produced from VUV photolysis of ethane (shown in red) is dominated by a major peak of $C_3H_5^+$ with other major peaks at ($C_4H_7^+$, $C_5H_9^+$ and so on) indicating ion fragments separated by CH_2 groups. These major ions are not fully saturated, suggesting the formation pathway of particles made from C_2H_6 introduces double bonds into the product molecules. The mass spectra of particles formed with ethylene (C_2H_4), shown in blue, appear very similar to those of ethane as they are separated by CH_2 groups, however the peaks have a slight shift to more saturated peaks at $C_3H_7^+$ and $C_4H_9^+$ and $C_5H_{11}^+$.

The composition of particles formed from acetylene (C_2H_2) are fundamentally different from that of ethane and ethylene particles. The mass spectra of from acetylene particles (shown in green) has a major peak at $C_3H_3^+$ and another at $C_7H_7^+$, both corresponding to peaks associated with aromatic compounds, which are likely major products because of the high degree of unsaturation of the acetylene. Also, on average the ion fragment produced via electron ionization are much larger than the fragments from ethane and ethylene. This is due to the increased stability of aromatic ions produced via electron ionization.

Figure 5.3 shows an effective way to visualize the high-resolution mass spectra of these particles via a two-dimensional "mass defect plot", which shows delta mass vs the ion mass. In these plots, the relative magnitude of individual ions is indicated by the area of the marker. The lines represent common

formulas: the black horizontal line (x axis) represents elemental carbon (Cn, which has no mass defect), the blue line indicates molecules with a formula of C_nH_n, (unsaturated species with H:C of 1) and the red line follows molecules with a formula of C_nH_{2n}, denoting essentially saturated species (alkanes). Figure 5.3(a) shows the mass defect plot of particles formed via the VUV photolysis of ethane. The majority of the ions are centered between the C_nH_{2n} and C_nH_n lines with the majority of the mass from ion fragments below 150 m/z. The mass defect for particles formed from ethylene (Figure 5.3(b)) is similar to that of

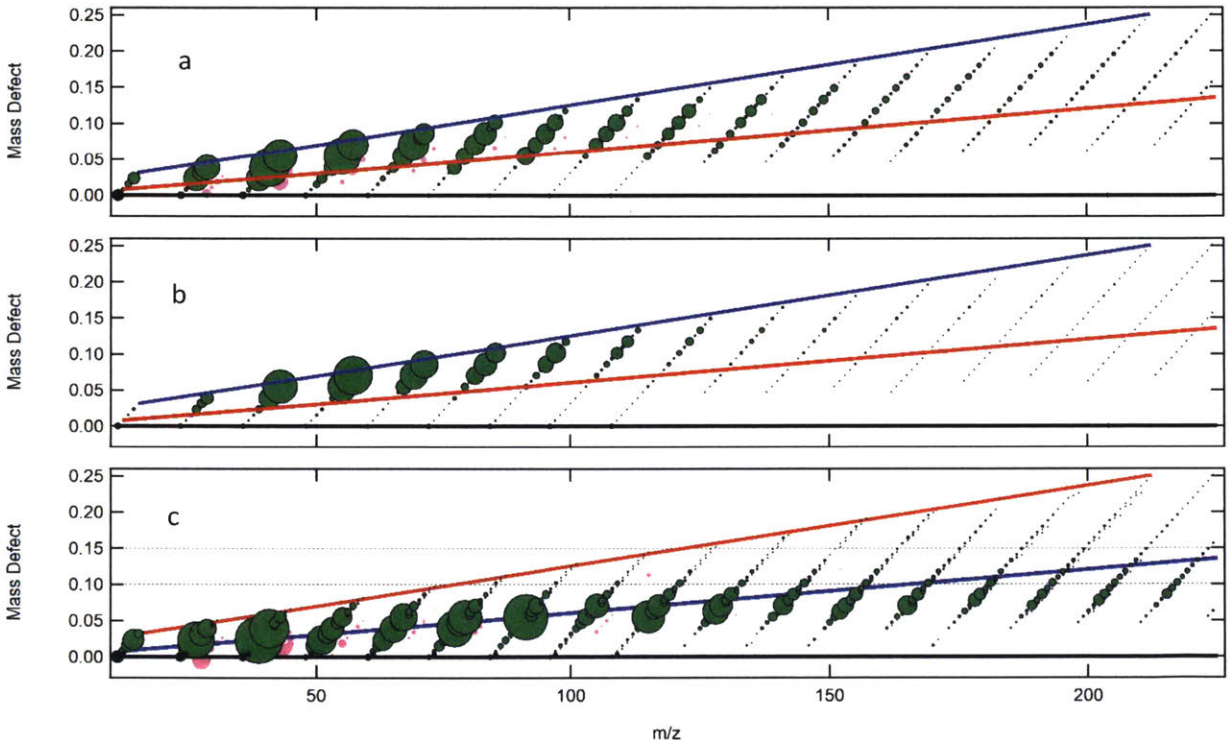

Figure 5.3 Mass defect plots for particles formed via VUV photolysis of ethane (top), ethylene (middle), and acetylene (bottom). The red line represents mass defects for fully saturated hydrocarbon molecules (C_nH_{2n}), the blue line represents molecules with the formula C_nH_n, while the black x-axis represents C_n molecules.

ethane, however, the mass is significantly focused in the smaller ion fragment masses. The majority of the signal also rests somewhat closer to the saturated C_nH_{2n} line in this plot, which indicates that the particles are composed of highly saturated organic species. The mass defect plot for acetylene, however, is again fundamentally different from that of both ethane and ethylene. The signal is distributed across a much larger range, extending well above a mass to charge ratio of 200. The mass spectrum also has a

much lower average mass defect when compared to either ethylene or ethane, indicating a significantly more reduced chemical composition. The majority of peaks are near or even below the C_nH_n line, especially for larger ion fragments. Ions below the C_nH_n line indicate highly unsaturated hydrocarbon fragments, with H:C values below 1; these may well include aromatic compounds. Indeed, ions corresponding to single and double aromatic hydrocarbon rings are detected. Peaks of ions associated with benzene, toluene and naphthalene are prominent in the mass spectrum and are visible at m/z 77, 91 and 128 respectively. Peaks below the C_nH_n line also show that molecules with extended carbon rings with limited hydrogen, such as PAH's may be formed as well though are not major products of the reactions as carried out in this research. The mass defect plots for ethane and acetylene show a small incorporation of oxygen in to the particles as indicated by pink markers in the figure. The total amount of oxygen incorporated into these particles is very small, with O:C ratios of 0.04 for each compound, and likely due to the inability to completely remove oxygen from the reaction cell or contamination in the precursor gases. It is unclear why the mass spectra of ethylene produces particles with very little oxygen, but is likely due to a higher purity of precursor gas.

The differing degree of unsaturation from the different systems can be expressed in terms of the double bond equivalents (DBE) of the measured ions. DBEs equal the sum of double bonds as well and rings in molecules and ions and is calculated using the formula: $DBE=n_c - n_H/2 + 1$. The majority of double bond equivalents presented are non-integer due to electron ionization process breaking molecules into radical ion fragments. Lower DBE values correspond to more saturated radical ion fragments. A DBE of 0.5, for instance, will correspond to fully saturated radical ion fragments, such as $C_3H_7^+$ and $C_4H_9^+$. Aromatic compounds, have DBE values of 3.5 and higher depending on the number of ring closures as

well as the degree of unsaturation of the substituted groups on the aromatic ring. Polycyclic aromatic hydrocarbons (PAHs) will have DBE values over 8.

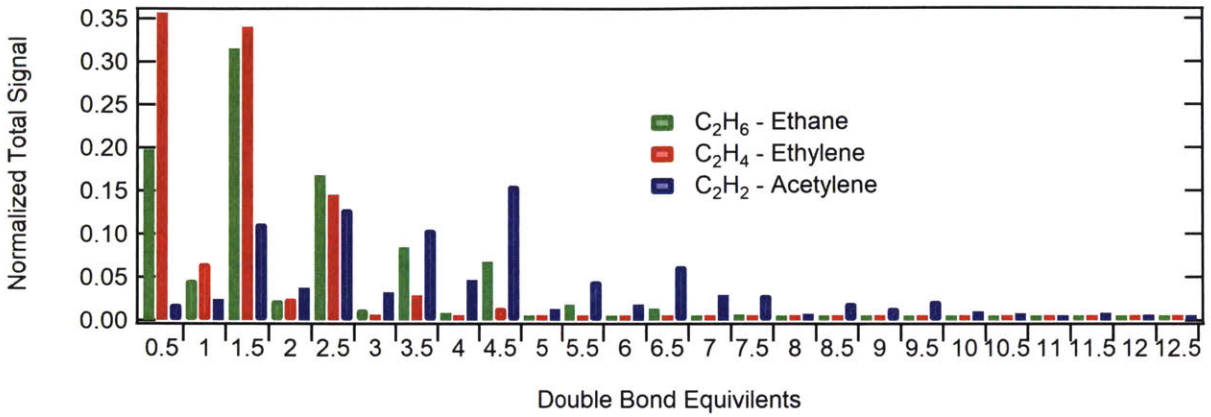

Figure 5.4 Aerosol Mass Spectra of particles formed from Ethane, ethylene and acetylene summarized via double bond equivalents (DBE). DBE values arise from ring closures as well as double and triple bonds in molecules. Particles formed from ethane and ethylene have DBE values mostly below 2.5 while particles formed from acetylene possess significantly higher DBE values averaging at 4.5 and going as high as 11.5. The majority of DBE values presented in this data are half values due to the molecular fragmentation which occurs during electron ionization mass spectrometry.

Figure 5.4 shows histograms of the DBE distribution for the mass spectra of particles formed from each C_2 precursor. The DBE values for ethane and ethane particles are very similar with the majority of signal coming below a DBE value of 3. This indicates the production of more highly saturated hydrocarbon compounds in the reactor which are expected as the starting reagents are themselves more saturated and there is enough free hydrogen in the system from ongoing photochemistry to maintain a higher degree of saturation. The DBE distribution from acetylene photolysis, however, is dramatically different, spread over a wider range of values (between 2.5 and 9.5), and ranging to much higher degrees of unsaturation (DBEs of 14) indicating higher degrees of ring closure and aromaticity. The peak DBE for acetylene is 4.5, which is significantly higher than that of ethylene or ethane, confirming that the particles produced are significantly more aromatic.

5.3.2 Elemental Composition

The high resolution mass spectrometer also provides elemental analysis of mass spectra (*16*). The hydrogen to carbon ratio of ethane and ethylene are 3 and 2 respectively. The particles from both ethane and ethylene both possess hydrogen to carbon (H:C) ratios of 1.95, which is very close to a ratio for saturated hydrocarbons, which will be closer to 2.2 for smaller saturated hydrocarbons and closer to 2.0 for larger saturated hydrocarbon molecules. Particles produced from acetylene, have a much lower H:C ratio of 1.26. The produced particles have different H:C when compared to elemental ratios of the starting materials. The H:C of acetylene is 1, while the particles have a slightly higher H:C ratio of 1.26. This means that the particles detected by the AMS have a slightly higher H:C than what is not being detected. The AMS strips away gases, suggesting it might possess a lower H:C ratio than the particles.

All the produced particles have very limited oxygen incorporation, with an O:C of 0.04. Oxygen is removed from the system by pumping the reaction vessel to 10^{-4} torr prior to filling with ultra-high purity nitrogen. This removes enough oxygen from the system to make the reaction of radical hydrocarbon with other hydrocarbons to be the dominant kinetic pathway even though there will still be some residual oxygen in the system. Any other oxygen in the system could also be due to impurities in the hydrocarbon mixtures as procured. Moreover, no nitrogen incorporation was observed in contrast to other recent laboratory simulations of haze particles (*12*, *13*). The organic nitrogen ion fragments of CN and CHN (m/z 26, 27) are typically seen in AMS spectra of titan analogs. AMS spectra from particles in this study show neither of these peaks nor other evidence of organic nitrogen in our particles. This is most likely due to the difference in starting material. The majority of other studies use methane as their starting material, which can form the CH radical via VUV photolysis. The CH radical can then react with N_2 to form CHN. This reaction cannot occur with the 2-carbon precursors used in this study because they do not form the CH radical.

While unsaturated and aromatic organic compounds were produced in this study, there was no evidence of the production of polycyclic aromatic hydrocarbons (PAHs) or soot. The SP-AMS did not

detect any increased signal above the mass detected via typical particle vaporization indicating that no organic molecules able to strongly absorb IR light were produced. Polycyclic aromatic hydrocarbons (PAHs), namely naphthalene (m/z 128) and phenanthrene (m/z 178) were detected mass spectra of haze particles produced from VUV photolysis of acetylene. However, these peaks do not dominate the signal of the mass spectrum, which is consistent with the lack of any signal in SP mode which indicates very large delocalized systems (e.g. graphene or soot). Under the right conditions, such as longer reaction time, lower pressure, or lower temperatures, it is possible that the VUV photolysis of acetylene could lead to soot type molecules, but they were not observed using the reaction conditions examined during this study.

5.4 Conclusions & Implications:

The chemistry associated with the production of particles through the VUV photolysis of two-carbon precursors is highly complex undergoing multiple generations of oxidation. Molecular growth occurring through radical reactions with other gas phase hydrocarbon species result in lower volatilities, and eventual partitioning into the particulate phase. Particles produced through the photolysis of ethane and ethylene result particles characterized by highly saturated organic compounds. While particles produced from ethane (C_2H_6) produce slightly less saturated particles, the mechanistic reason for this difference is unknown. Photochemical studies of ethylene show butane as a major product, which could lead to a higher saturation in particles compared to ethane (*17*). However, major first generation photolysis products only play a small role in particle formation as they must undergo many more rounds before growing large enough to nucleate particles. The chemistry associated with particulate production from the photolysis of acetylene is fundamentally different that of ethane and ethylene. The photolysis of acetylene produces an acetyl radical (C_2H), which can then react with other acetylene molecules starting a radical chain propagation, or react with another acetyl radical, forming a diacetylene molecule.

At this point, the chemistry becomes highly complex and the lack of available hydrogen combined with the high degree of unsaturation of the starting material serves to lead to highly unsaturated products, including aromatic compounds. While no strong evidence of PAH or soot formation was observed in SP mode, it is conceivable with different reaction conditions, such as lower pressure or longer reaction time, these could be produced. To fully understand the mechanism leading to the formation of particles from the photolysis of two-carbon precursors a detailed understanding of the production and evolution of secondary volatile and intermediate volatility organic compounds is necessary. This characterization could provide insight into the different generation of photo oxidation products that exist between precursor and particle.

5.5 References

1. M. G. Trainer *et al.*, Haze aerosols in the atmosphere of early Earth: manna from heaven. *Astrobiology*. **4**, 409–419 (2004).

2. P. Coll *et al.*, Experimental laboratory simulation of Titan's atmosphere: aerosols and gas phase. *Planetary and Space Science*. **47**, 1331–1340 (1999).

3. D. M. Hunten, The atmosphere of Titan. *Icarus*. **22**, 111–116 (1974).

4. E. L. Barth, O. B. Toon, Methane, ethane, and mixed clouds in Titan's atmosphere: Properties derived from microphysical modeling. *Icarus*. **182**, 230–250 (2006).

5. M. G. Trainer *et al.*, Aromatic Structures in Simulated Titan Aerosol. **1**, 1308 (2011).

6. D. W. Clarke, J. P. Ferris, Titan haze: structure and properties of cyanoacetylene and cyanoacetylene–acetylene photopolymers. *Icarus* (1997).

7. T. W. Scattergood, E. Y. Lau, B. M. Stone, Titan's aerosols I. Laboratory investigations of shapes, size distributions, and aggregation of particles produced by UV photolysis of model Titan atmospheres. *Icarus*, 1–8 (2002).

8. B. N. Tran *et al.*, Titan's atmospheric chemistry: Photolysis of gas mixtures containing hydrogen cyanide and carbon monoxide at 185 and 254 nm. *Icarus*. **193**, 224–232 (2008).

9. C. Sagan, W. R. Thompson, B. N. Khare, Titan - a Laboratory for Prebiological Organic-Chemistry. *Accounts of Chemical Research*. **25**, 286–292 (1992).

10. M. Cabane, E. Chassefière, Laboratory simulations of Titan's atmosphere: organic gases and

aerosols. *Planetary and Space Science*. **43**, 47–65 (1995).

11. E. C. Sittler *et al.*, Heavy ion formation in Titan"s ionosphere Magnetospheric introduction of free oxygen and a source of Titan"s aerosols? *Planetary and Space Science*. **57**, 1547–1557 (2009).

12. S. M. Hörst *et al.*, Laboratory investigations of Titan haze formation: In situ measurement of gas and particle composition. *Icarus*. **301**, 136–151 (2018).

13. M. G. Trainer, J. L. Jimenez, Y. L. Yung, O. B. Toon, M. A. Tolbert, Nitrogen Incorporation in CH 4-N 2Photochemical Aerosol Produced by Far Ultraviolet Irradiation. *Astrobiology*. **12**, 315–326 (2012).

14. P. F. DeCarlo *et al.*, Field-Deployable, High-Resolution, Time-of-Flight Aerosol Mass Spectrometer. *Anal. Chem.* **78**, 8281–8289 (2006).

15. T. B. Onasch *et al.*, Soot Particle Aerosol Mass Spectrometer: Development, Validation, and Initial Application. *Aerosol Science and Technology*. **46**, 804–817 (2012).

16. A. C. Aiken, P. F. DeCarlo, J. L. Jimenez, Elemental Analysis of Organic Species with Electron Ionization High-Resolution Mass Spectrometry. *Anal. Chem.* **79**, 8350–8358 (2007).

17. M. C. Sauer Jr., L. M. Dorfman, Molecular Detachment Processes in the Vacuum uv Photolysis of Gaseous Hydrocarbons. I. Ethylene. II. Butane. *J. Chem. Phys.* **35**, 497–502 (1961).

Chapter 6

Conclusion

5.1 Summary & Conclusions

An understanding of the sources of secondary organic aerosol is a necessity due to its impacts on human health, global climate, visibility and air quality as a whole. There exists a large uncertainty in the formation of secondary organic aerosol especially in the emissions and transformation of lower volatility organic gases in the atmosphere. Intermediate volatility organic compounds (IVOCs) have been shown to be efficient precursors to secondary organic aerosol, however measurements of IVOCs are lacking due to difficulties in quantification and detection. The goal of this thesis research is centered on understanding ***how*** to measure intermediate volatility organic compounds in the atmosphere and using that information better understand how they are emitted, evolve and are produced in the atmosphere.

Chapter 2 of this thesis focuses on how IVOCs are measured in the atmosphere and the characterization and development of the thermal desorption – electron ionization mass spectrometer (TD-EIMS). The TD-EIMS is an analytical technique designed prior to the start of the thesis work in the Kroll lab to provide a volatility separated bulk measurement of IVOCs. In the course of preparing the instrument for a field deployment the instrument was substantially characterized revealing a number of limitations in the original design. The instrument was redesigned utilizing a valve-less injection system, which replaces a mechanical 6-way valve in the original instrument design, as well as an improved collection loop. These major improvements, along with peripheral improvements to the system, improves the overall stability of the instrument producing more reliable and quantifiable measurements of IVOCs. With more reliable measurements of IVOCs come increased ease in data analysis and manipulation, which

easily is more time intensive than data collection. Instrument development is an ongoing process and the while the TD-EIMS is functioning well, more work on calibrations, especially of oxygenated species will improve the technique. The TD-EIMS took a major step forward in the process of this thesis work, the result of which is demonstrated in chapter 4 of this thesis.

Chapter 3 of this thesis examines the emission profiles of IVOCs from gasoline vehicles as a function of engine state and emissions controls tier. IVOC chemical composition is relatively uniform across engine states and are composed of alkanes and single-ring aromatics, regardless of the emissions control tier or engine state. However, the total emission rates of IVOCs are highly dependent on both factors. Cold start engine periods emit IVOCs at a much higher rate than once the engine has reached an operational temperature, including hot engine ignition events. The most modern emissions controls are the most effective at removing IVOCs and show an 80% reduction in emissions between the ULEV and newest SULEV tiers. This pattern does not follow that of volatile organic compounds, which show an 80% decrease in emissions between the LEV and LEV2 tier as well as a continued reduction in emissions with more stringent emissions controls. This decrease is not seen in IVOC emissions. This supports the notion suggested by Robinson et. al. and Gordon et. al. that a disproportionate reduction in IVOC emissions has led to a smaller reduction in SOA production in urban atmospheres (1, 2). Lastly, as emissions controls become more efficient at reducing emissions during normal operational conditions, specifically those of IVOCs, the cold start will contribute the most to SOA production in urban atmospheres.

Chapter 4 of this thesis focuses on the application of the newly developed valve less injection version of the TD-EIMS to measure the production and evolution of secondary IVOC during atmospheric "smog" chamber experiments. The chamber oxidation of α-pinene with OH and O_3 show two very different profiles in secondary IVOCs. In the case of α-pinene reacting with O_3, a wide volatility range of IVOCs grow in, exhibiting log(c*) values between 7 and 5.5. The IVOCs grow in at the beginning of the experiment, and then come to equilibrium. This is expected as the reaction of α-pinene with O_3 is, for the

most part, a one step process. When α-pinene reacts with OH, the case is different producing IVOCs that grow in over the first hour of the experiment, peak and then decay back to zero. This decrease is likely due to one of two pathways occurring. First, IVOCs decrease in volatility enough to partition into the particulate phase, and thus out of the detection of the TD-EIMS. IVOCs can also fractionate, producing two smaller oxidation products with higher volatilities, which also will be out of the detection range of the TD-EIMS. The case of cis-1,4 dimethylcyclohexane is different from both of the reactions of α-pinene. The OH oxidation experiment is characterized by a quick increase in IVOCs followed a gentle increase in IVOC loadings throughout the course of the experiment and is likely due to the slow reaction of DMCH yielding and a slow production of secondary IVOCs.

There has been a recent attempt to track the fate of all the carbon in the course of chamber oxidation experiments of α-pinene with OH that have successfully accounted for all the carbon after 24 hours of equivalent atmospheric oxidation. However, there exists an unmeasured fraction of carbon (as much 30%) at the beginning of the experiment that eventually shrinks as more of the carbon is identified and quantified throughout chamber oxidation experiments. The IVOC concentration profile closely matches this fraction of "missing" carbon. While it is likely that the TD-EIMS is not only sampling some of the missing fraction of carbon as there is likely overlap with other measurement techniques, it is highly possible that it is quantifying previously unaccounted for carbon in chamber experiments. By comparing TD-EIMS measurements with results from other analytical techniques, the extent of this overlap, and therefore the amount of "missing" carbon, can be characterized leading to a better understanding of the evolution of organic compounds in the production of secondary organic aerosol.

Chapter 5 represents a slight deviation from the focus on intermediate volatility organic compounds by focusing on the production of low volatility organic compounds produced from the VUV photolysis of two-carbon molecules in oxygen free environments. Produced from ethane, ethylene and acetylene, these low volatility organic compounds were measured once they had partitioned into the

particulate phase. Particles produced from ethane and ethylene are significantly more saturated with the majority of ion fragments produced during electron ionization possessing a double bond equivalence of 0.5 or 1.5. These values correlate with ions with a single or no double bonds, as would be expected when producing particles from more saturated precursors. The particles made from VUV photolysis of acetylene exhibit a fundamentally different chemical composition. Compared to particles formed from ethane and ethylene, the ion fragments are significantly larger and are significantly more reduced, many of them possessing H:C ratios below 1. While no significant signal indicating the presence of polycyclic aromatic hydrocarbons (PAHs) were detected, with the right reaction conditions they would be likely produced.

6.2 Implication and Future Research Directions

A better understanding of the evolution of organic carbon in the atmosphere, through improved measurements, is critical if there is going to be any reduction in the uncertainty in the formation of secondary organic aerosol. Low volatility organic compounds, specifically intermediate volatility organic compounds, represent an under-characterized class of compounds with high potential to impact the formation of organic aerosol in the atmosphere. The data presented in this thesis represents a step towards understanding the emissions, production and evolution of intermediate volatility organic compounds in the atmosphere. There exists potential for a significant growth in our understanding by the development of a new, more reliable analytical technique for measuring the mass, volatility, and composition of IVOCs in the atmosphere. As primary IVOC emissions from vehicles continue to decrease, a more time resolved understanding of emissions from vehicles, both gasoline as well as diesel, crucial to understanding the how vehicles contribute to SOA production in urban environments. The TD-EIMS could also provide a more time resolved characterization of not only primary IVOCs in vehicle emissions, but also the evolution of those emissions as they form SOA. By developing the TD-EIMS, secondary IVOCs were measured and potentially represent a substantial and previously unaccounted for fraction of carbon

during the oxidation of α-pinene by OH. While significantly more analysis needs to be performed to deconvolve the overlap between the TD-EIMS and other analytical techniques, there exists a wealth of information that the TD-EIMS could provide from chamber oxidation studies of other precursor systems. Lastly, measurements of the oxidation products in low oxygen systems could provide insight how particles are formed from the photolysis of small VOC species thus providing insight to processes occurring in planetary atmospheres as well as in soot production.

One concept stuck out to me the most in my time thus far studying atmospheric chemistry: the idea of ***collaboration***. In no other field is it common for a paper to have ten or twenty co-authors. It truly takes an army to characterize something as complicated as the atmosphere. In that notion, while I have a significant emotional investment in the TD-EIMS, it cannot be the only method used to characterize low volatility organic gases. Other techniques will always be better at measuring some specific compound or another. The best path forward in understanding the role IVOCs play in the atmosphere is to closely study them ***alongside*** other researchers utilizing other measurement techniques. By better understanding what exactly comprises the "bulk volatility separated characterization of IVOCs" we can provide modelers with better information to improve model output of SOA production; we again, cannot do it by ourselves.